

Fundamental Investigation of Fuel Transformations in Pulverized Coal Combustion and Gasification Technologies

Final Report: September 1, 2000 - August 31, 2004.

Principal authors: Robert Hurt, Brown University
Joseph Calo, Brown University
Thomas H. Fletcher, Brigham Young University
Alan Sayre, McDermott Technologies Inc.

Report Issue Date: April 29, 2005

DOE Award Number: DE-FG26-OONT40815

Submitting Organization: Brown University (R. Hurt)
Division of Engineering, Box D
Providence, RI 02912

ABSTRACT

The goal of this project was to carry out the necessary experiments and analyses to extend current capabilities for modeling fuel transformations to the new conditions anticipated in next-generation coal-based, fuel-flexible combustion and gasification processes. This multi-organization, multi-investigator project has produced data, correlations, and submodels that extend present capabilities in pressure, temperature, and fuel type. The combined experimental and theoretical/computational results are documented in detail in Chapters 1-8 of this report, with Chapter 9 serving as a brief summary of the main conclusions. Chapters 1-3 deal with the effect of elevated pressure on devolatilization, char formation, and char properties. Chapters 4 and 5 deal with advanced combustion kinetic models needed to cover the extended ranges of pressure and temperature expected in next-generation furnaces. Chapter 6 deals with the extension of kinetic data to a variety of alternative solid fuels. Chapter 7 focuses on the kinetics of gasification (rather than combustion) at elevated pressure. Finally, Chapter 8 describes the integration, testing, and use of new fuel transformation submodels into a comprehensive CFD framework. Overall, the effects of elevated pressure, temperature, heating rate, and alternative fuel use are all complex and much more work could be further undertaken in this area. Nevertheless, the current project with its new data, correlations, and computer models provides a much improved basis for model-based design of next generation systems operating under these new conditions.

TABLE OF CONTENTS

EXECUTIVE SUMMARY	5
PROJECT BACKGROUND.....	7
PROJECT OBJECTIVE AND APPROACH.....	8
CHAPTER 1 THE EFFECT OF PRESSURE OF COAL PYROLYSIS.....	10
CHAPTER 2: INTRINSIC REACTIVITY OF CHAR FORMED AT ELEVATED PRESSURE	51
CHAPTER 3: ELEVATED PRESSURE, HIGH TEMPERATURE COAL OXIDATION EXPERIMENTS AND MODELING	71
CHAPTER 4: DEVELOPMENT OF A NEW SEMI-GLOBAL RATE EXPRESSION FOR CHAR COMBUSTION MODELING.....	106
CHAPTER 5: THE ORIGIN OF POWER LAW KINETICS IN CHAR COMBUSTION.....	125
CHAPTER 6: CHAR COMBUSTION REACTIVITIES FOR A SUITE OF DIVERSE SOLID FUELS	145
CHAPTER 7: GASIFICATION KINETICS IN PRESSURIZED CO ₂	162
CHAPTER 8: IMPLEMENTATION OF ADVANCED COAL COMBUSTION SUBMODELS INTO B&W'S CFD CODE.....	201
CHAPTER 9: CONCLUSIONS.....	229

EXECUTIVE SUMMARY

The goal of this project was to carry out the necessary experiments and analyses to extend current capabilities for modeling fuel transformations to the new conditions anticipated in next-generation coal-based, fuel-flexible combustion and gasification processes. This multi-organization, multi-investigator project has produced data, correlations, and submodels that extend present capabilities in pressure, temperature, and fuel type. The main issue for pyrolysis is the effect of pressure for coals of various rank. By generating chars in both atmospheric and pressurized flat-flame burners (up to 15 atm), the team found a number of important trends. Chapters 1 and presents experimental data needed to extend coal pyrolysis models to high pressure, including effects on volatiles yield, swelling, H/C and O/C ratio, surface area, and char reactivity. Important differences are seen as a function of pressure, and the combined data allow these differences to be accounted for in CFD models. Chapter 3 describes high-pressure, high-temperature char combustion experiments and their analysis with a combination of Fluent and the CPD and CBK submodels. A different value of the char combustion reactivity (activation energy or pre-exponential factor) for each pressure condition for each coal, highlighting the importance of pressure effects that must be accounted for in advance combustor / gasifier design.

Chapters 4 and 5 present new results on char combustion kinetics and their extension to wide ranges of pressure and temperature. A major result is the first theoretical justification for the long-standing paradox of persistent, high fractional order in the char/oxygen reaction is surface heterogeneity. This work provides sufficient underpinning to justify the use of the power-law form in practical char combustion modeling. The use of the power-law form has practical advantages, but to date has lacked a fundamental basis and has led to much controversy and confusion in the field.

There continues to be interest in the development and applications of more detailed rate expressions. If the field proceeds in that direction, this work suggests that the common 2-step Langmuir form is unsuitable, as it cannot predict the high fractional orders almost universally seen at low temperature. A possible promising direction is the use of three-step or four-step semi-global mechanisms incorporating O₂-complex reaction as described here in Chapter 4. It remains to be seen if the added complexity relative to power-law approaches will make this a popular approach in design applications. The heterogeneous surface model of Haynes is also shown to be a promising framework for describing the major features in the char combustion database though it requires a statistical treatment of active sites.

Chapter 6 describes experimental work addressing the issue of fuel flexibility anticipated in next generation systems by providing a large database of comparative reactivities on coals and alternative solid fuels. A hybrid chemical/statistical model was developed that explains most of the observed reactivity variation based on four variables: the amounts of nano-dispersed potassium, nano-dispersed calcium and magnesium, elemental carbon wt-%, and nano-dispersed vanadium, listed in decreasing order of importance.

Chapter 7 deals with *gasification* mechanisms at elevated pressure. CO₂ gasification reactivities were determined for two char and the effects of total CO₂ pressure, CO₂ partial pressure, and the inhibition effect of CO on the reaction rate were investigated at elevated pressures. The results show that char reactivity increases monotonically with CO₂ partial pressure and the apparent activation energy *decreases* with *increasing* pressure. Further, reactivity *decreases* considerably with increasing CO partial pressure. Finally Chapter 8 describes a task in which advanced coal combustion submodels, Chemical Percolation and Devolatilization (CPD) and Carbon Burnout Kinetic (CBK) were modified and incorporated into a comprehensive computational CFD code.

Overall, the effects of elevated pressure, temperature, heating rate, and alternative fuel use are all complex and much more work could be further undertaken in this area. Nevertheless, the current project with its new data, correlations, and computer models provides a much improved basis for model-based design of next generation systems operating under these new conditions.

PROJECT BACKGROUND

Increased concern over energy supply and global warming is currently motivating a major research effort in the U.S. on future energy technologies with low CO₂ emissions. Research is needed to configure and design future coal-fired power-generation technologies with no or minimum impact on atmospheric CO₂ concentrations. A reduction in CO₂ emissions can be accomplished in the near term through increased efficiency with existing systems. Integrated gasification combined cycle (IGCC) systems have been used as the starting point for strategies to reduce CO₂ in the atmosphere, since (a) they are more efficient than conventional systems (50-60% as opposed to the current 34%) and (b) they promise to provide a concentrated stream of CO₂ by using steam and pure O₂ as the gasification agents (without N₂ as a diluent). Sequestration processes are currently under development that rely on IGCC, but this technology has not yet been widely demonstrated. In addition to IGCC, systems, combustion systems operating with enhanced oxygen concentration or pressure may also provide concentrated CO₂ streams.

Role of Model-Based Design

Within the last several years computational fluid dynamics (CFD) has firmly established itself as an important tool for the design, optimization, and retrofit analysis of full-scale combustion furnaces. CFD tools, when expertly applied, can identify firing configurations that significantly enhance performance and avoid the need for full-scale testing. Computer simulation is even more important for the design and development of next generation energy technologies based on oxygen-enriched combustion and/or gasification. These advanced systems cannot be reliably designed in an evolutionary way, as is often the case with current technologies, since there is no extensive database of operating experience with similar units. Model based design requires fuel-general submodels of coal transformations that are accurate under the combustion and gasification conditions unique to these processes.

Fuel Transformation Submodels

Successful furnace simulation requires predictive capabilities for many subprocesses including fuel transformation submodels to predict: (1) pyrolysis and char yield, (2) char oxidation and carbon burnout, (3) nitrogen release, and (3) mineral transformations. One of the P.I.s, (T. Fletcher) is the primary architect of the chemical percolation devolatilization (CPD) model (Fletcher et al. 1992), a mechanistic pyrolysis model based on a network description of the chemical structure of the parent coal. The model: (a) is suitable for application in large comprehensive models of coal combustion, and (b)

accurately describes key chemical structural features and reaction mechanisms of coal. Another of the Principal Investigators (R. Hurt) been engaged over the last eight years at the Combustion Research Facility at Sandia National Laboratories and at Brown University in the development of advanced submodels for char combustion, with emphasis on carbon burnout prediction. Carbon burnout has become a critical issue in the existing boiler stock as low-NO_x burner retrofits have increased carbon carryover and seriously impacted ash utilization markets at many sites in the U.S.. The experimental work has led to the Carbon Burnout Kinetic Model (CBK), a fuel-general kinetics package designed to predict carbon burnout under conditions relevant to current pulverized coal-fired boilers [Hurt et al., 1998]. Special emphasis is given to the late stages of combustion, which exert a strong influence on the burnout process that determines the carbon content of ash and thus ash utilization options [Hurt, 1998].

The fuel submodels listed above have been developed and applied for atmospheric pc-fired combustion systems. In this application they have found practical use in industry codes and have demonstrated some predictive capability, but further validation against field data is needed, as is extension to conditions found in next-generation energy processes. Although many of the condensed phase processes (internal diffusion, thermal annealing) can be directly carried over into models of gasification and O₂-enriched combustion, other reaction processes in the condensed phases require new data to make predictions under these conditions. Specifically new data is needed on: (1) the char formation process at high pressure, (2) char surface kinetics in enhanced oxygen and in the complex gasification environments, (3) nitrogen and inorganic release at high pressure and the concomitant high particle temperatures of enhanced oxygen combustion and oxygen-blown gasification systems, and (4) the development of engineering models that combine char property prediction with simplified surface kinetics for inclusion in practical flame codes.

PROJECT OBJECTIVE AND APPROACH

To carry out the necessary experiments and analyses to extend leading submodels of coal transformations to the new conditions anticipated in next-generation energy technologies. The work will use a combination of high-pressure TGA, atmospheric entrained flow reactor experiments, and experiments with a high pressure drop tube furnace to address volatile release, nitrogen release, inorganic release, and char properties and reactivity,

with particular emphasis on gasification environments under pressure and enhanced oxygen environments at atmospheric pressure. The CPD and CBK models will be validated against full-scale data on current pc-technologies with industry involvement (McDermott / B&W) and will be extended to the new conditions using the data generated in the experimental portion of the program.

To achieve the above project objective, a multi-university / joint industry team has been assembled, consisting of Brown University (P.I.s Robert Hurt and Joseph Calo), Brigham Young University (P.I. Thomas Fletcher), and McDermott's Babcock and Wilcox Power Generation Group (P.I. Alan Sayre). The research work will be divided into the following four tasks, with the leading participants identified:

- Task 1: Char Formation and Inorganic
(Fletcher, BYU)
- Task 2: Combustion Kinetics
(R. Hurt, Brown)
- Task 3: Gasification Kinetics
(Calo, Brown; Fletcher, BYU)
- Task 4: Validation and Extension of CPD and CBK Fuel Submodels
(Sayre, B&W)

The remainder of the report documents the results from this study organized along these task lines. Task 1 is covered in Chapters 1-3, Task 2 in Chapters 4-6; Task 3 in Chapter 7, and Task 4 in Chapter 8. Chapter 9 presents a brief summary statement that highlights the major conclusions and recommendations.

CHAPTER 1 THE EFFECT OF PRESSURE ON COAL PYROLYSIS

1.1 Literature Review

This literature review summarizes previous studies of coal devolatilization and char oxidation with emphasis on issues related to the effects of total gas pressure.

1.1.1 The Effect of Pressure on Coal Devolatilization

Coal pyrolysis at elevated pressure is reviewed here for three categories of reactors: TGA, wire-mesh, and drop-tube reactors.

1.1.1.1 TGA Reactor

The Thermogravimetric Analyzer (TGA) provides the most precise measurements of mass release of reacting material. However, this technique suffers from disadvantages such as low temperatures and low heating rates (<1 K/s). Seebauer and Staudinger (1997) used a TGA to investigate the effects of pressure, particle size, and heating rate on coal pyrolysis. They indicated that the total volatile yield decreased with increasing pressure, with a significant decrease in tar yield and a slight increase in light gas yield with increasing pressure. The TGA experiment alone is insufficient to derive kinetics parameters for pyrolysis reactions due to (a) the low heating rate, and (b) large effects from the bed of particles. Sun et al. (1997) studied the pyrolysis of two Chinese coals (0.4-4 mm) under pressure (1-13 atm) using a pressurized dual-chamber TGA with a heating rate as low as 0.33 K/s. Their results showed that the total volatile yield decreased with increasing pressure, while the total mass release was almost independent of pressure at low temperature (< 873 K). Arendt and van Heek (1981) performed high-pressure pyrolysis for five German coals using a wire mesh reactor and TGA respectively, and found similar trends with respect to pressure.

1.1.1.2 Wire-Mesh Reactor

The electrical grid or wire mesh reactor has been widely applied to coal pyrolysis due to the heating rate of the facility being well controlled. Anthony and Howard (1976) and Suuberg et al. (1978) showed that increasing pressure from 10^{-4} to 69 atm in 1000K/s experiments with 30 s hold reduced total volatile yield by roughly 5 wt% for lignite and

15 wt% for bituminous coal. Arendt and van Heek (1981) found that with increasing pressure, tar repolymerised and cracked more significantly, resulting in increased yields of char and hydrocarbon gases. Hydrogen was found to influence devolatilization significantly at increased pressures. Additional amounts of aromatic products were released by hydrogenation of coal itself, particularly between 773 and 973 K, and the yields of light products such as CH_4 and C_2H_6 increased significantly.

Griffin et al. (1994) studied the effects of pressure (1-10 atm) and temperature (750-1230 K) on pyrolysis of pulverized Pittsburgh No. 8 bituminous coal under a helium atmosphere, using an electrical screen heater reactor at a heating rate 10^3 K/s. They found that volatile yields decreased slightly with increasing pressure, the effect being more pronounced at higher temperature. Below 970 K, pressure had little effect on yields. This is similar to the results obtained by Anthony and Howard (1976) and Bautista et al. (1986), who studied high pressure pyrolysis for four different coals using an electric grid reactor at heating rates from 100-10,000 K/s. They found that the weight loss of Pittsburgh coal decreased rapidly with increasing pressures of helium and hydrogen to an apparent limiting value at 10 atm. The decrease in weight loss with increasing pressure was attributed to diminishing tar yields, only slightly compensated by increasing gas yields. The tar yields were identical in the inert and reducing atmospheres, so consistently higher gaseous yields under hydrogen resulted in the increased mass release. Cai et al. (1996) studied coal pyrolysis with a hydrogen pressure up to 70 atm in a wire-mesh pyrolysis reactor at heating rate 1 to 5000 K/s. They observed an increase of total volatile yield with increasing H_2 pressure, while tar yields decreased and the degree of reduction in tar yields decreased with increasing pressure. Cai's results showed that the influence of pressure on volatiles yields and tar yields became more significant at higher temperatures.

1.1.1.3 Drop-Tube Reactor

Lee et al. (1991) investigated the rapid pyrolysis behavior of a bituminous coal under rapid heating (10^3 - 10^4 K/s) and elevated pressure (up to 3.8 atm) relevant to gasification. They found that increasing pressure slowed the global release of volatiles, lowered the asymptotic volatile yields, and promoted secondary reactions of the volatiles, which

reduced the tar yields and changed the gas yields. Fatemi (1987) investigated the effect of pressure on devolatilization of pulverized coal particles up to a temperature of 1373 K and pressures of 68 atm in an entrained flow reactor. The results showed that tar yield is affected by pressure, decreasing significantly with increasing pressure up to 13.8 atm. Weight loss and gas yield decreased with increasing pressure up to 13.8 atm, but at higher pressures there was no significant effect. Yeasmin et al. (1999) studied the high-pressure devolatilization of brown coal using a pressurized drop tube furnace. The residence time of coal particles in the furnace was calibrated based on the effect of pressure and temperature. Partially devolatilized coal or char particles were collected using a collection tube, which was able to move up and down to control the residence time in the furnace. Weight loss decreased with increasing pyrolysis pressure. In a recent study, Matsuoka et al. (2003) examined three Japanese coals using a drop tube reactor, with temperature ranging from 600 to 700°C. The effect of pressure was significant on CH₄ and C₂-C₆ hydrocarbon fractions. The yields of CH₄ and CO₂ increased with increasing pressure, whereas C₂-C₆ yields monotonically decreased with increasing pressure.

1.1.1.4 Summary

In summary, the effects of pressure on devolatilization behavior vary with coal rank, gas environment and operating conditions. General trends observed from experiments can be summarized as follows:

The total volatile and tar yields decrease with increasing pressure, tar yield being more distinctly dependent on pressure. The reduction in tar and total volatile yields appears to be most significant for bituminous coals, but less pronounced for lignite. The effect of pressure on tar and total volatile yields appears to be more pronounced at higher temperature. The effect of pressure on the tar and total volatile yields appears to be less pronounced at high pressure. With increasing pressure, tar molecular weights are lower.

Although the effect of pressure on coal pyrolysis has been extensively researched, entrained flow high pressure coal pyrolysis research is still needed. TGA pyrolysis tests

are limited by low temperature and low heating rate. Wire-mesh reactors have the drawback of interaction between coal particles and the wire mesh. Many current drop tube reactors can not achieve high temperatures ($>1200^{\circ}\text{C}$) at high pressure, and the particle heating rate typically only reach 10^4 K/s compared to 10^6 K/s in industrial facilities. A high-pressure flat flame burner was therefore developed in this study to overcome these problems.

1.1.2 Effect of Pressure on Resulting Char Physical Properties

Coal devolatilization affects the combustion performance of pulverized fuel boilers in many different ways. The primary influences of coal devolatilization on char combustion are (a) the amount of mass released as volatile matter, and (b) the heating value of pyrolysis product, which have been discussed in section 1.1.1. An equally important aspect is mass remaining in the char. The physical structure of char subsequent to devolatilization (i.e. diameter, internal surface area, pore size, and porosity) determines the rate of char oxidation. This section focuses on the effects of coal devolatilization at elevated pressure on the physical structure of the char products. Coal swelling, morphology, surface area, and pore size will be discussed.

1.1.2.1 Coal swelling ratio during devolatilization

The swelling ratio may be the most distinct phenomenon of coal physical structure transformation during devolatilization, which can affect char particle size, pore size, porosity, density, and reactivity. The swelling ratio can be affected by coal properties such as particle size, coal rank, maximum temperature, heating rate, and oxygen content. This issue becomes more complicated when considering the diversity of the behavior of individual particles during heating due to the variation of the coal maceral constituents among the particles within the same coal sample (Benfell et al., 2000). Instead of a comprehensive review of coal swelling research, this section only focuses on pulverized coal swelling at elevated pressure.

Direct observations (Essenhigh and Yorke, 1965; Gao et al., 1997; Strezov et al., 2003) of coal swelling at low heating rates were relatively easy compared to harsh industrial flame conditions. It was observed that coal particles undergo significant changes of

swelling and shrinking, followed by a rapid contraction repeating until resolidification occurred. Fletcher (1993), Gale et al. (1995), and Zygourakis (1993) observed the transient swelling of fuel particles in situ at high heating rates during pyrolysis at 1 atm. The general trend of coal particle swelling ratio with heating rate is shown in Figure 1.1. Coal particle swelling ratio increases with increasing heating rate to $10^3 \sim 10^4$ K/s, and then decreases at higher heating rate.

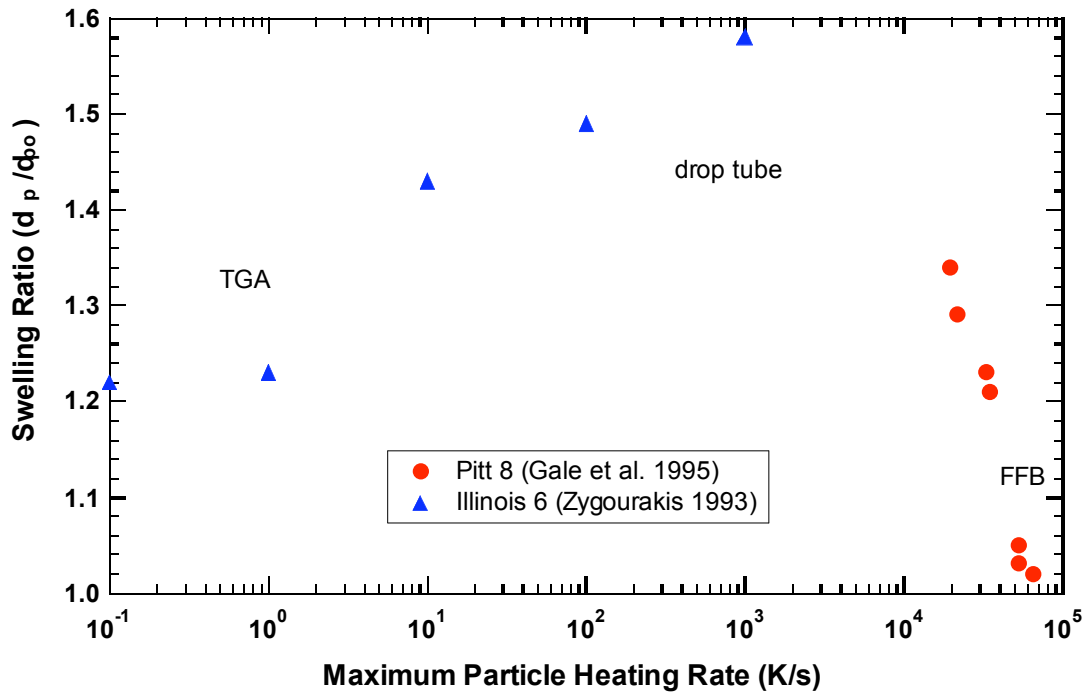


Figure 1.1. Swelling vs. heating rate at 1 atm (Gale et al., 1995).

Lee et al. (1991) studied the effect of pressure on the swelling behavior of Illinois #6 coal pyrolyzed at 1189 K in an inert Nitrogen atmosphere. At 1 atm, coal particle swelling was not significant. At 8 atm, swelling based on diameter increased about three times at 0.3 s and thirty times at 0.8 s, suggesting swelling may occur during later stage of pyrolysis. However, at 22 atm, the extent of swelling dropped significantly, and swelling occurred in the early stage of pyrolysis, where significant mass release occurred. Wu et al. (2000) studied an Australian bituminous coal using a pressurized drop tube furnace. The char characteristics were found to be influenced significantly by the system pressure.

Results obtained indicated that the coal and char fragmentation might have occurred during devolatilization at high pressure. The char size (as characterized by the swelling ratio) was also observed to increase with system pressure. The measured swelling ratios of the char sample fall well below the data by Lee et al. (1991) at all system pressures. This may be caused by differing furnace temperatures or heating rates, which are compared in Table 1.1. Yu et al. (2003) studied the effect of initial coal density fractions on their swelling ratio. The mass release, swelling ratio, and the porosity decrease with increasing parent coal density. Results of size fraction samples suggest that a larger swelling occurs in DTF (drop-tube furnace) when the particle size decreases.

Table 1.1 Comparison of Experimental Conditions for 2 Pressurized Drop Tube Experiments

	Lee et al.(1991)	Wu et al. (2000)
Coal	Illinois No.6	Australian Bituminous coal
Particle size	62 μ m mean particle diameter	63-90 μ m
Apparatus	HEF (high-pressure entrained-flow furnace)	PDTF (pressurized drop-tube furnace)
Heating rate	$\sim 10^4$ K/s	$\sim 10^4$ - 10^5 K/s
Temperature	1189 K	1573 K
Pressure	0.1-3.8 MPa	0.1-1.5 MPa
Atmosphere	N ₂	N ₂ with small amounts of O ₂

A number of attempts have been made to model the coal swelling (Oh et al., 1989; Sheng and Azevedo, ; Solomon and Hamblen, 1985; Yu et al., 2002). It is commonly agreed that metaplast fluidity and bubbles formed during coal devolatilization play an important role on determining coal swelling ratio and char structure. The fluidity of the metaplast of the softening coal can be improved by increased pressure, due to the retention of volatiles which act as a plasticizing agent (Khan and Jenkins, 1984). The increased fluidity facilitates bubble transport to the particle surface. Elevated pressure also increases the resistance to expansion of the plastic coal melt (Lee et al., 1991). The maximum swelling ratio occurs at the point that initial pressure build-up inside coal melt achieves a balance with bulk pressure. When the bulk pressure is higher than the inflection point, bubble




contraction can be observed. Bubble growth and coalescence can also be used to explain char physical structure change with density (Yu et al., 2002).

1.1.2.2 Coal morphology and surface area during devolatilization

Char morphology has been extensively studied during past decade (Alvarez et al., 1997; Cloke et al., 1997; Lester and Cloke, 1999; Lester et al., 1996). Recently, Wu et al. (2000) and Benfell et al. (2000) studied the effect of pressure on char morphology. By analyzing char SEM (Scanning Electron Microscopy), chars were categorized based on criteria shown in Table 1.2.

Typically, Group I particles have a very porous structure, with large voids inside the particle and a thin wall, Group II particles have a medium porosity and wall thickness, while Group III char particles have low porosity. This classification is the first such attempt. Effects of coal rank and density on coal morphology were also studied by Bailey et al. (1990) and Benfell et al. (2000). Essentially, coal rank and density are indexes of coal petrography. The morphology of the chars shows a strong relationship with increasing vitrinite content (Benfell et al., 2000).

Table 1.2 Char Classification System (Benfell et al., 2000; Wu et al., 2000)

Char groups	Group I	Group II	Group III
Two-dimensional schematic representation			
Porosity (%)	>70	Variable, 40–70	<50
Average wall thickness (mm)	<5	>5	>5
Shape	Spherical subspherical	Subspherical	Angular
Typical swelling ratio	>1.3	<1.0	<0.9
Typical residual mass ratio	0.1–0.5	0.1–0.5	1.0

Pressure has a strong influence on coal morphology. When furnace pressure increases, the overall proportion of Group I chars formed increases, while the proportions of Groups II and III chars decrease. Mean diameter and sphericity of coal A increased with pressure.

Mean diameter and porosity of coal CV increased at pressure between 5 and 10 atm, then decrease from 10 to 15 atm, probably due to char fragmentation. Microscopic observation of this char showed that the group I particles had thinner walls and a more spherical structure than those of lower pressure chars, factors which made this sample more susceptible to fragmentation within the furnace and during handling (Benfell et al., 2000). Compared to the low-pressure char, the average macro-porosity of high-pressure chars was higher, and they had larger number of bubbles with smaller sizes (Yu et al., 2003).

The internal surface area of char is one of the significant parameters used for char combustion and gasification modeling. Only two data sets have been presented for the surface area of chars produced under high-pressure conditions. Lee et al. (1991) investigated the development of CO₂ surface area of char as a function of mass release and pressure for Illinois No. 6 bituminous coal under a low heating rate condition (Table 1.1). The surface area of char is generally lower under higher pressure pyrolysis conditions. The development of surface area is relevant to the thermal-plastic property of coal during heating. A recent study presented the CO₂ surface area for chars produced from Australian bituminous coals in a pressurized drop tube furnace at various pressures (Benfell et al., 2000). Generally, the surface areas of chars decreased as pressure is increased. The effect of pressure on char surface area is believed to be related to the fluid behavior during devolatilization (Lee et al., 1991).

1.2 Objectives

The objective of this part of the project is to study the effects of pressure on coal pyrolysis at high heating rate, typical of practical pulverized coal combustion. High-temperature, high-pressure pyrolysis experiments were conducted on four bituminous coals. The resulting chars were collected and analyzed to find the effect of pressure on the coal pyrolysis process and the char structure properties. This chapter focuses on the following aspects: mass release during pyrolysis processes, char elemental composition, char swelling ratio, char physical structure, and char surface area.

1.3 High-Pressure Facility at BYU

The conditions required for high temperature, high pressure coal pyrolysis and oxidation experiments place strict demands on the test facility, especially when simulating industrial-scale pulverized coal combustion conditions. Basically, the following conditions need to be met for a realistic experiment:

1. High particle heating rates ($10^4\sim 10^6$ K/s);
2. High gas temperature for coal pyrolysis and high particle temperature (1700~2200 K) for char combustion;
3. Stable temperature zone for coal particles to react during the oxidation process;
4. Reaction residence times and gas compositions for particle oxidation must be stable and adjustable;
5. Single particle reaction behavior.

The difficulties associated with implementing these requirements are reasons that there is a lack of reliable high temperature, high pressure coal combustion data.

1.3.1 Review of Char Oxidation Facilities

Coal pyrolysis and char oxidation experiments have been conducted for over several decades, and have mainly been studied in heated grids and thermogravimetric analyzers (TGAs). Some coal pyrolysis and char combustion experiments are also performed with flat flame burners, or shock tubes. The previous section evaluated the advantages and disadvantages of drop-tube furnaces, heated grids, and TGAs. Flat flame burners (FFBs) were used widely in atmosphere coal combustion studies (Fletcher, 1993; Mitchell, 2003), since they can closely approximate pulverized fuel combustor conditions, have high heating rates and high gas temperatures, and are easy to start up. On the other hand, flat flame burners use methane or carbon monoxide as fuel, limiting the gas compositions of combustion products (e.g., there are significant concentrations of steam for methane flame). Isothermal temperature profiles in FFBs are also difficult to maintain.

Shock tubes can be operated at elevated pressure without being too expensive, but several drawbacks limit their usefulness: (1) The short reaction time (several milliseconds) result in very unsteady particle temperature histories (Lester et al., 1981); (2) particles cannot be sampled in various stages of burnout; (3) the range of gas concentrations is limited; and (4) particle dispersion and agglomeration have proven to be problematic (Essenhigh, 1981).

Although one apparatus may be better than others in one or several aspects, certain prerequisites need to be satisfied to achieve a reasonable simulation of pulverized coal combustion. For the elevated pressure coal combustion study, basic prerequisites are (Niksa et al., 2003):

1. Pressure: a uniform pressure should be maintained through reaction process.
2. Thermal history: Sufficient information must be available to assign the temperature of the samples as a function of time throughout an entire process. High heating rate ($>10^5$ K/s) is needed at coal/char initial heating stage, and high gas temperature (>1400 K) is needed for char combustion experiments.
3. O₂ partial pressure: Uniform O₂ levels in the free stream throughout a combustion history can only be imposed with very dilute coal suspensions. O₂ partial pressure can be controlled.

These prerequisites may be closely approximated by a drop-tube furnace. A drop-tube furnace consists of a long, vertical reaction tube through which passes a laminar flow of gas. Two gas flows are introduced at the reactor entrance. The primary flow is introduced at the center of the reaction tube through an injection probe. The secondary flow, preheated to a certain temperature, enters the reaction zone through the annulus between the reaction tube and the injection tube. Carried by the primary flow, the small stream of particles enters the reaction zone, and flow along the reaction tube axis, reacting with the surrounding gases. These reactions are quenched as the particles enter the cooled collection probe, located at the reactor exit. The injection tube or the collection probe is moveable to allow various particle residence time. Electric wall heaters are normally used

to provide heat to the reaction tube, and the preheating is achieved by plasma, a combusting flame, or electric heaters.

Drop-tube furnaces have been widely used in high-pressure coal pyrolysis and char combustion studies (Lee et al., 1991; Monson, 1992; Reichelt et al., 1998; Wu et al., 2000). There are several drawbacks related to drop-tube furnaces. The heating rate of particle in drop tube furnace can only be as high as 10^4 K/s, caused by the slow heat transfer rate from the secondary flow to coal particle. It has also been observed that insulating characteristics of the refractory degraded sharply with increasing pressure (Monson, 1992), which make it very difficult to achieve a high temperatures. One possible solution to this dilemma is to introduce a flat flame burner in drop tube furnace. This attempt was implemented in the current project and will be described in the following sections.

1.3.3 BYU HPDT Reactor

A high pressure drop tube (HPDT) reactor was previously designed and constructed for use in both devolatilization and char oxidation tests (Monson, 1992). This drop tube reactor was later upgraded by changing from molybdenum disilicide heating elements to an Iron-Chrome-Aluminum ceramic-coated high temperature heater, which had greater longevity than the original heating elements (Hambly, 1998).

Figures 1.2 and 1.3 show schematics of the high pressure drop tube reactor. The drop tube reactor (Figure 1.2) is an electrically-heated laminar flow drop tube which was operated at pressures as high as 15 atmospheres (Monson, 1992). Maximum particle heating rates were about 10^4 K/s. Separate cylindrical electrical resistance heaters were used in the preheater and drop tube sections, each with separate set points and control thermocouples. Each control thermocouple was kept at a constant operating temperature by a PID controller. The pre-heater section heated the (secondary) nitrogen stream to about 625 K before it entered the drop tube. A water-cooled injection probe entrained the coal particles in a small (primary) nitrogen flow and prevented the particles from being heated until they left the probe. The residence time was changed by either raising or

lowering the injection probe, or by changing the gas flow rate. The particles were injected at a slow rate ($\sim 1\text{g/hr}$) in order to approximate single particle behavior. The secondary (pre-heated) and primary (injection probe) nitrogen flows were set so as to attempt to match their radially-averaged gas velocities (about 0.7-0.85

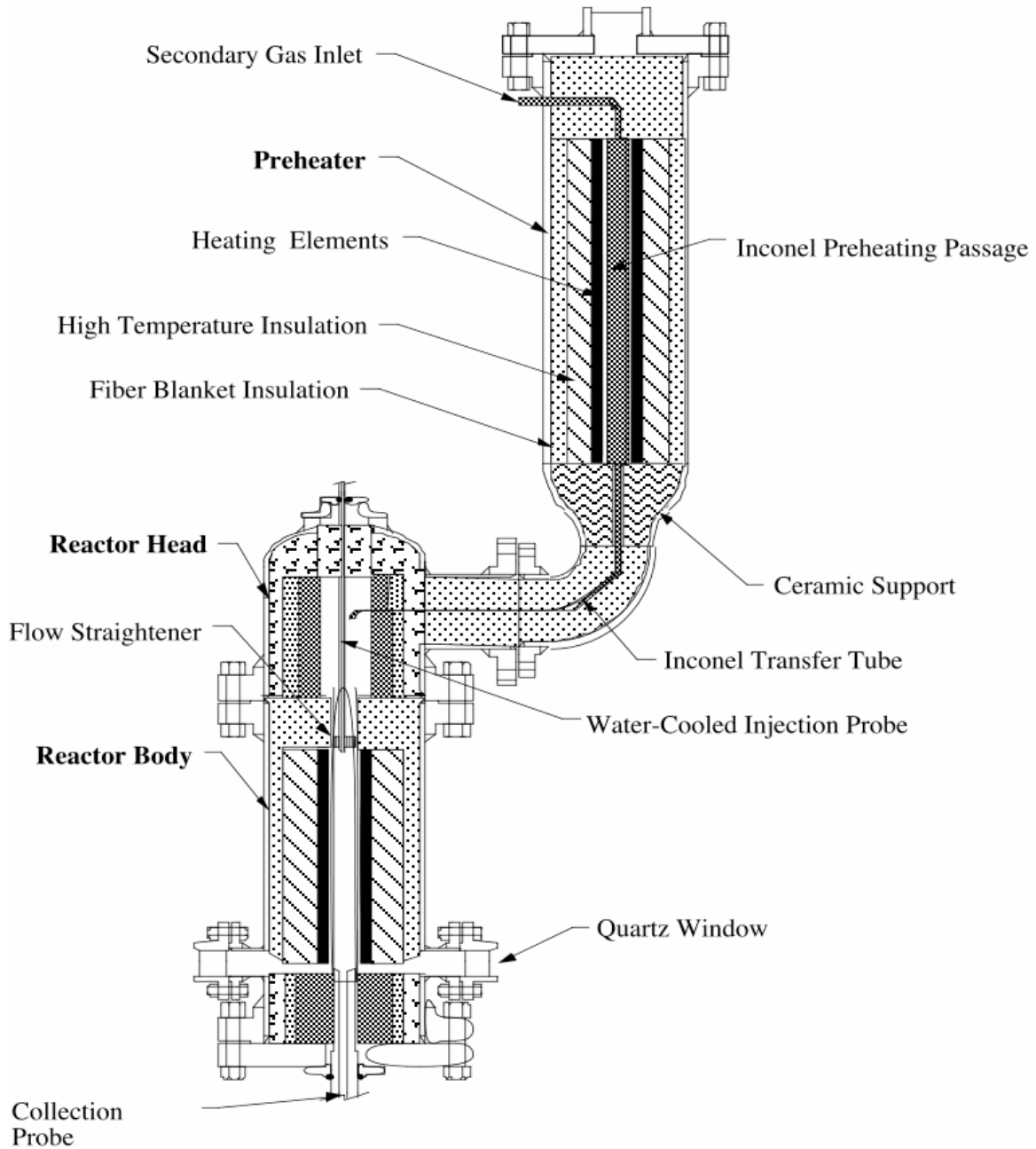


Figure 1.2. Schematic of High Pressure Drop Tube Reactor (Hambly, 1998).

m/s). In this way it was hoped to minimize turbulence at the point of injection so that the particles would flow down the center axis of the drop tube with minimal dispersion. The direct observation of particle flow near the reaction tube exit showed that particles flowed along the centerline.

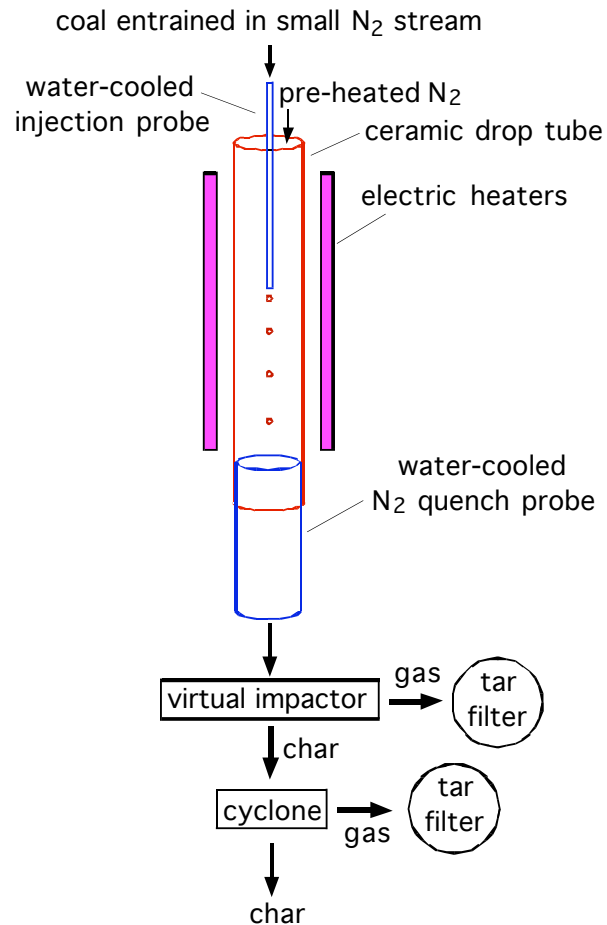


Figure 1.3. Schematic of drop tube reactor sample collection configuration(Perry, 1999).

Gas temperatures along this center axis were carefully measured with the injection and collection systems in place (except for the cyclone) using a type S thermocouple inserted from beneath the virtual impactor. Measured gas temperatures were corrected for radiative losses from the thermocouple bead. Pyrolysis products in the drop tube were immediately quenched by dilution with cool (300 K) nitrogen gas upon entering a water-cooled collection probe. Char was separated from most of the tar by a virtual impactor followed by a one-inch cyclone (Perry, 1999).

The HPDT could not achieve high temperatures at elevated pressures. Figure 1.4 shows the centerline temperature profiles of HPDT at different total pressure and a fixed gas flow rate. By adjusting the set point of the heaters, the temperature profiles were maintained at 1200 K. At 15 atm total pressure, the set point of preheater had to be lowered down to 580°C to avoid failure of the controller unit. Most hear loss was observed at elevated pressure, since denser gas promoted heat loss through the insulation on the reactor wall.

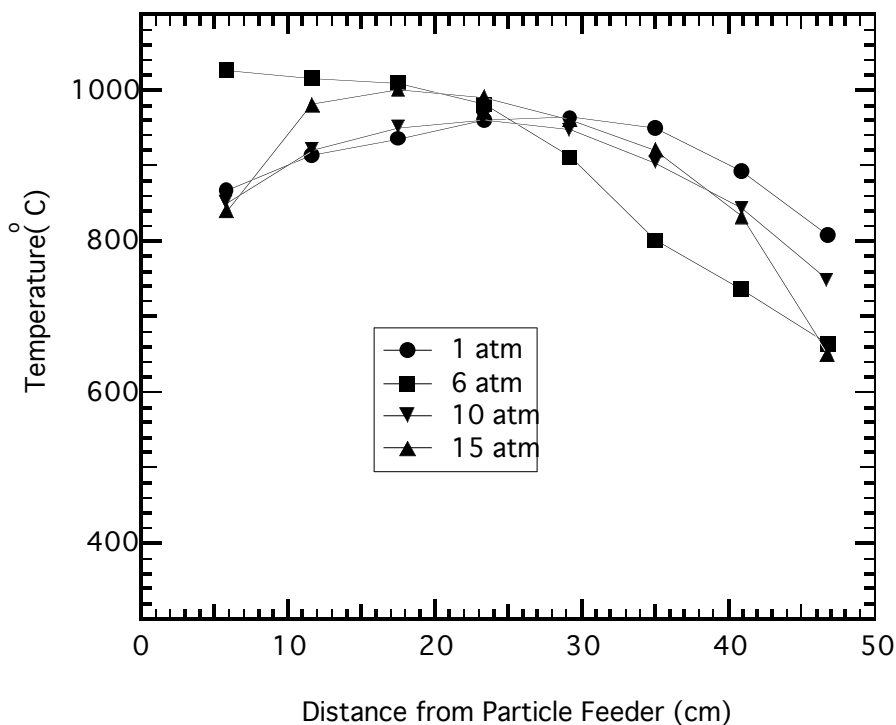


Figure 1.4. Measured gas temperature profiles in the HPDT.

A series of devolatilization tests of Pitt #8 coal were conducted on HPDT at 1, 6, and 11 atm total pressures. The hydrogen contents of the chars collected were around 2 wt%, which is much higher than the hydrogen content (0.5%) of char normally collected from an atmospheric flat flame burner. Since it was not possible to obtain fully pyrolyzed chars in the HPDT at elevated pressures, due to heat loss limitations, it was necessary to develop another system.

1.3.3 High Pressure Flat-Flame Burner (HPFFB) Reaction System

The high-pressure flat flame burner developed in this project was designed based on an atmospheric pressure FFB used by Ma (1996). The atmosphere FFB was also used for some comparison tests in this project. A schematic of the HPFFB is shown in the Figure 1.5.

The high-pressure flat flame burner uses the hot products of methane combustion to heat the particles. As shown in Figure 1.5, methane flows through hypodermic tubes and combusts with oxidizer, which is either air or a mixture of air/O₂. The “flat-flame” therefore consists of an array of small diffusion flamelet located about 1 mm from the burner surface. The combustion in these flamelets in completed quickly (flame thicknesses at 0.5 to 1 mm), providing an uniform post-flame environment. Post-flame gas temperature and composition can be adjusted by changing the equivalence ratio or oxidizer composition. Residence time can be changed by raising or lowering the burner relative to the collection probe. Coal particles were injected along the center axis of a 2 inch diameter quartz tube. In order to approximate single particle behavior (i.e. no particle-particle interactions), the coal particles were fed at a rate of less than 1 g/hr by entrainment in a small stream of nitrogen. Maximum particle heating rates in the flat flame reactor were about 10⁵ K/s.

Figure 1.6 is a flow diagram of the HPFFB facility. High pressure nitrogen, air, oxygen, and methane were provided by a reservoir of high pressure gas bottles, with pressure regulators set to 400 psig. Four Porter flow controllers were used to control the flow rates of primary gas (N₂), methane, air, and oxygen. Nitrogen flow used to pressurize the system was monitored by a flow meter, and the flow rate was manually adjusted. Nitrogen quench flow was also controlled in the same manner. Air and oxygen were premixed during char oxidation experiments to increase oxygen concentration. The O₂ concentration in the reactor exit stream was monitored with an O₂ sensor before each coal experiment. An Omega PID controller read the reactor pressure from a pressure transducer, and then controlled the system pressure by adjusting orifice size of a valve located in the reactor exhaust line (after the particle collection system). An electronic

heater was used to decrease the heat loss from the reactor walls at elevated pressure. Platinum-rhodium thermocouples were installed along the length of reaction tube to monitor gas temperature, and a PID controller was used to control the temperature of the heater.

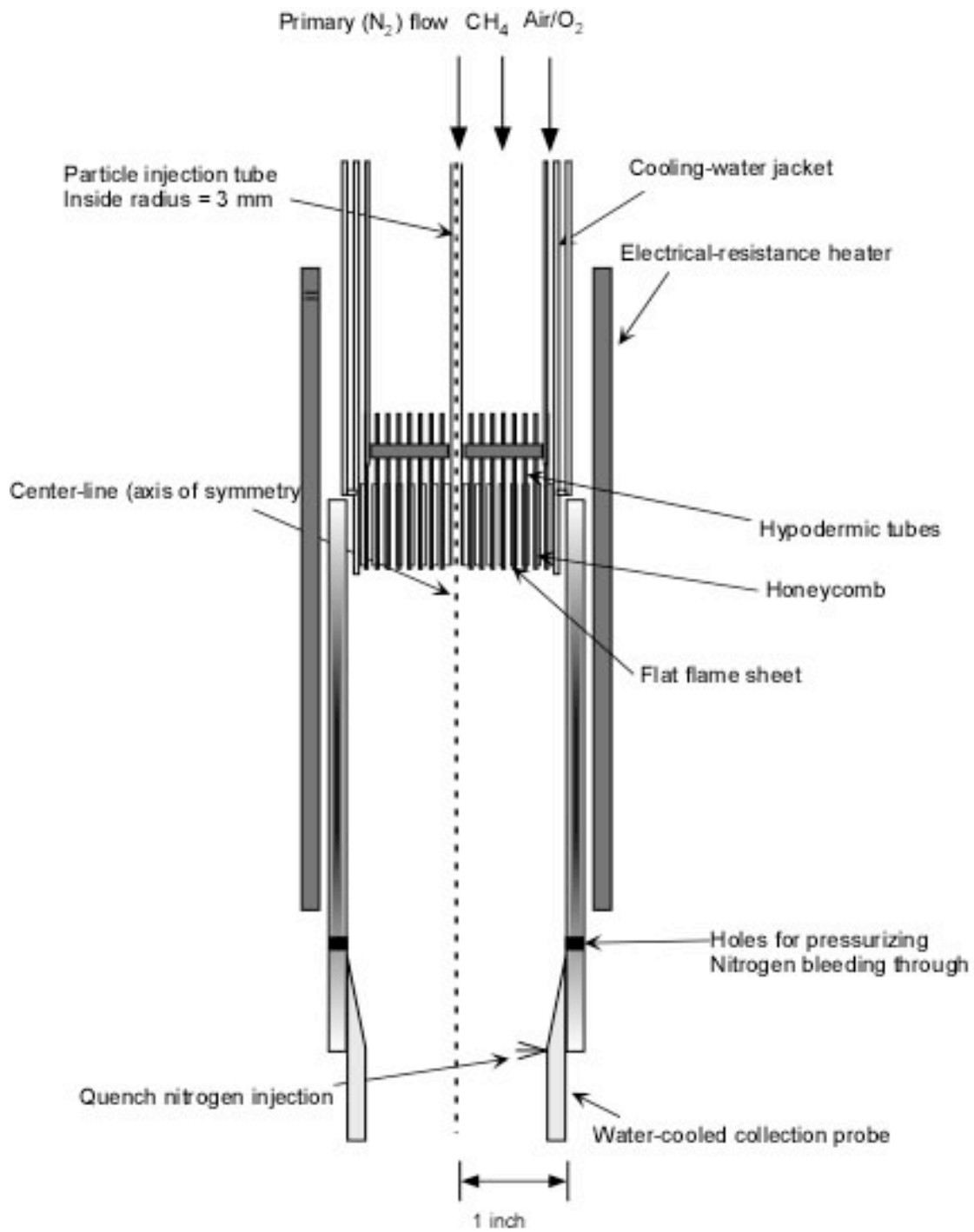


Figure 1.5. Schematic of the HPFFB.

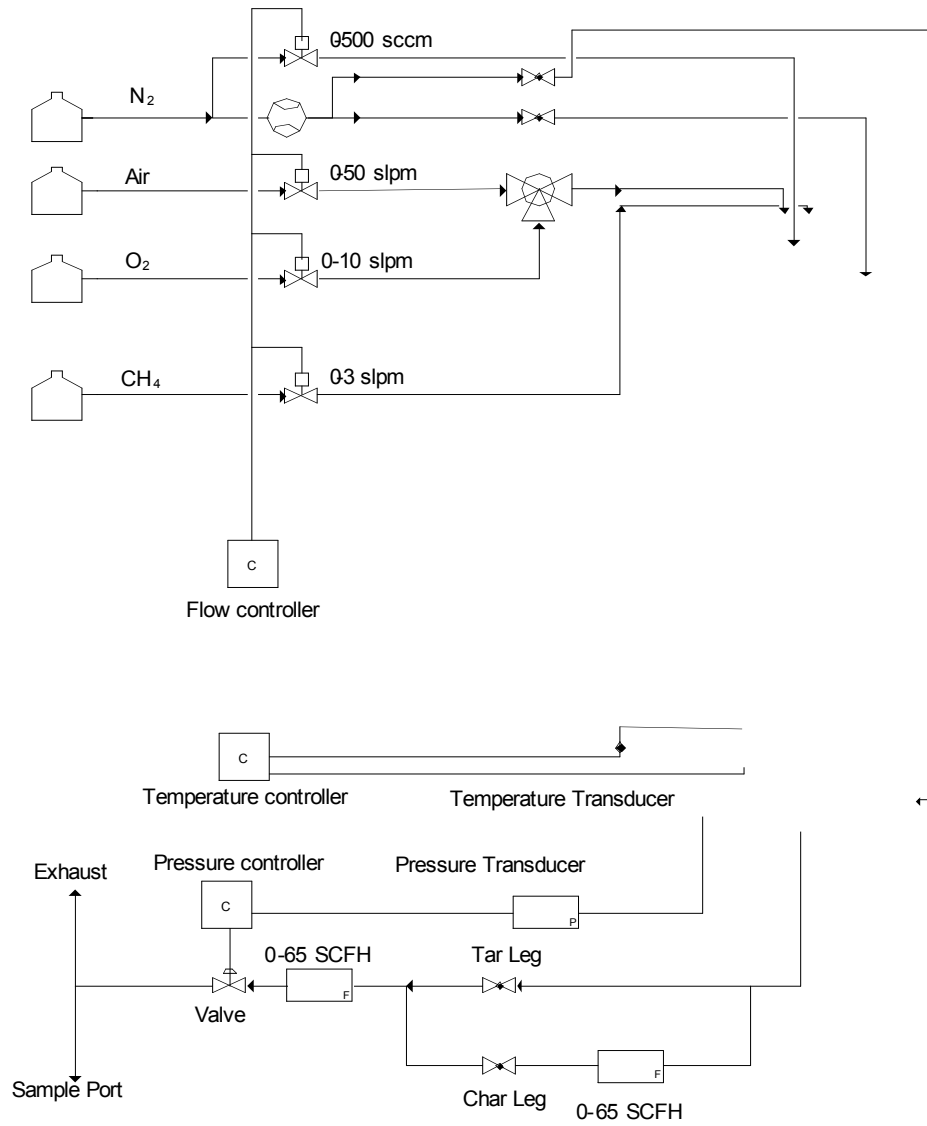


Figure 1.6 Schematic of the High Pressure Flat Flame Burner flow system.

1.4 Coal Pyrolysis and Resulting Char Properties

1.4.1 Coal Characterization

The main body of pyrolysis experiments was conducted on the four coals listed in Table 1.3, ranging from lignite to high-volatile bituminous coal. The size of coal particles used ranged from 45 to 130 μm . Typical particles used in pulverized coal furnace applications have a mean diameter of $\sim 50 \mu\text{m}$. Oxygen content was determined by difference.

Because the sulfur values as determined by the elemental analyzer include both organic and inorganic sulfur, the oxygen values are somewhat underestimated.

Table 1.3 Characteristic of Coals

Coal	Rank	d (μm)	Proximate Analysis (Wt %)			Ultimate Analysis (wt%, daf)				
			Moisture	Ash (dry)	VM (daf)	C	H	N	S	O ^a
Pitt #8	HvA-Bit	63-90	1.44	10.7	34.34	84.58	5.47	2.00	0.49	7.44
Ken #9	HvB-Bit	44-74	8.21	8.43	42.11	76.72	5.27	1.81	3.72	12.4
Ill #6	HvC-Bit	74-90	3.31	9.35	53.83	78.02	5.45	1.36	4.14	10.5
Knife River	Lignite	45-75	11.91	20.3	47.86	62.23	4.23	0.95	1.28	31.3

a. $O = 100 - (C + H + N + S)$

1.4.2 Reaction Conditions for the Pyrolysis Experiments

All of the elevated pressure chars preparation experiments were conducted using the methane-air high-pressure flat flame burner (HPFFB). Maximum gas temperatures were 1300°C at pressures of 2.5 to 15 atm, with particle heating rates of 10^5 K/s . Atmospheric pressure (0.85 atm) char preparation was conducted using an atmosphere flat flame burner.

In ideal experiments, the pressure could be changed without changing temperature history, residence time, or heating rate. However, this is not possible in an entrained flow

experiment. At high pressure, gas velocity decreases when mass flow rate is held consistent. Gas velocity can be adjusted by increasing the total mass flow rate of entrainment gas, but this changes the heating characteristics (i.e., gas temperature) in the reactor. Residence time is adjusted by changing the reaction length, which was changed by moving the burner up and down. However, excessive heat was lost to the water-cooled burner when the burner was lowered significantly into the furnace.

The high-temperature coal pyrolysis process is usually completed in less than 50 ms, after which little reaction occurs. In this study, all pyrolysis experiments had a residence time longer than 120 ms, and hence collected samples were fully pyrolyzed. The initial plan was to conduct all of the pyrolysis experiments under fuel-rich post-flame conditions, since this worked well in atmospheric FFB experiments. However, the fuel-rich CH₄ flame produced soot at elevated pressures, which contaminated the char samples and affected the experimental results. To avoid this, all of the pyrolysis experiments were conducted in a slightly oxidizing condition (0.2~0.4 mol% O₂) in the post-flame. Such a low concentration of O₂ had a negligible effect on resulting char properties. An O₂ analyzer was used to monitor the composition of the gases exiting the reactor.

The desired flow rates of the combustion gases were determined (a) by computing the adiabatic flame temperatures, and (b) by comparing the measured temperature profiles and O₂ concentrations at different pressures. Table 1.4 lists the flow rates of CH₄ and Air at different pressures.

Table 1.4 Flow Rates Used in the HPFFB

Condition	2.5 atm	6 atm	10 atm	15 atm
CH ₄ (slpm)	1.74	2.16	2.49	2.85
Air (slpm)	17.5	21.5	25	28.5
O ₂ in product (mol%)	0.41	0.32	0.2	0.17
Total flow rate (g/min)	24.295	30.096	34.511	41.732

The centerline gas temperature profile was measured using a type S platinum/rhodium thermocouple inserted from bottom of reactor. The thermocouple bead diameter was 200 μ m. Figure 1.7 shows the measured gas temperature profiles for the four conditions listed in the Table 1.4. Thermocouple readings were corrected for radiation losses. Temperature decreased dramatically at longer distances from the burner as pressure increased. This was caused by larger heat loss at high pressure.

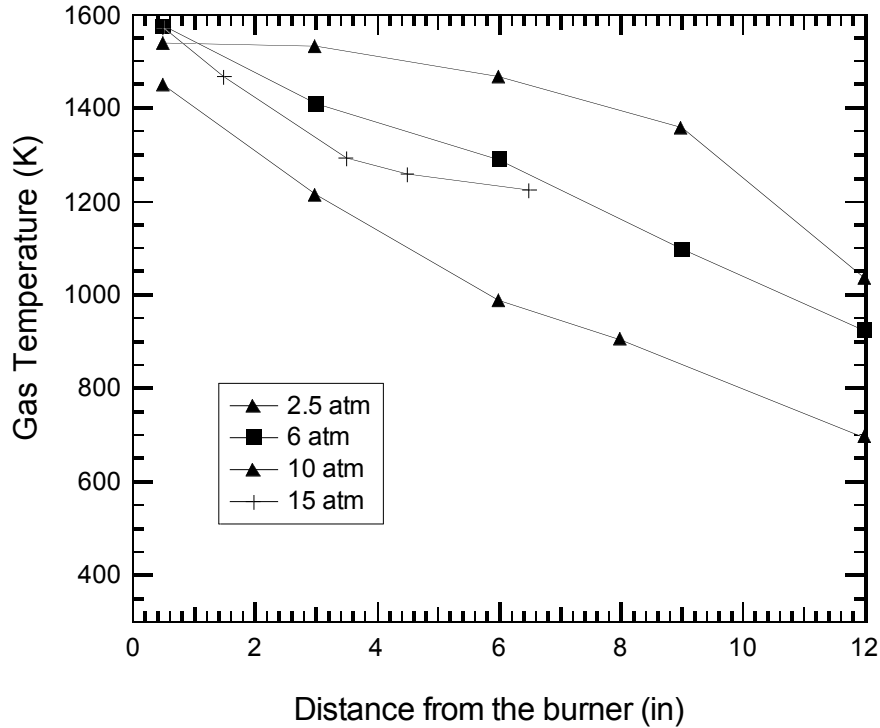


Figure 1.7. Measured gas temperature profile in the HPFFB.

The particle velocity was modeled using Fluent, and the particle velocity profile and gas temperature profile were modeled using the CPDCP code (Fletcher et al., 1990). The effect of primary gas was considered with Fluent modeling. The particle energy conservation equation used in the CPDCP code is:

$$\dot{m}_p c_p \frac{dT}{dz} = h A_p (T_g - T_p) \frac{B}{e^B - 1} - \dot{m}_p A_p (T_p^4 - T_w^4) - \dot{m}_p \frac{dm}{dz} \dot{A}H \quad (1.1)$$

where $h = Nu k_g / d_p$. In this equation, particle properties are known, and velocity (v_p) was obtained from Fluent modeling results. Gas properties changed with CH_4 /air flow rates,

temperature, and pressure, and were modeled using a chemical equilibrium code. Particle temperature histories calculated at early residence times, characteristic of pyrolysis times, are shown in Figure 1.8 for each pressure. Each condition had a maximum particle heating rate of 10^5 K/s.

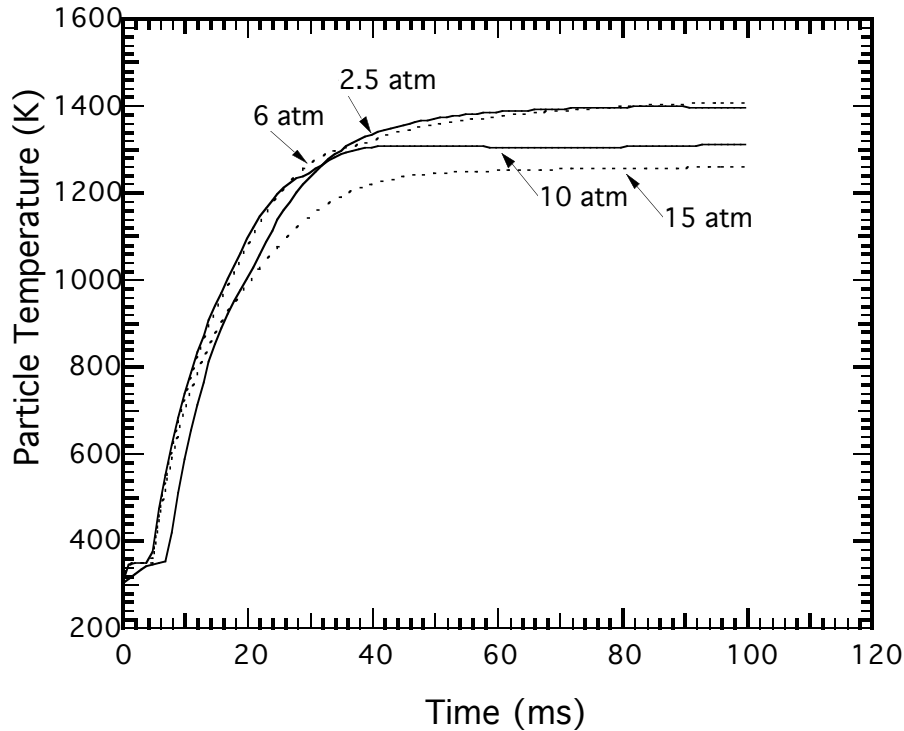


Figure 1.8. Calculated early particle temperature histories for the different pressure conditions in the HPFFB. These particular calculations were for the Ill #6 coal.

1.4.3 Mass Release during Coal Pyrolysis Process

The HPFFB coal pyrolysis data were obtained in the 1573 K gas temperature condition at residence times ranging from 231 ms to 2 sec and pressures ranging from 2.5 atm to 15 atm. The atmospheric pressure data (actually 0.85 atm in Utah) were obtained at 1300 K in a separate atmospheric flat-flame burner facility (Zhang and Fletcher, 2001) where the char samples were collected immediately above the luminous devolatilization zone. The total volatiles yield data for the four coals are shown in Figure 1.9 as a function of pressure. The measured volatiles yields exceeded the ASTM total volatiles yields (see Table 1.3) for all coals at low to moderate pressures (< 7 atm); this is apparently caused

by the high pyrolysis temperature, the high heating rate, and the single particle behavior in the HPFFB experiment. The measured volatiles yields of all four coals decreased with increasing pressure. The effect of coal rank on coal mass release is not very clear in this figure, due to the changes in particle temperature profiles and residence times for the different conditions.

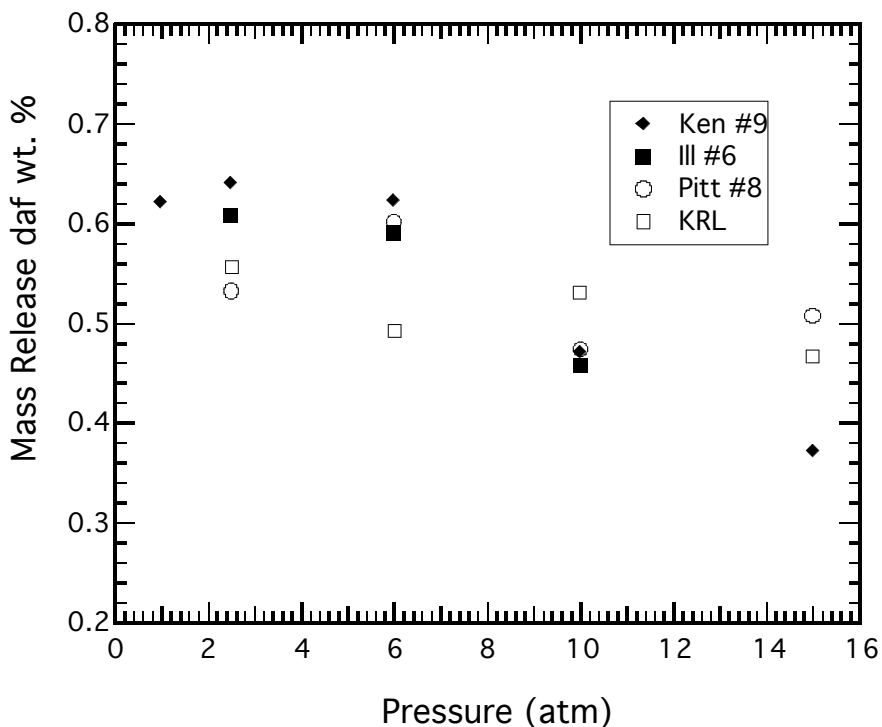


Figure 1.9. Measured mass release due to pyrolysis for chars, obtained at different pressures.

The decreased volatiles yield at increased pressure during devolatilization is commonly thought to be caused by two physical processes: vapor-liquid equilibrium effects and transport effects (Fletcher et al., 1990). Bituminous coal tars exhibit a broad molecular weight distribution. As total pressure is increased, tar precursors with high molecular weights no longer have sufficient vapor pressure to evaporate, and are retained in the condensed phase (Solomon and Fletcher, 1994). Elevated pressure also increases the resistance of volatiles leaving the coal particle, possibly decreasing the total volatiles yield (Lee et al., 1991).

The Chemical Percolation Devolatilization (CPD) model (Fletcher et al., 1990; Fletcher, 1989; Grant et al., 1989) was developed to predict devolatilization behavior of rapidly heated coal based on the chemical structure of the parent coal. In this study, coal-dependent input parameters for the CPD model were calculated using proximate and ultimate analysis data using a correlation of previous ^{13}C NMR analyses (Genetti et al., 1999). These input parameters are listed in Table 1.5. Model constants were not tuned to match the volatiles yield data.

Table 1.5 Coal Structure Parameters Used in CPD Modeling

Coal	M_{\square}	MW_{cl}	p_0	$\square+1$	c_0
Pitt #8	29.1	344.4	0.5	4.8	0.0
Ken #9	39.2	386.7	0.5	5.2	0.0
Ill #6	40.5	381.4	0.5	5.2	0.0
Knife River	53.3	337.3	0.7	3.7	0.2

In the CPD model, a vapor-liquid equilibrium submodel, based on the molecular weight of tar precursors, accounts for the change in tar yield observed as the total pressure is changed. The CPD model was used to predict the coal mass release using the measured gas temperature profile, the gas velocities predicted using FLUENT software, and the aforementioned particle energy balance (Eq. 1.1). CPD model predictions are shown in Figure 1.10, including predicted tar yields. Each pressure condition was modeled using the appropriate particle temperature history, although lines are drawn through the modeling results for convenience. Modeling results are generally comparable to the experiments for pressures up to 6 atm, and slightly underestimates the measured amount of mass release in this experiment.

1.4.4 Elemental Composition of Chars Prepared at Different Pressures

The elemental compositions of coal chars collected at different pressures are shown in Figure 1.11. For the Kentucky #9 coal, the decrease in H/C ratio between 0.85 and 2.5 atm was due to the difference in temperature between the two experiments (1300 K at 0.85 atm vs. 1573 K at elevated pressures). At higher pressures, the H/C and O/C ratios

increased because less tar escaped from the char due to vapor pressure effects at elevated pressures. Although a decrease in mass release was observed when pressure was increased from 10 atm to 15 atm, both H/C and O/C ratios remained relatively stable when pressure was higher than 6 atm. For the Illinois #6 coal, both H/C and O/C ratios were relatively stable, though the measured mass release decreased slightly with increasing pressure.

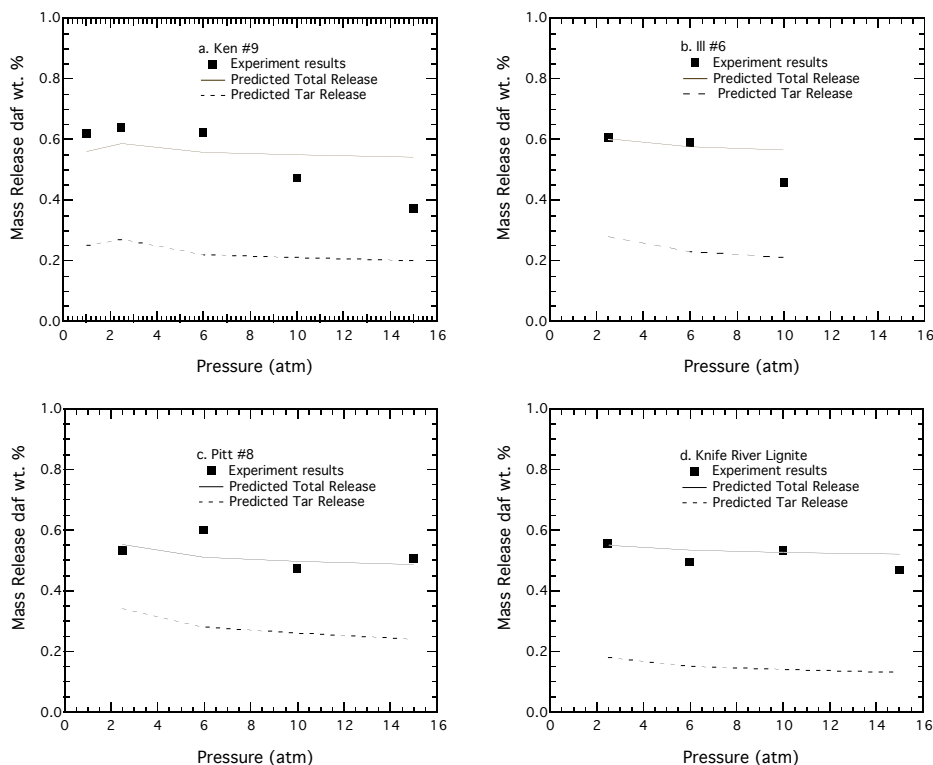


Figure 1.10. Predicted and measured mass release as a function of pressure. The solid lines represent predicted volatiles yields using the CPD model, while the dashed lines represent predicted tar yields. (a) Ken #9, (b) Ill #6, (c) Pitt #8, (d) Knife River Lignite.

The stable H/C ratio in the chars at elevated pressure can be explained based on several competing phenomena. First, at increased pressure, the tar yield decreases due to vapor pressure effects in the high molecular weight tar precursors. Thus, the heavier tars are only vaporized at lower pressures. Second, the heavier tars are enriched in carbon and depleted in hydrogen, due to their higher carbon aromaticity than the lighter tars. The tar

that vaporizes at elevated pressure is therefore enriched in hydrogen (Solomon and Fletcher, 1994) beyond the tar evolved at low pressure, but less tar yield is observed at the higher pressure. The tar molecules that would have vaporized at lower pressures, but that stay in the char at elevated pressure, are slightly higher in hydrogen content than the char. These heavier tar precursors that remain in the coal particle serve as light gas precursors, and the evolution of light gas from the char removes hydrogen-rich side chains. Thus, the light gas yield increases as pressure increases, and the light gases are enriched in hydrogen compared to the char. The net effect is that the char H/C ratio remains relatively constant at the elevated pressures.

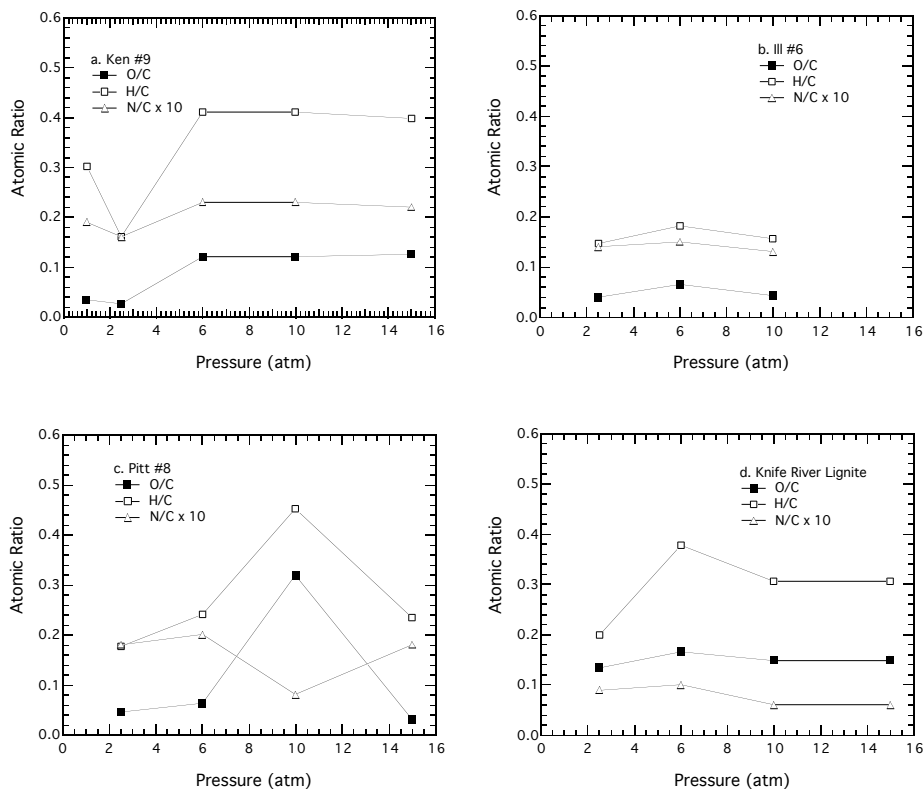


Figure 1.11. Elemental compositions of chars as a function of pressure. (a) Ken #9, (b) Ill #6, (c) Pitt #8, (d) Knife River Lignite.

Another factor influencing the char H/C ratios in these experiments may be the effect of residence time. The particle residence time in these experiments ranged from 0.3 s to 2.0 s when pressure was increased from 2.5 atm to 15 atm. The total mass flow rate of gas into the reactor increased only slightly with pressure in order to keep the gas temperature

at 1300°C, so as pressure increased, and hence gas density increased, the velocity had to decrease. The ultimate hydrogen content of char can be affected by both the temperature and the reaction time (Genetti et al., 1999). This residence time effect may also offset the higher H/C ratio caused by elevated pressure.

The N/C ratios in the chars do not change significantly as a function of pressure, as shown in Figure 1.11. The fraction of the initial amount of nitrogen that remains in the char can be calculated from the elemental compositions of the coal and char and from the mass remaining (m/m0). Figure 1.12 shows that at least for two of the coals (Ken #9 and Ill #6), more nitrogen remains in the char at increased pressures. The nitrogen release data for the other two coals (Pitt #8 and KRL) are more scattered, but seem to indicate that the fraction of nitrogen remaining in the char stays relatively constant with pressure.

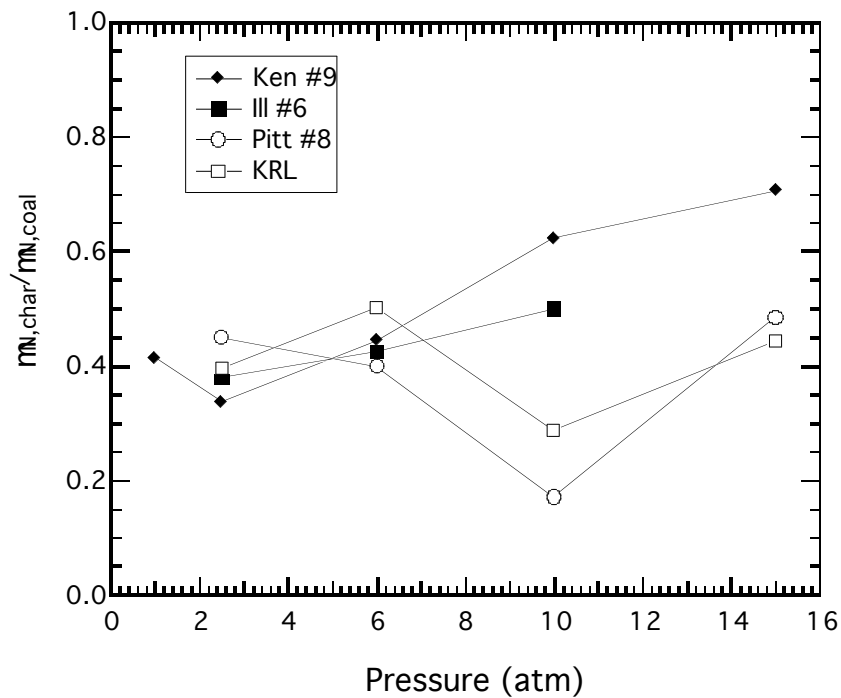


Figure 1.12. Fraction of initial nitrogen remaining in the char ($m_{N,char}/m_{N,coal}$) after pyrolysis as a function of pressure.

1.4.5 The Effect of Pressure on Coal Swelling Ratios

Figure 1.13 shows measured apparent densities as a function of pressure from 1 atm to 15 atm. Fig 1.14 shows the swelling ratios of chars collected at different pressures. The

heating rate of the HPFFB char in this study was estimated to be about 10^5 K/s (see Figure 1.8). This heating rate is higher than the drop tube reactor because there is no wake from the water-cooled coal injector; the particles in a FFB are convectively heated as they pass through a flame front. The experimental conditions of this experiment are compared with other studies (Lee et al., 1991; Wu et al., 2000) in Table 1.6.

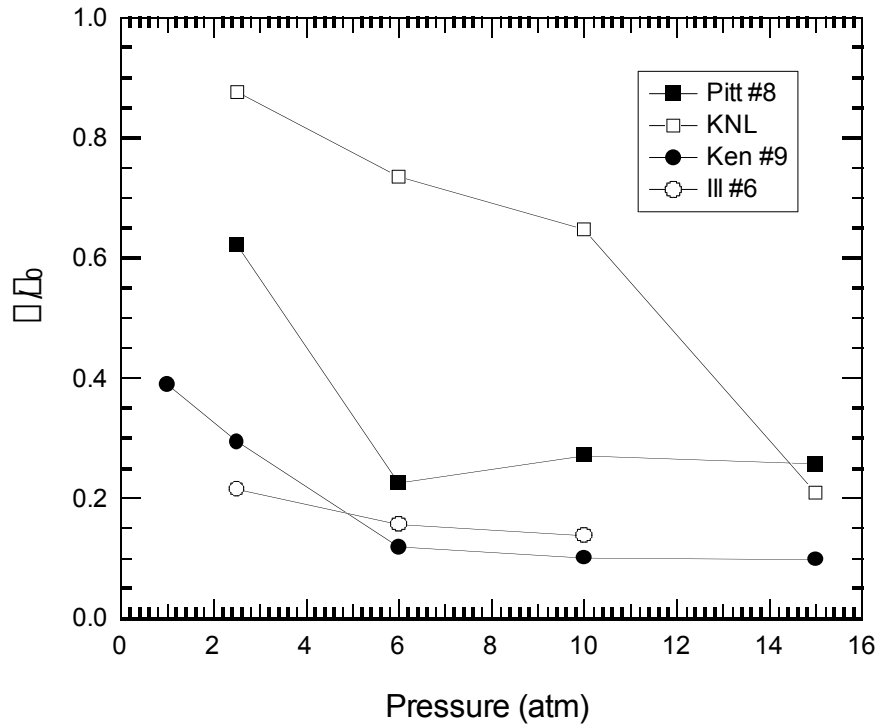


Figure 1.13. Apparent densities for chars prepared in the HPFFB.

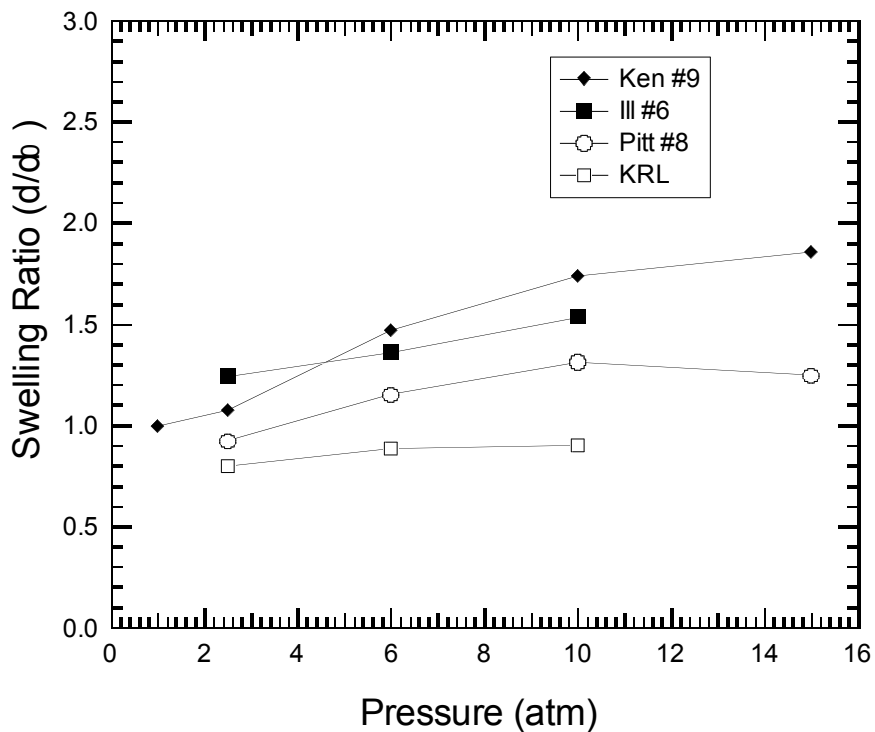


Figure 1.14. Swelling ratios of four coal chars as a function of preparation pressure.

Table 1.6 Comparisons of Experimental Conditions

	Authors		
	Lee et al.(1991)	Wu et al. (2000)	Current work
Coal	Illinois No.6	Australian Bituminous coal	Two US bituminous coals and one lignite
Particle size	62 μ m mean particle diameter	63-90 μ m	75 μ m average diameter
Apparatus	HEF (high-pressure entrained-flow furnace)	PDTF (pressurized drop-tube furnace)	HPFFB (high-pressure flat flame burner)
Heating rate	$\sim 10^4$ K/s	$\sim 10^4$ - 10^5 K/s	$> 10^5$ K/s
Temperature	1189 K	1573 K	1573 K
Pressure	0.1-3.8 MPa	0.1-1.5 MPa	0.1-1.5 MPa
Atmosphere	N ₂	N ₂ , with O ₂ to burn volatiles	Combustion product of CH ₄ /Air

This high heating rate condition (10^5 K/s) strongly changed the devolatilization characteristics during the early stages of coal pyrolysis, as shown by the comparison of swelling ratios in Figure 1.15. The swelling ratios for coals in the HPFFB were smaller

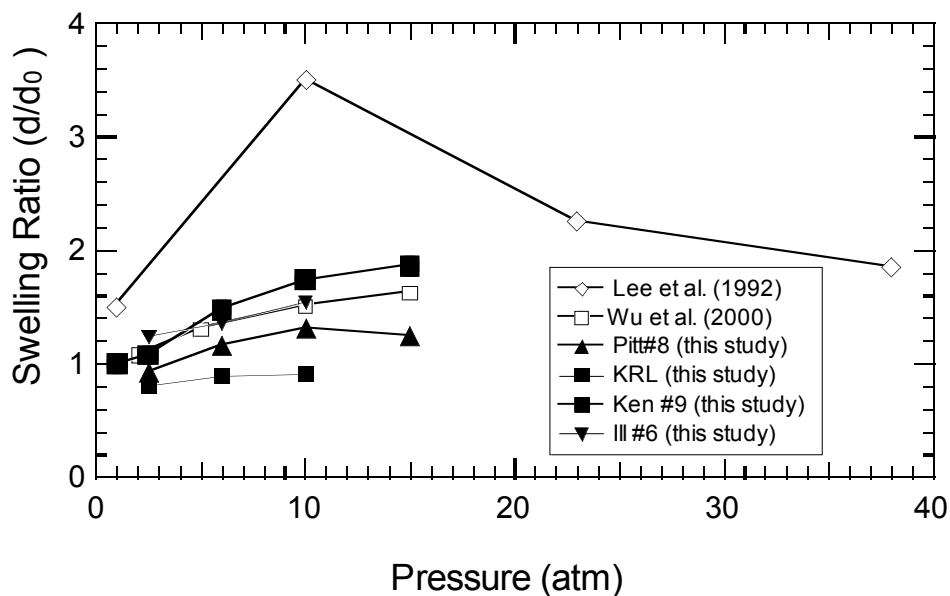


Figure 1.15. Comparison of swelling ratio in the HPFFB with other studies.

than observed in the PDTF (Wu et al., 2000) or the high-pressure entrained-flow furnace (Lee et al., 1991). Swelling ratios for HPFFB chars still increased with the increase of char preparation pressure. However, the swelling ratios at any pressure for the HPFFB chars are smaller than reported in the experiments with lower heating rates. The swelling ratio of Pitt #8 coal increased when pressure increased, reaching a maximum value at 10 atm, and then dropped at 15 atm. The other coals also exhibited increasing swelling ratios within the pressure range of 1-15 atm, indicating that the effect of pressure on the coal swelling ratio is rank dependent. Similar rank dependent results were reported by Lee et al. (1991).

1.4.6 The Effect of Pressure on Char Morphology

Scanning electron micrographs (SEM) of the chars collected in this study are shown in Figure 1.16. The SEM of cross sections of Pitt #8 and Knife River lignite char samples are shown in Figure 1.17 and Figure 1.18, respectively. The Pitt #8 char particles show evidence of softening bubble formation, and large blow holes where bubbles have ruptured. The 10 atm particles seem to have smaller surface holes than the 6 atm char, which is consistent with the small increase in swelling behavior shown in Figure 1.15. The general features of the lignite chars seem to be void of softening behavior.

Both heating rate and pressure affect swelling characteristics during coal pyrolysis. At low heating rates (such as in a TGA, or ~ 1 K/s), volatiles can diffuse through the pores without causing an internal pressure high enough to cause the particle to swell. At moderate heating rates (such as in a drop tube, or 10^4 K/s), the volatiles formed in the particle interior are formed faster than they can escape through the pores, and swelling occurs if the particle has softened. At high heating rates (approaching 10^5 K/s), the volatiles are formed faster than the swelling process can accommodate, and the bubbles burst. At elevated pressure, higher molecular weight tar precursors do not vaporize, causing more plasticity in softening coals. Hence if conditions are right, enhanced swelling is observed at increased pressures. However, at high heating rates, the surface tension in the bubble walls is overcome and the bubbles burst before significant swelling occurs. For low rank coals and lignites, little softening occurs, and the discharge of moisture and light gases with little tar formation can actually cause particle shrinkage.

The physical structure of the char significantly affects its high temperature oxidation or gasification rate. A comprehensive coal oxidation model needs precise prediction of the swelling ratio. A correlation of coal swelling ratio with pressure and

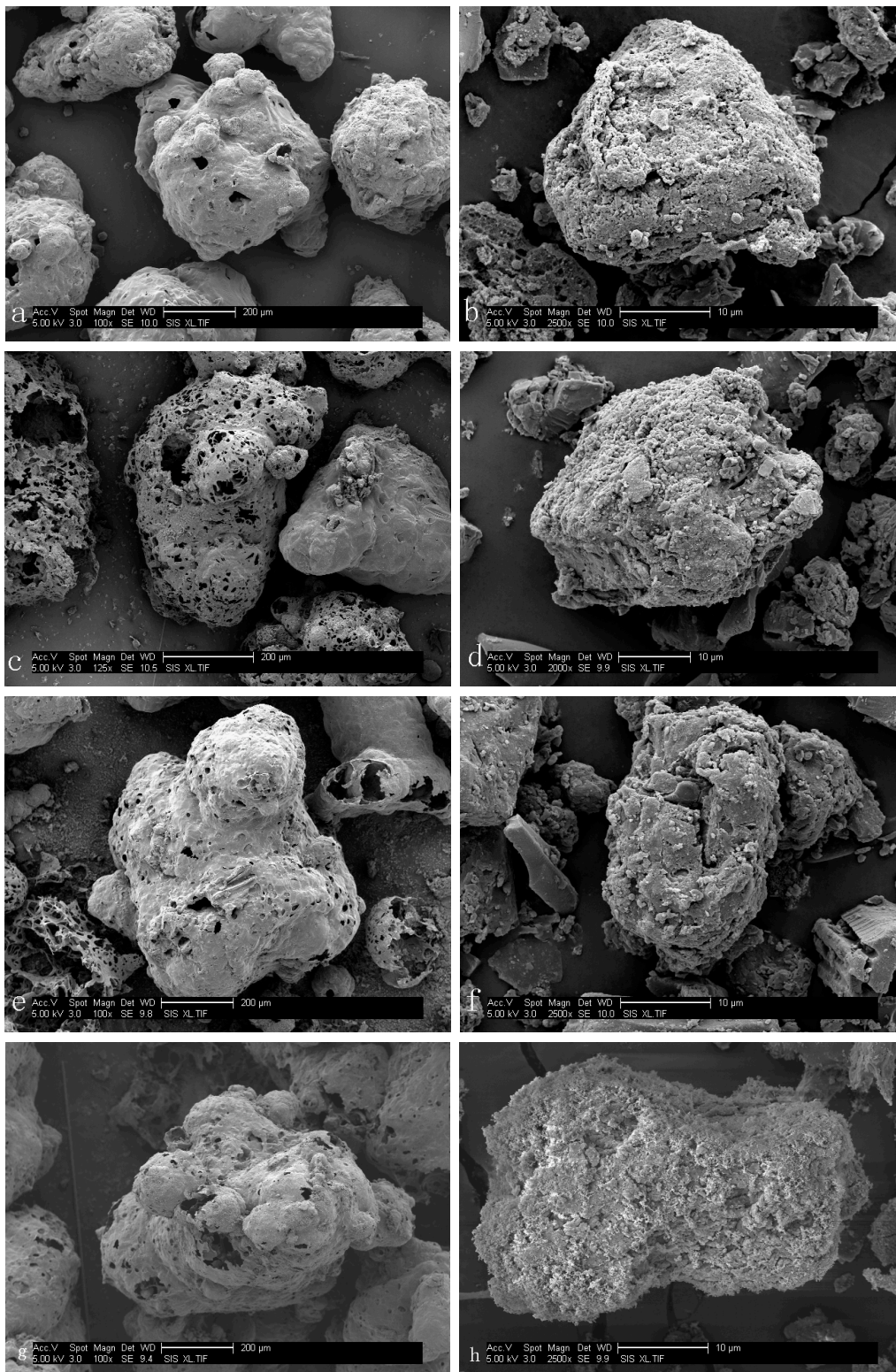


Figure 1.16. SEM micrograph of char produced from pyrolysis of Pitt #8 coal and Knife River Lignite. (a) Pitt #8 1 atm, (b) KRL 1 atm (c) Pitt #8 6 atm, (d) KRL 6 atm, (e) Pitt #8 10 atm, (f) KRL 10 atm, (g) Pitt #8 15 atm, (h) Pitt #8 15 atm.

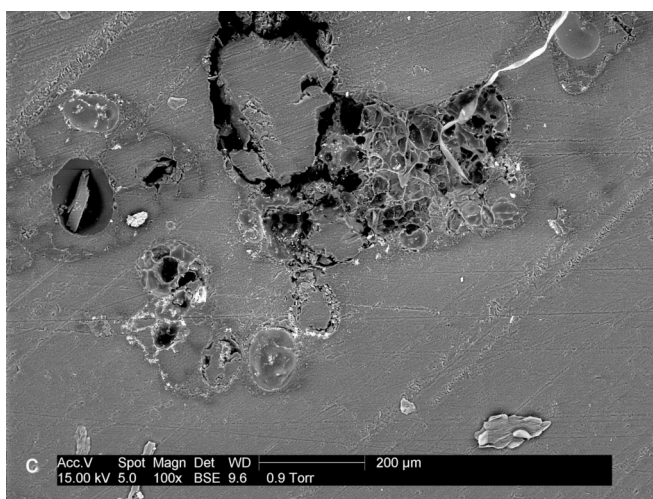
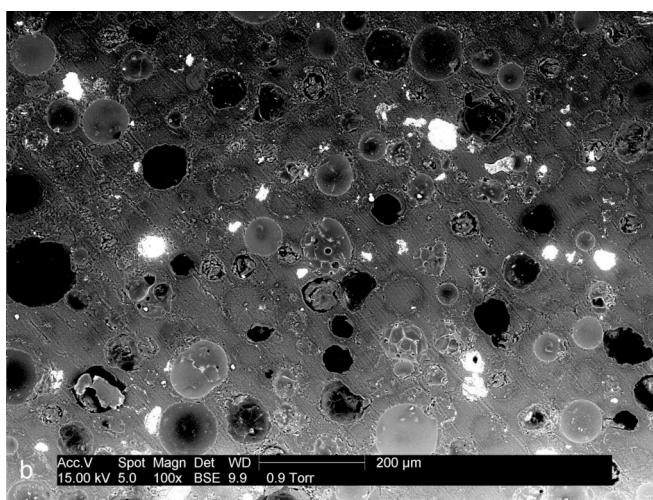
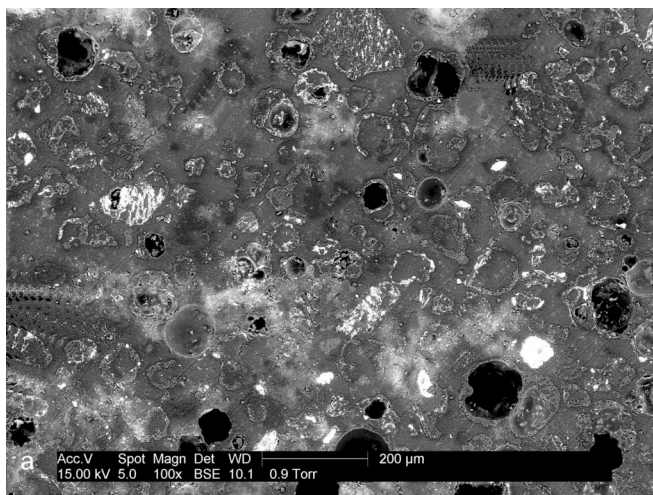


Figure 1.17. SEM micrograph of char cross section produced from pyrolysis of Pitt #8 coal (a) 2.5 atm (b) 6 atm (c) 15 atm.

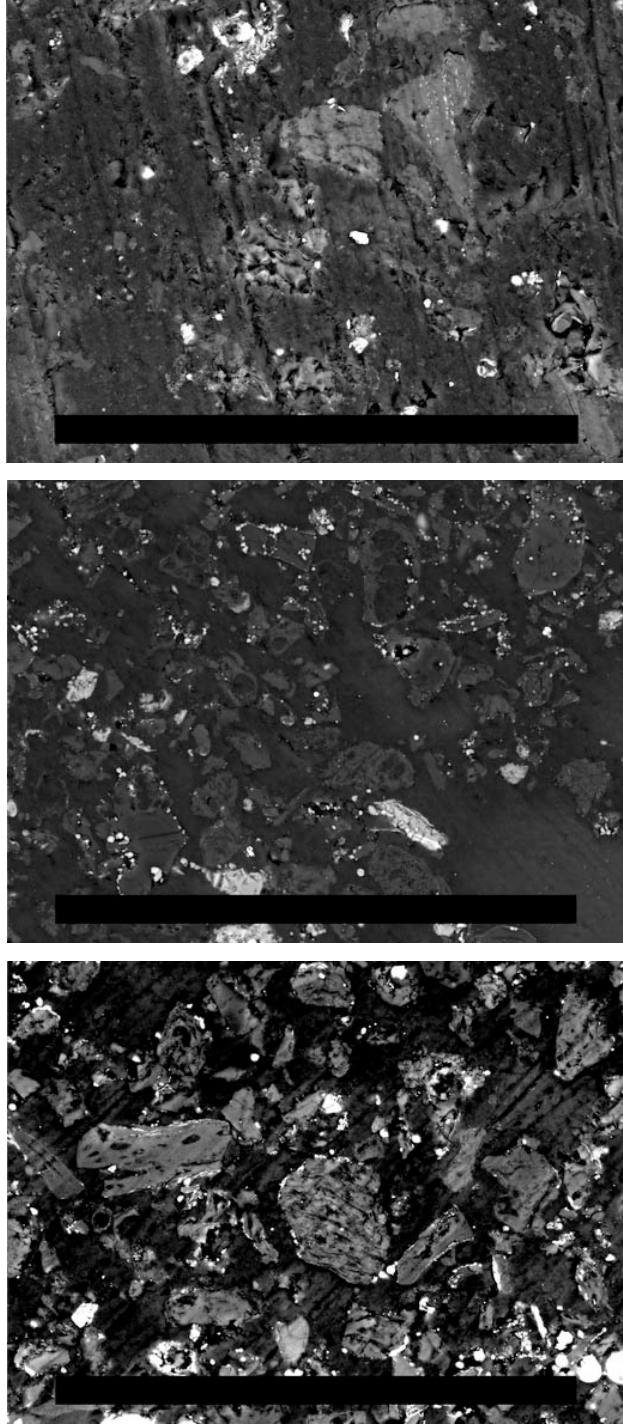


Figure 1.18. SEM micrograph of char cross section produced from pyrolysis of Knife River Lignite (a) 2.5 atm (b) 6 atm (c) 15 atm.

carbon content of the parent coal was developed by Benfell (2001), which predicts change of the coal swelling ratio with increased pressure from medium heating rate coal pyrolysis ($\sim 10^4$ K/s), but overestimates swelling ratio for high heating rate pyrolysis ($\sim 10^5$ K/s). Since practical pulverized coal combustion occurs at high temperature (2000K) and heating rate (10^6 K/s), such correlations should include the effects of heating rate.

SEM images of the external surface of the Kentucky #9 chars produced at pressures of 0.85, 2.5, 6, 10, and 15 atm are shown in Figure 1.19. The letters a-e in the top left corner of each image represents increased pressure condition, respectively. The exterior morphology of char particles clearly changed with increasing pressure. The surfaces of chars produced at 0.85 and 2.5 atm show similar characteristics. The particles have a porous external surface, with blow holes created by volatiles as the internal particle pressure overcame the surface tension of the softened particle. Some smaller char fragments were also observed, possibly caused by fragmentation at these high heating rates. The char particle surface became less coarse as pressure increased from 6 atm to 15 atm, and bubbles were clearly visible beneath the particle surface, which implies a thin wall. Only a small number of fragments were visible at the elevated pressures, and blow holes were not observed like in the char produced at lower pressure.

Cross section SEM images of the Kentucky #9 char particles are shown in Figure 1.20. Char bubble structure appears to be affected by the pressure. The char particles produced at lower pressure tend to have one or several large bubbles in the central area, with small bubble clusters appearing near the outer surface of the char particles (i.e., the char “skin”). For char particles produced at elevated pressures, bubbles are more evenly distributed throughout the particle interior, and the walls between pores are thinner than in the chars made at lower pressure. Similar phenomena can also be observed from Pitt #8 chars (see Figure 1.17). The observed phenomena can be explained using char structure evolution mechanism of Yu et al. (2002). The bubble structure of chars produced at lower pressure is in the later stage of structure evolution, and chars produced at higher pressure are in the early stage. The char structure evolution is restrained by elevated pressure. Considerable

amounts of volatiles are transported through bubble movement. Small bubbles are created during the initial stage of devolatilization, and then

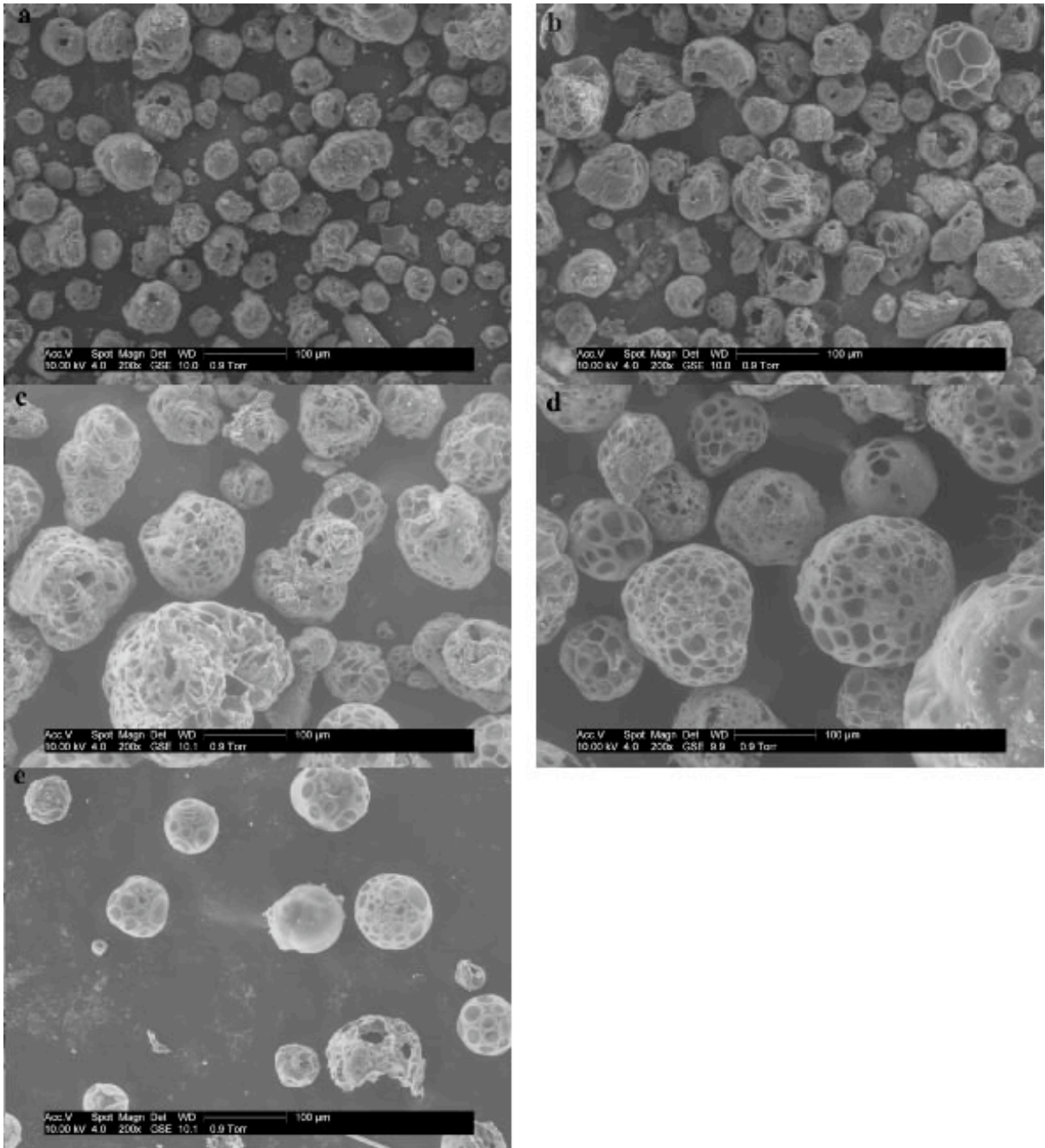


Figure 1.19. SEM micrograph of char produced from pyrolysis of Ken #9 coal (a) 1 atm, (b) 2.5 atm (c) 6 atm (d) 10 atm (e) 15 atm.

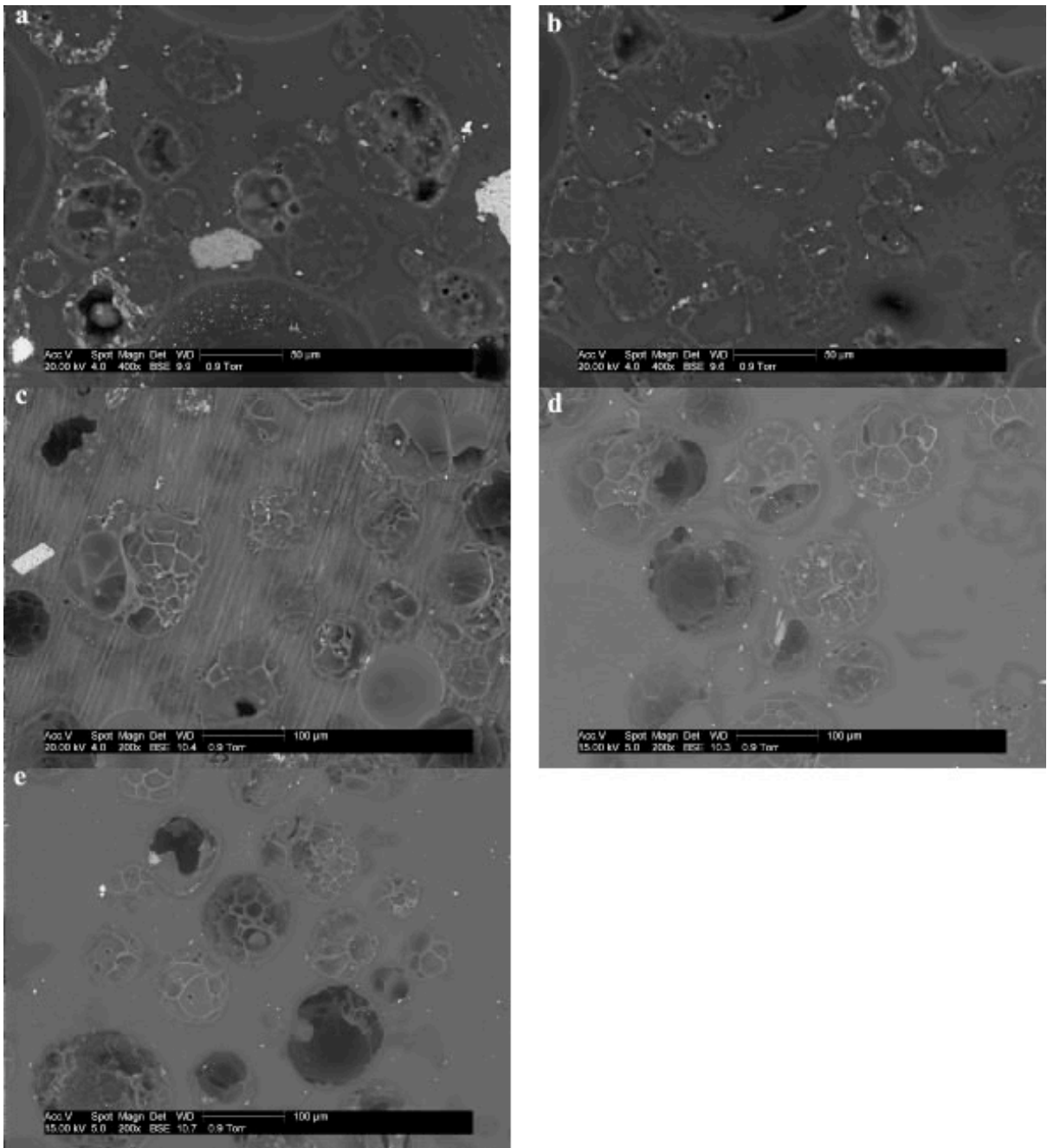


Figure 1.20. SEM micrograph of char cross section produced from pyrolysis of Ken #9 coal (a) 1 atm, (b) 2.5 atm (c) 6 atm (d) 10 atm (e) 15 atm.

these small bubbles merge together to form larger bubbles. The larger bubbles move to the particle exterior surface and finally burst open. At high pressure, transport of bubbles is more difficult, and a char with characteristics of the early stage of bubble evolution is produced. The char structure observed illustrates one possible reason for lower mass release at elevated pressure.

The effect of pressure on coal particle swelling ratio was discussed previously (Figure 1.14). Here the swelling ratios are interpreted using char morphology. Within the range of pressures tested in this study, the swelling ratios of all four coals studied increased with increasing pressure. The morphology of the Kentucky #9 char consistently illustrates the trend of increased swelling ratio with elevated pressure. At higher pressures, the char became more fluid because of the increased amount of metaplast. Bubbles were created and trapped within the particle by the increased resistance created by high pressure. These bubbles expanded and formed thinner inter-bubble walls, until a force balance was achieved with the reactor pressure exterior to the particle. At lower reactor pressures, bubbles merged or burst open because of a smaller mass transfer resistance compared to the high-pressure condition, thus forming thicker walls and blow holes on the particle exterior surface. Therefore, smaller swelling ratios were observed at the lower pressures, and even fragments in some particles were observed. This swelling effect is governed by many factors such as coal rank, heating rate, and pressure. These same types of effects were observed in the other bituminous coals studied in this experiment. In contrast, very few changes were observed in the morphology of Knife River lignite chars as a function of pressure, since lignites do not go through a softening regime.

1.4.7 Char Surface Area

The internal surface area of char is an important factor affecting the reactivity of char oxidation or gasification, but only a few studies have reported the effect of pressure on char surface area. Lee et al. (1992) found that chars generated at higher pressure have lower N₂ surface areas, and that CO₂ surface areas increase with pyrolysis time. Similar trends were also reported by Wall et al. (2002). In the contrast, Roberts et al. (2003)

found that both CO₂ and N₂ surface area increased with pressure during coal pyrolysis. CO₂ surface areas of chars were more sensitive to increases in pressure. In the current study, both CO₂ and N₂ surface areas of chars decreased with increasing pressure (see Figure 1.21). The CO₂ surface area was larger than the N₂ surface area at all pressures. CO₂ surface areas are usually representative of micropore surface, and N₂ surface areas are representative of meso and macropores. These trends mean that chars produced at high pressure have fewer micropores than low pressure chars. This trend is consistent with the SEM analysis, where high pressure chars exhibited more distinct bubbles than low pressure chars. This trend is consistent with the SEM analysis, where high pressure chars exhibited more distinct bubbles than low pressure char, and the texture of solid part of the char was denser and less porous.

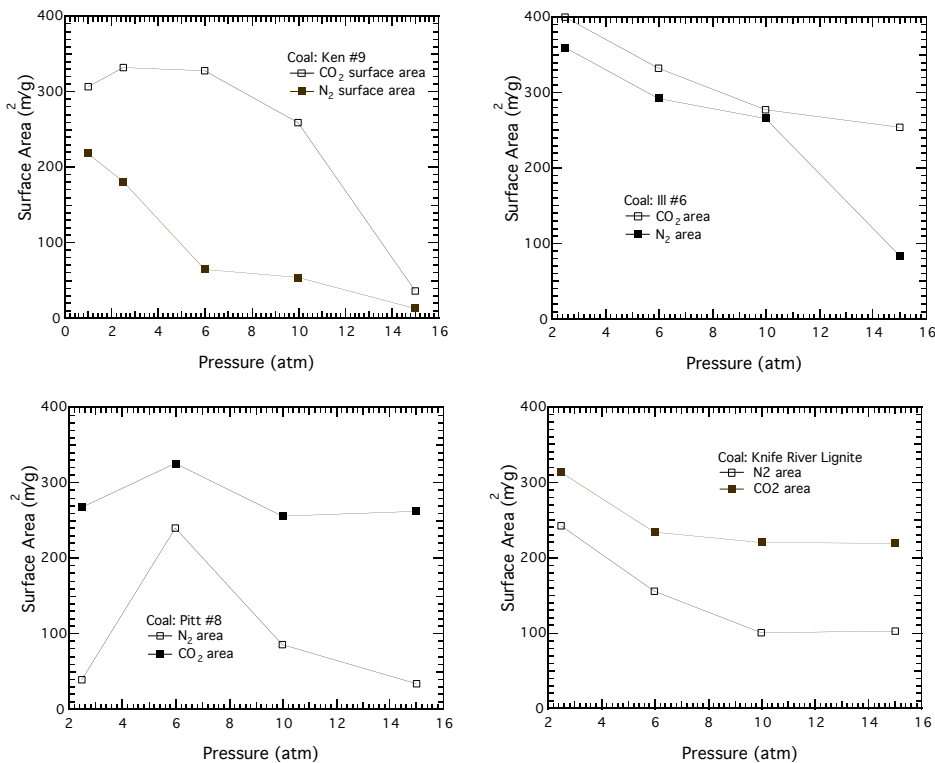


Figure 1.21. Surface area of chars prepared at different pressures.

1.5 Chapter 1 Conclusions

Four coals with a broad rank distribution, including Kentucky #9, Illinois #6, Pitt #8, and Knife River Lignite, were pyrolyzed in an atmospheric flat-flame burner and a high-pressure flat-flame burner. Resulting chars were collected at pressures of 0.85, 2.5, 6, 10,

and 15 atm. The chars were analyzed to find the formation the effect of pressure on char properties.

The measured decreases in total volatiles yields with increasing pressure were predicted using the CPD model using only the elemental composition and ASTM volatiles yields of the parent coals as changeable input parameters that relate to coal chemical structure. The H/C and O/C ratios in the resulting chars initially increase with increasing pressure, but remain relatively constant at pressures from 6 to 15 atm. The H/C ratio in the char is thought to be affected by the decrease in tar yield at increased pressures, the change in the hydrogen content of the tar with pressure, and the increase in light gas yield as pressure increases. The change in residence time at different pressures in these experiments may also have played a role in the hydrogen release.

Swelling ratios of the lignite chars were less than 1.0, and only about 1.3-1.8 for the bituminous coals. All coal chars showed slight increases in swelling behavior as pressure increased. The swelling behavior observed for the Pitt #8 coal char at each pressure was lower than reported in high pressure drop tube experiments, supporting earlier work at atmospheric pressure showing that particle swelling decreases as heating rates approach 10^5 K/s. The morphology of chars produced at different pressures were analyzed using SEM. Chars formed at high pressure were in the early stage of foam structure evolution, while chars formed at low pressure were in later stages of foam evolution. The swelling ratio of chars increased with increasing pressure, and is attributed to bubble evolution.

Char surface areas using both CO₂ and N₂ as adsorption gases decreased with increasing pressure. The amount of micropores is less for chars produced at high pressure. These chars are more porous but have a denser framework.

CHAPTER 2 INTRINSIC REACTIVITY OF CHAR FORMED AT ELEVATED PRESSURE

2.1 Literature Review : Effect of Pressure on Resulting Char Reactivity

The pressure at which the parent coal is devolatilized also plays an important role in the reactivity of the resulting char. Sha et al. (1990) noted a significant decrease in the reactivity of the char as pressure was increased, postulating that reactivity was affected by changes in pore structure. Van Heek and Mühlen (1991) noted that the steam reactivity for chars is not affected by pressure if pyrolysis is performed under inert conditions. Under a hydrogen atmosphere, increased pressure resulted in a decrease in the steam reactivity of the resulting char. Cai et al. (1996) found combustion reactivities (calculated as the maximum rate observed during the conversion profile at 773 K) decreased during hydro-pyrolysis at pressures up to 40 atm and increased at pressures above 40 atm. The eventual increase in reactivity was reportedly the result of some char conversion by H₂ at the higher pressure, which exposed a fresh and enlarged carbon surface. Lee et al. (1992) investigated the structure and reactivity of Illinois No.6 coal char following pyrolysis at elevated pressure. They found that increasing the pressure slowed the rate of release of volatiles, increased the amount of char remaining after pyrolysis, and altered the composition of the volatile products. Their data also demonstrated how pressure hinders the development of the mesopore system that develops after the coal passes through the plastic phase of pyrolysis. The increased fluidity that resulted from higher-pressure pyrolysis led to enhanced ordering of carbon layers and the subsequent loss of gasification reactivity in the char residue.

Roberts et al. (2000) measured the apparent and intrinsic gasification rates of an Australian coal char collected from a pressurized drop tube furnace (PDTF) under various pressures. Char reactivity varied significantly with pressure, whereas the intrinsic rates, which were obtained by normalizing the apparent rate by internal surface area, were almost independent of pressure over a range of 1 to 15 atm. Comparisons of the initial apparent and intrinsic gasification rates of vitrinite- and inertinite-rich char samples from the same coal were given by Benfell et al. (2000). The inertinite-rich sample had a faster

apparent gasification rate than the vitrinite-rich sample when made at 5 atm, but a slower apparent gasification rate when made at 15 atm. However, it was shown that the intrinsic reaction rates of these char samples did not systematically show large variations with pressure or maceral concentrations in the parent coal. This suggests that the pressure significantly influences the physical structure of coal chars, as discussed above, but has little effect on the chemical structure of char, which largely determines the intrinsic char reactivity. Such a conclusion has significant implications for interpreting char reaction rates and mathematical modeling of char burnout.

In summary, chars produced at different pressures were reported to have different apparent reaction rates, but similar intrinsic rates. However, pressure may have a significant influence on char morphology. High pressure pyrolysis forms more porous char particles. The morphology contributes to the difference in apparent reactivity. Chemical structures of chars formed at different pressures seem similar, as long as the char preparation temperature is low. Further studies are needed to determine the effects of high pyrolysis temperatures (>1673 K) and high pyrolysis pressures on the properties of char.

2.2 Objective

The objective of this part of the project is to study the effects of pressure on the TGA (i.e., low temperature) oxidation rate of coal chars formed at high temperatures and high heating rates, typical of industrial pulverized coal combustion.

2.3 High Pressure Thermogravimetric Analyzer (HPTGA)

The Deutsche Montan Technologie (DMT) high pressure Thermogravimetric analyzer (HPTGA) (Figure 2.1) is an electrically-heated apparatus that allows the control of temperature, pressure, gas concentrations, and flow rates. A sample is placed in some type of basket that is suspended from a chain attached to the microbalance, and is lowered into the furnace. The weight of the sample is then measured and recorded

throughout the experiment by a computer. Time, temperature, and pressure are also recorded at a function of time. The temperature is monitored with thermocouples. Pressure is controlled by a PID controller, with an accuracy of $\pm 1\%$. The gas compositions and flow rates are controlled by mass flow controllers, with flow rates ranging from 0.1 to 10 L/min. The maximum reactor temperature is 1100°C. The maximum heating rate achievable in the reactor is 100°C/min. The entire vessel is rated at a maximum pressure of 100 bar. Some of the gases that have been used in the HPTGA include helium, nitrogen, oxygen, carbon dioxide, carbon monoxide, argon, hydrogen, and methane.

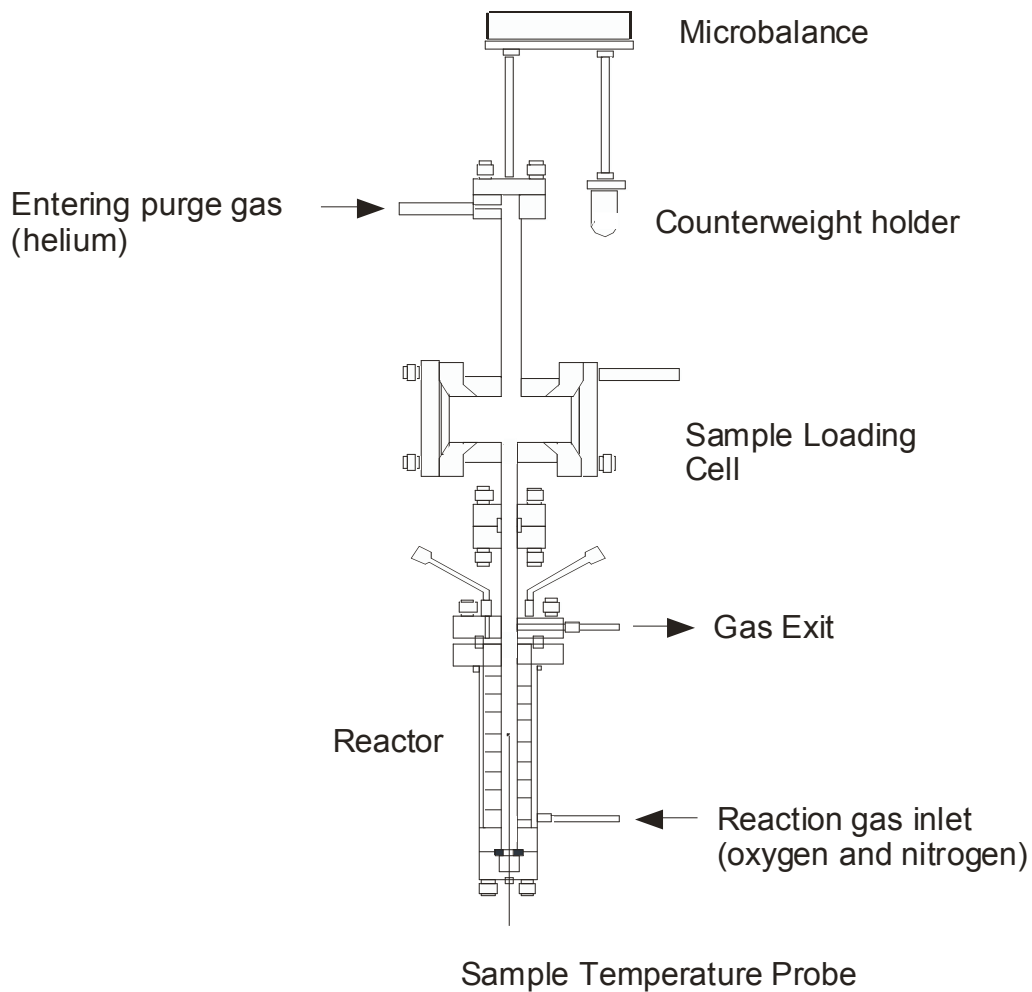


Figure 2.1. Schematic of the DMT high pressure Thermogravimetric Analyzer.

The HPTGA was characterized to ensure that the experiments were carried out under conditions such that the reaction rate was controlled only by chemical processes and was

not affected by mass or heat transfer effects. Temperature ranges, carrier gas, gas flow rates, and sample amount were chosen accordingly. Helium was chosen as the inert gas environment due to its high thermal conductivity and low density, which should minimize the thermal delay and buoyancy effects, and hence increase the accuracy of the data. A 4 mg sample size was used for all of the HPTGA tests and reported here.

2.4 Descriptions of HPTGA Tests

High-temperature, high-pressure pyrolysis experiments were conducted on three bituminous coal chars. Chars were collected at different pressures in the HPFFB. These chars were then oxidized using the same high-pressure Thermogravimetric Analyzer (HPTGA). Char intrinsic combustion reactivities were calculated based on mass vs. time data. This chapter will discuss the experiment procedure, the effect of pressure on resulting char reactivity, and reaction of mechanisms.

2.4.1 Char Preparation

Coal chars from Pitt #8, Ill #6, and Knife River Lignite were tested using the HPTGA. The properties of these coals were reported in the previous chapter. Chars were prepared using same procedure described in Chapter 1. All of the coals were pyrolyzed at 2.5, 6, 10, and 15 atm. Resulting chars were collected, and then stored in a refrigerator. Chars were dried at 110°C for 2 hours prior to each HPTGA test. The properties of these char were reported in the previous chapter.

2.4.2 HPTGA Test Procedure

TGA char oxidation experiments are usually conducted on small amounts of sample (~4 mg) in order to minimize bed effects. Careful characterization is needed to minimize the experimental error. The HPTGA used in this study was also used to conduct char combustion experiments at elevated pressure by Hecker et. al (2003). Based on their work, a certain experimental procedure was introduced to the current study to minimize the effect of buoyancy, flow rate, and gas composition, thus an intrinsic reactivity of char

oxidation which is free of mass transfer effects can be obtained. First of all, the total inert gas flow rate was set to 4 l/min. This flow rate was found to effectively minimize the effect of boundary diffusion, as well as conserve helium and facilitate pressure control in the reaction chamber. Second, helium was selected as the inert gas rather than nitrogen, because helium has significantly higher thermal conductivity than nitrogen. Third, samples less than about 4 mg were found to introduce weighing errors. Finally, gas compositions were carefully selected to avoid heating from char oxidation, and the reaction temperature was selected to be in the region of chemical reaction control.

Hecker et al. (2003) found that char intrinsic char oxidation rate, determined on a $(g_{\text{avail}}/(g_{\text{avail},s}))$ basis, is independent of char burnout level, and that kinetic parameters are not affected by changes in total pressure. Char intrinsic char oxidation rate ($-r$), activation energy (E), and oxygen reaction order (n) were defined by an n-th order kinetic equation:

$$-r = A e^{-\frac{E}{RT}} P_{O_2}^n \quad (2-1)$$

and found to be independent of the total pressure. It was been that the nth order kinetic model fits both atmospheric and elevated pressure char oxidation data very well, with n = 0.7 for both chars studied. The char studied by Hecker and coworkers were all formed at atmospheric pressure.

The results of Hecker et. al (2003) are consistent with some other studies (Suuberg et al., 1988). Since all the chars used in Hecker's experiments were produced at 1 atm, char intrinsic reactivity should have been essentially the same. However no experiments were performed to see if the char intrinsic reactivity changes if the chars were formed at different pressures. The experiments in the current study were performed precisely to study this effect. Table 2.1 shows the matrix of experiments performed in the HPTGA. For the three coals examined, chars were collected in the HPFFB at four total pressures (0.85, 6, 10, and 15 atm), and then tested at the same pressure in the TGA. Oxygen partial pressure and temperature were changed at each total pressure to find the char oxidation kinetic data. These conditions were carefully selected to minimize the effects of mass transfer and sample heating due to reaction.

Table 2.1 Matrix of Experiments in the HPTGA

	P _{Tot} = 1 atm	P _{Tot} = 6 atm	P _{Tot} = 10 atm	P _{Tot} = 15 atm
Pitt #8	√	√	√	N/A
Ill #6	√	√	√	√
KNL	√	√	√	N/A

2.4.3 Kinetic Analysis

Figure 2.2 shows a typical data set obtained from the HPTGA. The weight of the basket and sample is recorded continuously by the microbalance. These data were rescaled to the initial weight of sample (without the basket). The data were then fitted to an equation:

$$mass = A + Be^{\square C \square r} \quad (2.2)$$

The constants a, b, and c in equation 2.2 were obtained from a least squares analysis using Microsoft Excel. The oxidation rate of char was then calculated using:

$$\square r = \frac{1}{m_{avail}} \frac{dm_{avail}}{dt} \quad (2.3)$$

An example of the char oxidation rate is shown in Figure 2.3. The weight measurements in the HPTGA are not stable at the initial stages of experiment. The reactivity increases dramatically at burnout levels, as seen in Figure 2.3 for char burnout levels larger than 90%. This high reactivity is caused by using the available weight in the reactivity determination (Eq. 2.3).

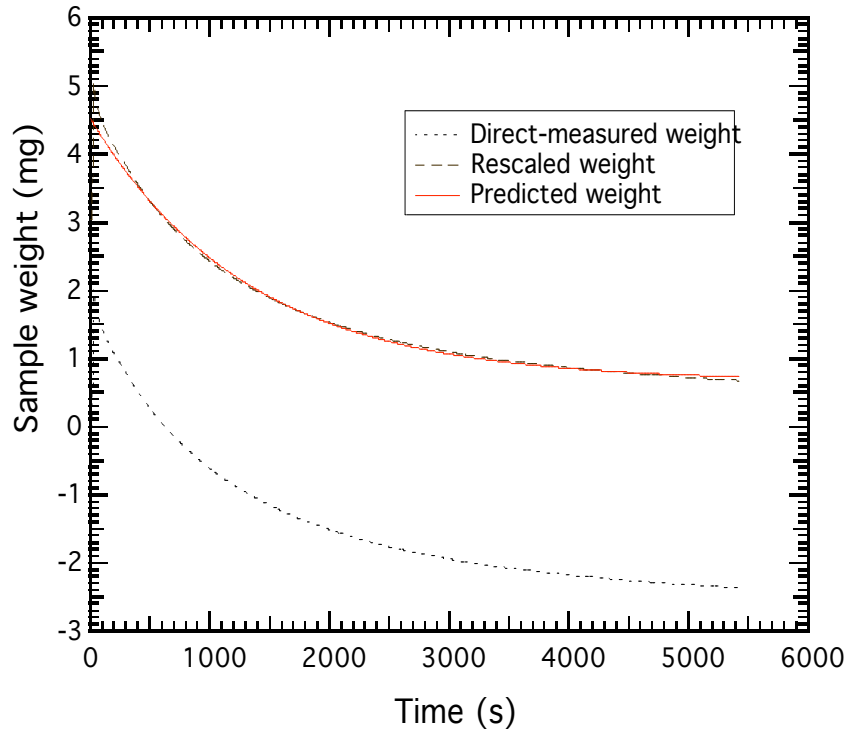


Figure 2.2. Measured and fitted data set obtained from a HPTGA test.

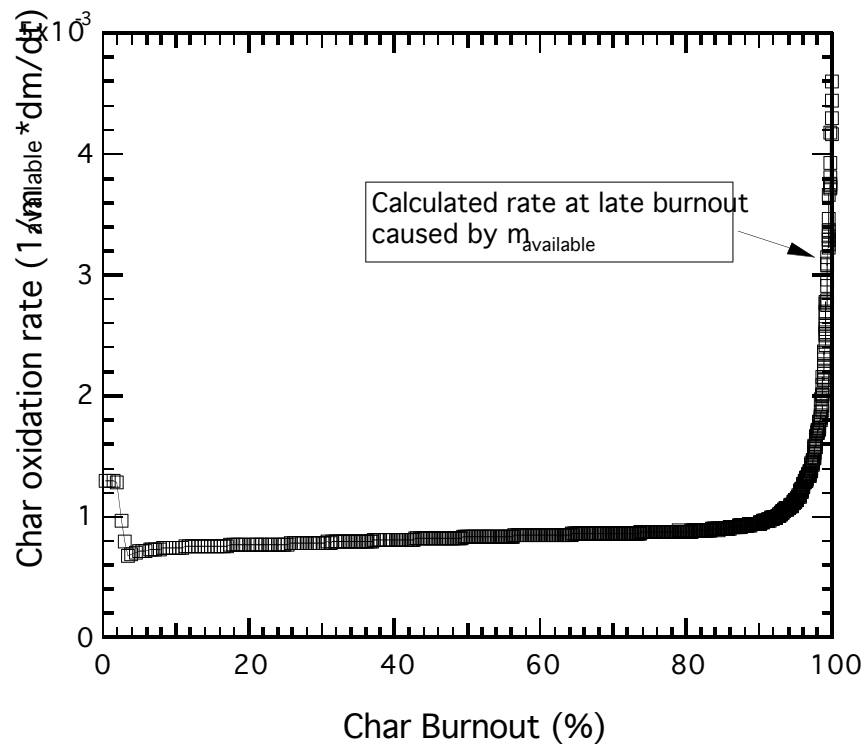


Figure 2.3. Char oxidation reactivity as a function of burnout.

The reactivity can also be interpreted using following equation:

$$\bar{r} = \frac{dx_i}{dt} = \bar{r} \frac{1}{m_{initial}} \frac{dm_{avail}}{dt} \quad (2.4)$$

Figure 2.4 shows the same data processed using equation 2.4. The reactivity is not reasonable at the beginning of test because of instability of microbalance. The reactivity during the later stages of char burnout decreases to almost zero, which is caused by full consumption of the carbonaceous material. This data processing method can help to eliminate the problem of equation 2.3. However, in reality, the reactivity changes with burnout based on the remaining mass. Therefore, all HPTGA rate data were normalized by the instantaneous mass in this study (see Eq. 2.3).

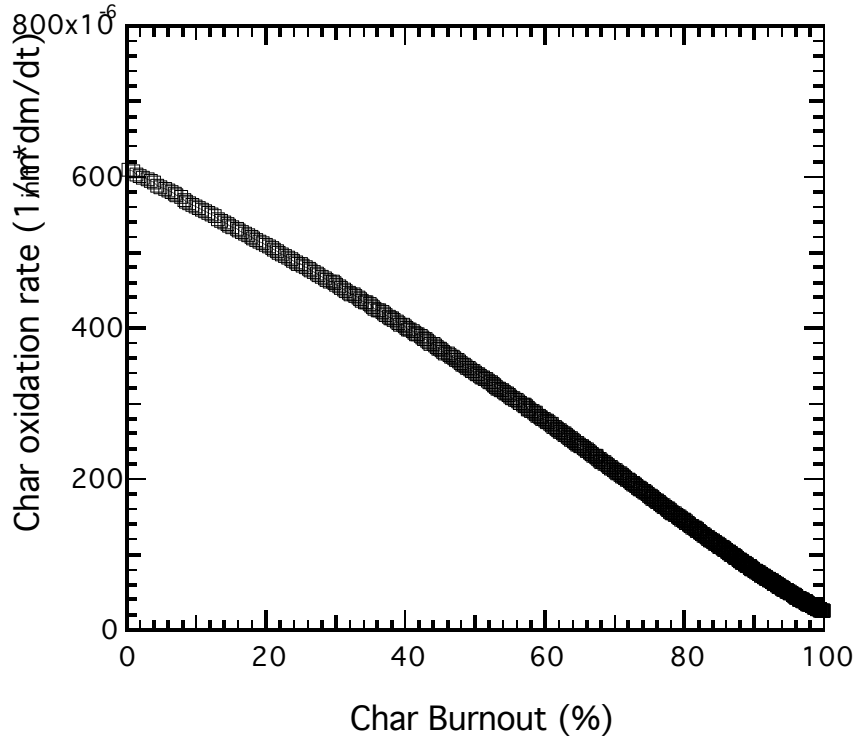


Figure 2.4. Char oxidation reactivity as a function of burnout

There are wide variations in the methods used in the literature regarding how to interpret TGA data from char oxidation tests. Previous researchers have used average reactivity over a certain range of char burnout, maximum reactivity, initial char reactivity, or the reactivity at 20% burnout (Cai et al., 1996; Hecker et al., 2003; Roberts and Harris, 2000;

Roberts et al., 2003). Initial reactivities vary in an unpredictable manner due possibly to movement of the sample basket or slow degassing of a small amount of pyrolysis products. Therefore, in this study, reactivities are compared at TGA char burnouts between 20% and 60%. At the end of each TGA test, the sample was burned completely at higher temperatures and O₂ levels in order to determine the ash content for that sample. The sample and basket were then weighed on a separate, more accurate balance, to improve the accuracy of the reactivity data. Each TGA test was repeated three times. The average reactivity value and standard deviation value were computed from the repeat samples at intervals of 5% in the char burnout, and error bars were set at ± 2 standard deviations.

The activation energy and oxygen order of n-th order rate expressions of Pitt #8 coal and Ill #6 coals were also calculated. Activation energies were determined from standard Arrhenius plots (ln[rate] vs. 1/T at constant oxygen partial pressure). Oxygen reaction orders were determined from a power law model by determining slopes of ln[rate] vs. ln[P_{O₂}]. The total pressure during these TGA tests was kept the same as the char formation pressure, so as to simulate a continuous combustion process. TGA conditions used here were temperatures ranging from 693 to 753 K and oxygen partial pressures ranging from 0.2 to 0.8 atm. The low temperatures ensure that intrinsic rates were measured. Resulting O₂ mole fractions were 20 to 50% for the 1 atm test, and lower than 13% for the 6, 10, and 15 atm tests. Low O₂ mole fractions are preferred to minimize the degree of char heating from the heat of the combustion.

2.5 Results and Discussion

2.5.1 Char Intrinsic Reactivity

The effect of pressure on the resulting char combustion reactivity is shown in Figure 2.5 for the Pitt #8 coal, Figure 2.6 for the Illinois #6 coal, and Figure 2.7 for Knife River lignite. Pitt # 8 chars were oxidized in the HPTGA at a partial pressure of O₂ of 0.32 atm and a temperature of 715 K. KNL char oxidation conditions were P_{O₂} = 0.28 atm and T =

615 K. The oxidation conditions of Ill #6 chars were $P_{O_2} = 0.4$ atm and $T = 693$ K. The temperatures and oxygen concentrations were low enough for each char to avoid mass transfer effects. All of the chars were oxidized at the same total pressure as their respective char preparation pressure (i.e., 2, 6, 10, and 15 atm). The different oxidation conditions for different coals were used to maintain a reasonable reaction time. For example, Knife River lignite is the lowest rank coal, so its reaction temperature and oxygen partial pressure were set lower than for the other coals.

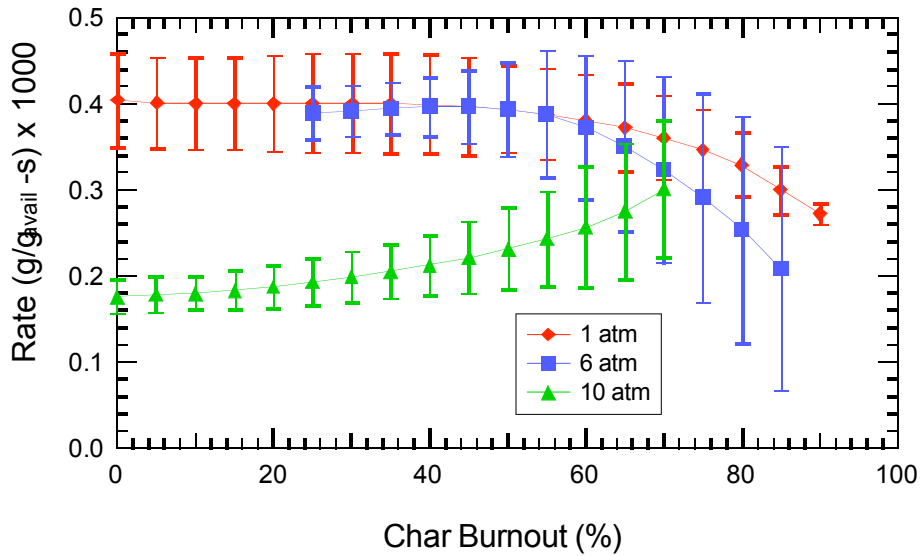


Figure 2.5. Pitt #8 char oxidation reactivity as a function of burnout.

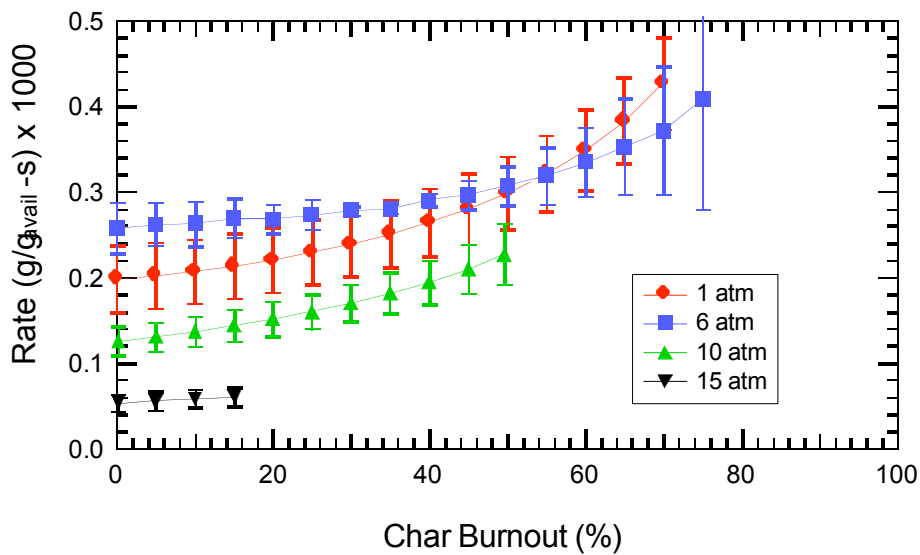


Figure 2.6. Ill #6 char oxidation reactivity as a function of burnout.

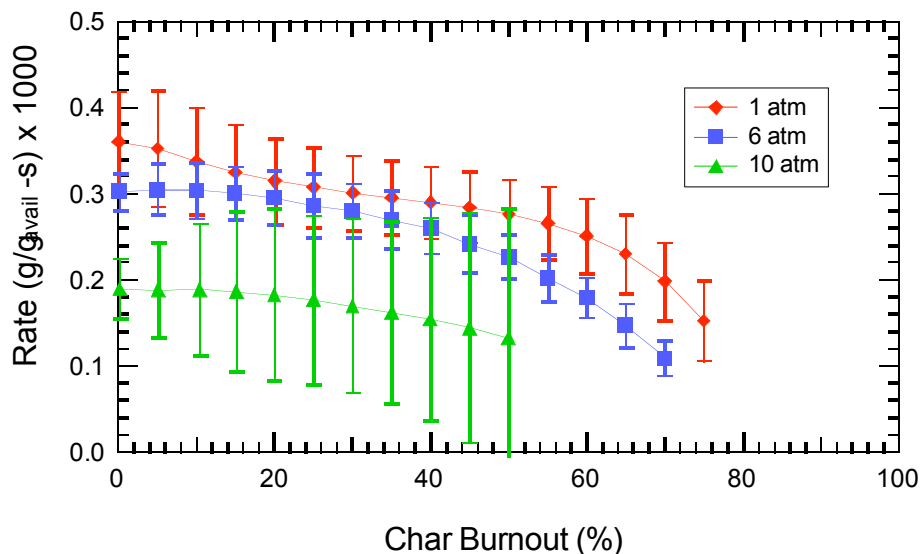


Figure 2.7. KNL char oxidation reactivity as a function of burnout.

As seen in Figure 2.5, each of Pitt #8 char reactivity curves is relatively constant for char burnouts from 30 to 60%. This region of constant char reactivity is consistent with results presented by Hecker et al. (2003), where chars produced at atmospheric pressure in a FFB were examined in a HPTGA.

Hecker's results also indicated no change in TGA O₂ reactivity for the same starting char as total pressure was increased. In contrast, Figure 2.5 shows that after 60% burnout, the 6 atm HPPFB char is observed to decrease in reactivity faster than the 1 atm FFB char. At this degree of char burnout, activated sites may have been mostly consumed and initial pore structure destroyed, causing char reactivity changes. The reactivity of the 10 atm Pitt #8 char is about 50% lower than the reactivities at the lower pressures. This decrease in reactivity with pressure differs from results reported previously in the literature (Roberts et al., 2003).

Figure 2.6 shows the char reactivity of Ill #6 char with burnout. In general, char produced from Ill #6 coal decreased in reactivity as the pressure during pyrolysis increased. This is consistent with the results from the Pitt #8 coal. The reactivity curve of

15 atm char became unstable above 50% char burnout, due to instability in the mass measurement. When the HPTGA was operated at high pressure, it usually took longer time for the microbalance to be stabilized after lowering the char sample basket into the furnace. As mentioned previously, the mass measured at the early stages of oxidation is not suitable for use in calculating the burnout rate. Therefore, the reported reactivities are theoretically from the early stages of burning, but actually are from partially reacted char samples.

Another interesting result from Figure 2.6, and from the 10 atm curve in Fig 2.5, is that char reactivity increases with increasing burnout rate. Since active sites were consumed when char oxidizes, the reactivity should decrease, especially at the late stage of burning. However the results obtained from these chars are apparently different. The effect of experimental uncertainty has been eliminated by repeating the tests at the same condition for different kinds of chars. One of the possible causes of this result may be the calculation of averaging, since the late burnout has larger error bars. Another way to comprehend this result is to remember that the reactivity is normalized by the current dry ash-free mass (see Eq. 2.3). When a small amount of sample was used in TGA test such as this study (3-5 mg), $m_{\text{available}}$ can be very small at the late stages of burnout, and approaches zero on an ash-free basis. This provides a high degree of uncertainty when the burnout rate is high. The value of dm/dt actually decreases at the late stages of burnout for all of conditions, but this decrease was counteracted by the change in m_{avail} . This effect can be controlled somewhat by increasing sample size, but then the extra combustion heat of combustion can simultaneously raise sample temperature.

Figure 2.7 shows that the lignite reactivities also decrease monotonically with increasing pressure. This is an interesting result, since the lignite char does not soften and resolidify during pyrolysis, and also since the effect of pressure on lignite pyrolysis yields are thought to be minimal. Explanations for this behavior are left for further studies.

The effect of pressure on resultant char reactivity has been studied under a variety of reaction conditions (Cai et al., 1996; Chitsora et al., 1987; Kajitani and Suzuki, 2003; Lee et al., 1992; Roberts et al., 2003; Sha et al., 1990; Van Heek and Muhlen, 1991).

Different pyrolysis atmospheres and temperature were used; char reactivities included oxidation rates as well as H₂O, and CO₂ gasification rates. Among them, three references (Chitsora et al., 1987; Kajitani and Suzuki, 2003; Sha et al., 1990) used high temperature (700-930°C) in their reactivity tests, and hence are not used for direct comparison since mass transfer may have affected their results. Roberts et al. (2003) pyrolyzed three Australian coals at 5, 10, and 15 atm. Char oxidation reactivities were measured at 10 or 15 atm at 723K in 50% O₂. The initial reaction rate for one char increased with increasing pressure, while no clear trend with pressure was observed for two other chars. However, the reactivities after normalization by the char CO₂ surface areas were the same. Cai and coworkers (1996) examined chars formed during hydrolysis (i.e., pyrolysis in H₂) as a function of pressures. They found that Pitt #8 and Linby char combustion reactivities decreased with pressure at low to medium pressures (20-30 bar), then increased at increased pressures. Lee et al. (1992) found that Illinois char reactivity generally decreased with increasing char formation pressure, but that this decrease was not as significant for coal pyrolysis residence times longer than 1 s. Lee and coworkers found no correlation between the micropore surface area (CO₂) of chars and char oxidation reactivity.

Generally, at low to medium pressures (1-40 atm), most of these studies showed that char reactivity decreased as char formation pressure increased. One study found that char reactivity increased with increasing pressure. Increasing pressure is thought to decrease the tar yield, and hence increase the hydrogen content in the char. Increased hydrogen contents in char generally translate to higher reactivities. Increased hydrogen contents in the char at increasing pressure are generally observed. However, high-pressure also increases the fluidity of the char, making the char surface more ordered, which generally means lower reactivity. This resolidification process can also be affected by residence time, causing lower char reactivity (Lee et al., 1992). Char surface area may also contribute to reactivity change with pressure, and will be discussed later in this chapter.

2.5.2 Activation Energy and Oxygen Order in N-th Order Kinetic Rate Expression

A series of TGA experiments were performed to 1, 5, 10, and 15 atm Pitt #8 chars to determine reaction orders and activation energies, following the basic TGA test procedure of Hecker et al. (2003). Temperatures used in these TGA experiments ranged from 693 to 753 K, and oxygen partial pressures ranged from 0.2 to 0.8 atm. The low temperatures ensure that intrinsic rates were measured (i.e., negligible effects of heat and mass transfer). The reaction orders and activation energies were calculated based on the average reactivity from 20-60 % burnout. Resulting O₂ mole fractions were 20 to 50% for the 1 atm test, and lower than 13% for the 6, 10, and 15 atm tests. Low O₂ mole fractions are preferred to minimize char heatup from reaction. The reaction orders and activation energies determined from these experiments are shown in Table 6.2 Except for the data point at 6 atm, the activation energy stays roughly constant with total pressure, and the oxygen order stays relatively constant at 0.7, in agreement with Hecker's results (2003).

Table 2.2 Activation Energies and Oxygen Orders of Pitt #8 Coal Chars

Total Pressure (atm)	Activation Energy (kcal/mol)	Oxygen Order
1	29.15	0.78
6	18.90	0.64
10	37.76	0.74
15	30.86	0.73

Similar sets of TGA experiments were performed on the 1, and 6 atm Ill #6 chars to determine reaction orders and activation energies. TGA experiments were conducted at temperature ranging from 663-723.5 K and oxygen partial pressures ranging from 0.2-0.5 atm. The results show a large variation in order than for the Pitt #8 coal char.

Table 2.3 Activation Energies and Oxygen Orders of Ill #6 Coal Chars

Total Pressure (atm)	Activation Energy (kcal/mol)	Oxygen Order
1	29.85	0.67
6	23.26	0.84

2.5.3 The Relationship between Surface Area and Char Reactivity

The internal surface area of the char is an important factor affecting the reactivity of char oxidation or gasification. However, only a few studies have been reported that treat the effect of pressure on char internal surface area. Lee et al.(1992) found that chars generated at higher pressures have lower N₂ surface areas, and that chars exhibit larger CO₂ surface areas with increasing pyrolysis time. Similar trends are also reported by Wall et al.(2002) In contrast, Roberts et al. (2003) found that both CO₂ and N₂ surface area increased with increasing pressure during pyrolysis, and that CO₂ surface areas were more sensitive to the increases in pressure. In the current study, both CO₂ and N₂ surface areas of chars generally decreased with increasing pressure, as shown in Figure 1.21, with the exception of the Pittsburgh #8 data at 2.5 atm. Measured CO₂ surface areas were larger than the N₂ surface areas at all pressures. CO₂ surface areas usually correspond to micropore surface area (< 2 nm pore sizes), and N₂ surface areas correspond to meso and macro pores (2 to 50 nm pore diameters). The trends shown in Figure 1.21 and the SEM of chars shown in Figure 1.17 and 1.20 imply that chars produced at high pressure have fewer amounts of micropores than low pressure chars. Even though high pressure chars exhibit more distinct bubbles than low pressure chars in the SEM, the texture of the solid part of the high pressure char (i.e., the bubble wall) is denser and less porous.

Pressure effects on char reactivity can also be related to surface area, with either CO₂ or N₂ as the adsorption gas. The normalized reactivities are calculated using the following equation:

$$r_{\text{normalized}} = \frac{r_{\text{intrinsic}}}{A_{\text{CO}_2 \text{ or } \text{N}_2}} \quad (2.5)$$

where $A_{\text{CO}_2/\text{N}_2}$ is the CO_2 or N_2 surface area in m^2/g , respectively. The intrinsic reactivity $r_{\text{intrinsic}}$ is defined as:

$$r_{\text{intrinsic}} = \frac{1}{m_{\text{avail}}} \frac{dm_{\text{avail}}}{dt} \quad (2.6)$$

Intrinsic reactivity data obtained in a high pressure thermogravimetric analyzer (HP-TGA) for chars prepared in the HPFFB facility were reported on a dry, ash-free basis in a previous section. The intrinsic reactivity ($r_{\text{intrinsic}}$) can be viewed as an “overall” intrinsic reactivity, which includes contributions by both the char surface activity and the “available” reaction area. However, it is difficult to quantify these effects individually. By normalizing the reactivity by the char internal surface area, the effect of char surface property on reactivity can be determined. It was difficult to obtain the initial char reactivity at 0% char burnout because of instabilities at the beginning of each HPTGA experiment. The intrinsic reactivities of Pitt #8, Ill #6, and KRL coal char were therefore taken from the time at which 5% char burnout was achieved in the HPTGA. The surface areas used in the normalization were measured using the original char. These surface area values were assumed not to change after 5% char burnout at the low temperature conditions used in the HP-TGA experiments.

It is not clear in the literature which surface area measurement can be treated as the “available area” for char oxidation, even at the relatively low TGA reaction temperatures. Both N_2 and CO_2 surface areas were therefore used to reduce the data. The values obtained may not precisely reflect the true active surface area, but can provide a qualitative insight into the effect of char surface area on reactivity.

Figures 2.7-2.9 show HP-TGA reactivity data for the Ill #6, Pitt #8, and KRL coals, respectively. The intrinsic reactivity has units of $\text{g}/(\text{g}\cdot\text{sec})$ and was multiplied by 10^3 in this figure, while the normalized reactivity has units of $\text{g}/(\text{sec}\cdot\text{m}^2)$ and was multiplied by 10^5 in this figure for comparative purposes. For all coals, the reactivity normalized by CO_2 surface area was smaller than the rate normalized by N_2 , since the CO_2 surface area

is always larger than the N₂ surface area. The normalized reactivity remained relatively constant as a function of pressure for the Illinois #6 coal and the lignite for both the CO₂ and N₂ surface area; more pressure dependence was seen in the non-normalized intrinsic reactivity for these chars. The Pitt #8 char data at 2.5 atm showed one inconsistent data point for the reactivity normalized by the N₂ surface area, otherwise the normalized data showed a minimal change with pressure.

These results imply that the decrease in intrinsic char intrinsic reactivity is mainly due to changes in the internal surface area. Chars prepared at low pressure have larger internal surface areas available for low temperature oxidation. The temperatures used in the TGA experiments were low enough to minimize the effects of pore diffusion. Differences in char chemical structure, as indicated by the H/C and O/C ratios, can not explain the difference in reactivities observed at different pressures. This observation of the importance of internal surface area is somewhat consistent with the results of Roberts et al. (2003) However, in the current study, it is hard to distinguish the relative importance of CO₂ versus N₂ surface area, since almost the same trend was observed for

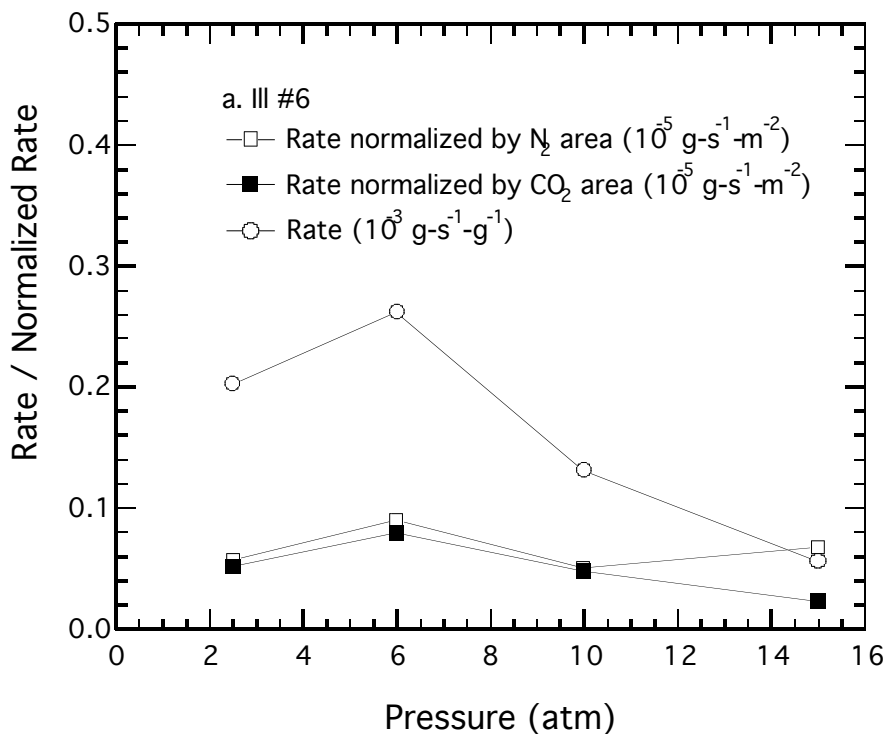


Figure 2.7. Ill #6 char reactivity and normalized reactivity.

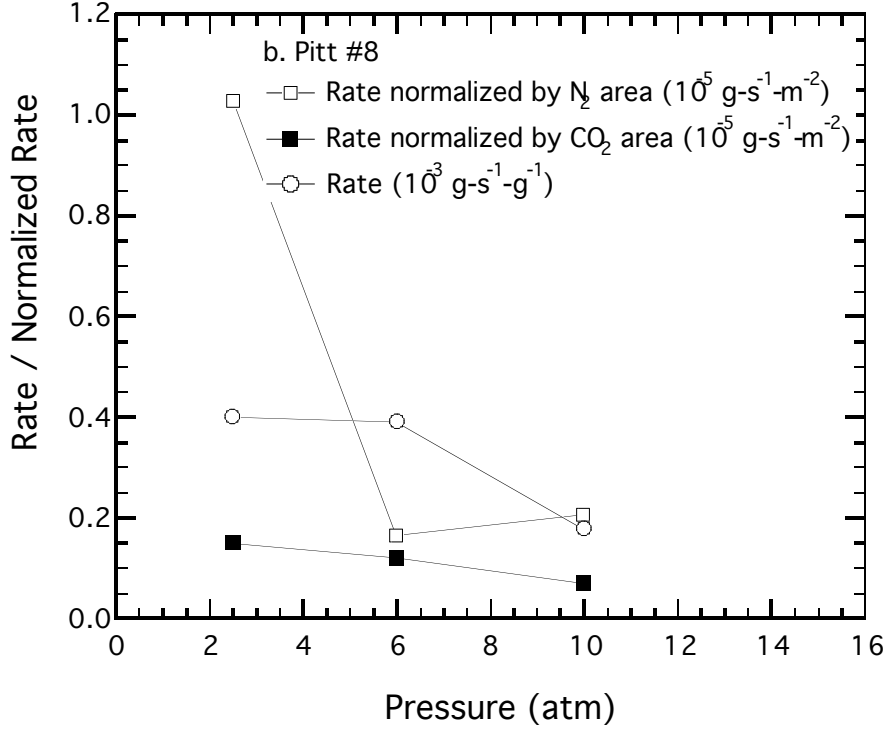


Figure 2.8. Pitt #8 Char reactivity and normalized reactivity.

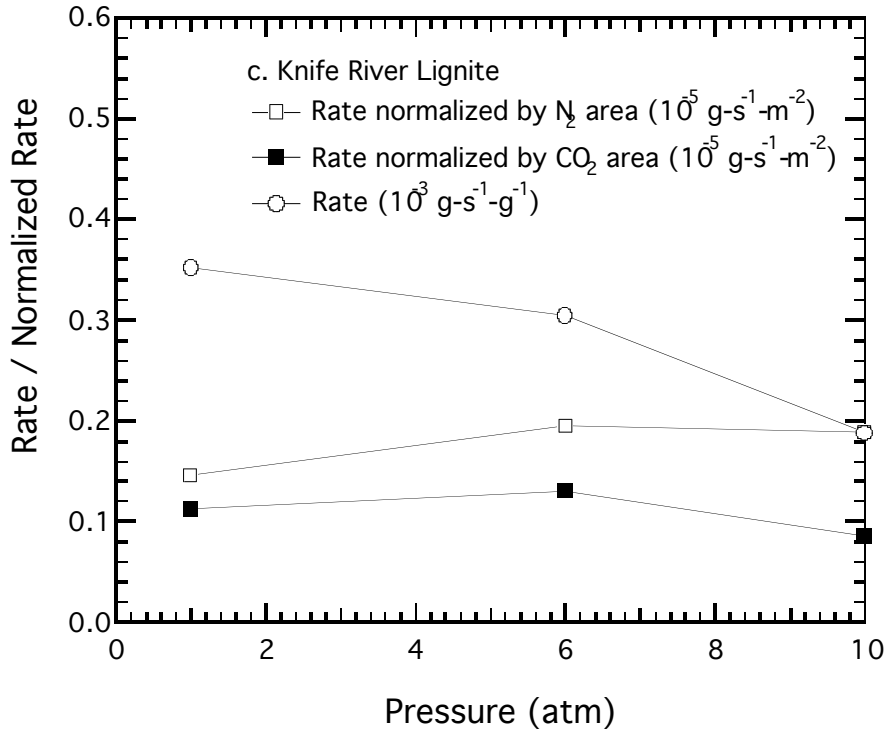


Figure 2.9. KNL char reactivity and normalized reactivity.

each surface area normalization. Further studies are still required to determine the correct available surface area that describes char oxidation as a function of pressure.

2.6 Chapter 2 Conclusions

A flat-flame burner was used in a high pressure laminar flow facility to conduct high temperature, high heating rate coal pyrolysis experiments. Particle heating rates were approximately 10^5 K/s, which is higher than in conventional drop tube experiments. Char samples from coals such as Pitt #8, Ill #6, Ken #9 coal, and lignite were collected at 1300°C at 2.5, 6, 10, and 15 atm.

TGA char oxidation reactivities were measured at the same total pressure as the char preparation pressure. The general trend was that the TGA reactivity on a gram per gram available basis decreased with increasing char formation pressure for both Pitt #8 and Knife River lignite coal chars. The Pitt #8 char intrinsic activation energy and oxygen reaction order remained relatively constant with increasing pressure.

The intrinsic char- O_2 reactivity was measured in a HP-TGA on a $\text{g/g}_{\text{avail}}\text{-s}$ basis. The intrinsic reactivity at 5% char burnout was then normalized by either the N_2 or CO_2 internal surface area. The resulting normalized reactivity was found to be relatively constant with increasing pressure for both the N_2 and CO_2 normalizations. The reactivity that was normalized by the N_2 surface area was higher than that normalized by the CO_2 surface area, as expected. The fact that the normalized reactivity is constant with pressure strongly implies that the majority of the change in char reactivity with pressure can be attributed to changes in internal surface area.

**CHAPTER 3 ELEVATED PRESSURE, HIGH
TEMPERATURE COAL OXIDATION
EXPERIMENTS AND MODELING**

3.1 Literature Review

A review of published data from high pressure coal combustion and char oxidation experiments is listed in Table 3.1.

Table 3.1 Test Conditions for Various High Pressure Oxidation Rate Measurements

Investigator(s)	Fuel	diameter (μm)	T_p (K)	P_{total} (atm)	x_{O_2} (%)
Monson (1992)	chars	63-75	1300-2100	1-15	5~21
Mathias (1996)	Coals, chars	6, 9 mm	900-1300	0.86-5	6-18
Ranish and Walker (1993)	graphite	flakes	733-842	1-64	100
Banin et al. (1997)	chars	~6	1200-1800	8	0-100
Croiset et al. (1996)	chars	90-106	850-1200	2-10	1.5-10
Moors, J.H.J (1999)	char	<10	1300-3000	6-11	0-100
Roberts and Harris (2000)	chars	600-1000	723	15	50
Hecker et al. (2002)	chars	64-76	598-723	1-32	2.5-80

Monson (1992) investigated high-pressure and high-temperature char oxidation using a high-pressure controlled-temperature profile drop-tube reactor. The measurements were performed for Utah and Pittsburgh coals at reactor temperatures between 1000 and 1500 K and total pressures of 1, 5, 10 and 15 atm. At constant oxygen mole fractions (0.05, 0.10 and 0.21), increasing total pressure from 1 to 5 atm led to a slight increase in the reaction rate, with the rate decreasing with further increases in total pressure from 5 to 15 atm. Monson (1992) used a global n -th order char oxidation model to fit his data. The calculated apparent rate coefficients showed significant pressure dependence, since both the activation energy and frequency factor decreased with increasing pressure. Since these rate coefficients should not vary with pressure, this appears to show that the global n^{th} order approach is inadequate in modeling char oxidation rates when total pressure is varied.

Mathias (1996) performed oxidation experiments on char particles of mostly 8-mm diameter with a Cantilever Balance Attachment (CBA) in a drop tube reactor. The gas temperatures were 825, 1050, and 1200 K (measured by a type-S thermocouple 1.2 cm

above the particle). The gas velocities were 0.08, 0.32, and 1.28 m/s. The pressures tested were 0.86, 3.0, and 5.0 atm. Major findings included: 1) An increase in the partial pressure of oxygen resulted in a significant increase in the char oxidation rate on the runs performed at atmospheric pressure; 2) An increase in total pressure, while maintaining the same partial pressure of oxygen, drastically decreased the oxidation rate; 3) Increasing the total pressure from 0.86 and 5.0 atm while maintaining oxygen mole fraction at 21% produced a small increase in the oxidation rate; 4) Correlating the oxidation rate to the mole fraction of oxygen rather than to the partial pressure of oxygen better described the trends in the experimental data.

Ranish and Walker (1993) studied the oxidation rates of highly crystalline graphite flakes at oxygen pressures between 1-64 atm and temperatures ranging from 733-842 K. The global activation energy (defined as the slope of the log [reaction rate] vs. $1/T_p$ curve, the term “global” arising from the fact that the form of the reaction rate is unknown) for the reaction was found to be 204 ± 4 kJ/mole and was independent of carbon burnout. The intrinsic reaction order decreased from 0.83 to 0.69 as the reaction temperature increased from 733 to 813 K

Banin and Veefkind (1997) studied the combustion behavior of pulverized char in drop-tube experiments. The gas temperature was varied between 1200 and 1800 K and the gas pressure was about 8 atm. The oxygen partial pressure was varied between 0.3 and 8 atm. In all cases, 95% of the coal and char particles had diameters less than 6 μm . The apparent reaction order at high oxygen pressure was observed to be as low as 0.3. This could not be explained as Zone I combustion since the char particles were observed to burn with shrinking diameters, and the particle temperatures (1480 ~ 2850 K) were beyond the temperature range where Zone I combustion typically occurs.

Croiset (1996) performed combustion experiments on Westerholt bituminous coal char in a fixed-bed reactor at 2, 6, and 10 atm and temperatures between 850 and 1200 K with particle diameters in the range of 90-106 μm . The reported reaction was first order in both Zone I and Zone II. The pre-exponential factor, A , decreased when the total

pressure increased from 2 to 6 atm. Above 6 atm, the effect of total pressure was very weak. High pressure also favored the combustion regime controlled by pore diffusion. Attempts were made to apply the Langmuir rate equation to these data. However, the mole fraction of oxygen was used instead of the oxygen concentration. The theoretical basis behind the use of between the mole fraction and concentration needs to be explored.

Moors (1998) investigated combustion of Göttelborn char in a high temperature and high pressure shock tube. The particle temperature varied between 1300-3000 K. The total gas pressure varied between 0.6-1.1 MPa. He concluded that the combustion of Göttelborn char particles occurs in the rough-sphere regime (defined by Moors as regime in which the external surface area of the particle is much larger than the internal surface area involved in the combustion process). The penetration of oxygen into the pores was small. Internal transport of reactant had no influence on the apparent kinetics. Based on an energy balance, a mass balance and a carbon dioxide production calculation, the kinetics were found to be of a Langmuir type. Adsorption of oxygen at active sites determines the overall reaction rate at partial pressures higher than about 0.4 MPa. The reaction order decreased from unity to zero when the oxygen partial pressure increased. When internal transport influenced the apparent combustion kinetics, the reaction order decreased to one half as the pressure increased. Moors also found that the particle size distribution and the temperature history of the particles influenced the kinetic reaction rates obtained. The shock tube gave smaller activation energies than other reactors. This difference was due to a difference in burnout time and a more pronounced influence of thermal annealing for the reactors with a longer burnout time.

Roberts (2000) measured the intrinsic reactivities of two Australian coal chars (produced at 1100°C nitrogen for 3hr) to O₂, CO₂, and H₂O at pressures up to 30 atm. Measured reaction orders in CO₂ and H₂O were not constant over the pressure range investigated, whereas reaction order in O₂ was unchanged. The differences in reaction order transition appeared to be related to the rate of the reaction. Activation energies of all three reactions were not found to vary as the pressure was increased. These results demonstrated that a physical rather than a chemical change is the reason for the observed variations in the

apparent reaction order. However, the authors pointed out a need for high-temperature high-pressure measurements of reactivities in order to validate their conclusion.

Hecker et al. (2003) examined the intrinsic oxidation of two coal chars prepared at high temperature and high heating rate at atmospheric pressure. High pressure TGA experiments were conducted over a pressure range of 1 to 32 atm, a temperature range of 598 to 823 K, a range of oxygen partial pressures from 0.03 to 12.8 atm, and a burnout range of 20 to 60%. Under these conditions, it was found that intrinsic char oxidation rate, determined on a g/g_{actual} -s basis, was independent of char burnout level, and that kinetic parameters were not affected by changes in total pressure. More specifically, under the conditions of this study, intrinsic char oxidation rate, activation energy, and oxygen reaction order were found to be independent of total pressure. It was also reported that the n th order kinetic model fits both atmospheric and elevated pressure char oxidation data very well, with $n = 0.7$ for both chars studied.

In summary, elevating reaction pressure increases char oxidation reactivity. The reaction rate may be almost independent of total pressure at total high pressure. Char oxidation rates at elevated pressure may increase with an increase in total pressure from atmospheric pressure to almost 10 atm, and then reduce at even higher pressure.

More work should be performed in order to firmly establish the kinetics of high pressure char oxidation. One particular area that should be studied is the intrinsic kinetics of chars produced at elevated pressure. Chars produced at elevated pressures may exhibit different behavior compared to chars produced at atmosphere pressure. In addition, it is possible that the internal surface area of the char changes significantly as experimental conditions vary. Many mechanistic models of intrinsic reactivity normalize the reactivity by the internal surface area. Changes in the internal surface area may account for the changes in reactivity with total pressure or burnout predicted by some of these models. Finally, high temperature, high pressure char reactivity data are needed.

3.2 Objectives

The objectives of this chapter are: (1) obtaining the char high temperature, high pressure reactivity data, (2) modeling of char combustion process using char burnout kinetic model (CBK).

3.3 Conditions of Combustion Tests

3.3.1 Coal Selection

Coal oxidation experiments were performed with three fuels: two size fractions of Pittsburgh #8 (63-76 μm , 90-125 μm) and one size fraction of Illinois #6 (74-90 μm). These are common U.S. coals that have been widely studied in char oxidation experiments. Samples of the coals were ground, dried and stored in refrigerator before experiments.

3.3.2 Experimental Conditions

All of elevated pressure coal combustion experiments were conducted using the methane-air high-pressure flat flame burner (HPFFB) that is described in Chapter 1. Three kinds of Coal were injected into the HPFFB, varying O_2 concentration, residence time, and total pressure.

The previous high-pressure char combustion experiments (Banin and Veefkind, 1997; Croiset et al., 1996; Mathias, 1996; Monson, 1992; Monson et al., 1995; Moors, 1998; Ranish and Walker, 1993) were usually conducted using char formed at atmosphere pressure. The use of the same starting char was convenient for char kinetic analysis. Unfortunately, this approach neglected changes in the characteristics of the chars due to pressure. Several char oxidation kinetic models have been developed and applied to explain several sets of high-pressure char oxidation data (Hong et al., 2000; Niksa et al., 2003). This study will only compare previously-developed models to the char oxidation data obtained in this project.

In this study, parameters such as coal type, coal size, total pressure, bulk oxygen composition, and reaction distance were varied during the experiments. Two sizes of Pitt #8 coal were tested. Samples of Ill #6 coal char were collected at two reaction distances to test residence time effects. The test matrix for all of the coal oxidation experiments conducted is shown in Table 3.2.

Table 3.2 Matrix of Coal Oxidation Experiments^a

	P _{Tot} = 1 atm	P _{Tot} = 6 atm	P _{Tot} = 10 atm
Pitt #8 (63-76 m)	0-19.24 % O ₂	0-9.76 % O ₂	N/A
Pitt #8 (90-125 m)	0-19.24 % O ₂	0-9.76 % O ₂	0-11.97 % O ₂
Ill #6 (74-90 m) (ST*)	0-15.13 % O ₂	0-9.76 % O ₂	0-8.69 % O ₂
Ill #6 (74-90 m) (LT**)	0-15 % O ₂	0-12.4 % O ₂	N/A

* Short reaction distance

** Long reaction distance

^aall concentration are given in mol%

The post-flame O₂ concentration was adjusted by changing the CH₄/air ratio. The desired flow rates of each gas were first calculated using an equilibrium code such as NASA-Lewis code, and were controlled by adjusting the mass flow controllers. The oxygen concentration for each condition was examined using an O₂ monitor.

3.3.3 Gas Temperature Profile

The particle residence time is an important factor affecting the char burning rate. The reaction length was determined by measuring the distance from the burner to the collection probe.

Gas temperature profiles were measured for each reaction condition before char collection experiments were conducted. At each pressure, the flow rates of CH₄ and air were held constant, and the O₂ flow rate was adjusted to control the post-flame O₂

concentration. The flow rates of CH₄, air, and O₂ used in different experiments are shown in Table 3.3. Thermocouple measurements of gas temperature were adjusted for the effects of radiation, and are shown in Fig 3.1. These temperature profiles show two characteristics: (1) the dramatic decrease of temperature versus distance from about 1700 K to 1000 K at 2.5 atm, or to 700 K at 10 atm; and (2) the fact that gas temperature remained relatively constant at a given pressure when the O₂ concentration was changed from 0-15 mol%.

Table 3.3 Gas Flow Rates Used in the HPFFB

	Post flame O ₂ concentratio	CH4 (l/min)	Air (l/min)	O2 (l/min)
1 atm	5.75%	1.74	16.55	1
	9.76%	1.74	16.55	2
	15.13	1.74	16.55	3.3
6 atm	2.98%	2.16	20.5	0.7
	4.97%	2.16	20.5	1.25
	9.76%	2.16	20.5	2.5
	12.44%	2.16	20.5	3.3
10atm	4.97%	2.49	23.5	1.25
	5.67%	2.49	23.5	1.6
	9.76%	2.49	23.5	2.5
	9.86%	2.49	23.5	2.9

* All concentrations are given in mole percent.

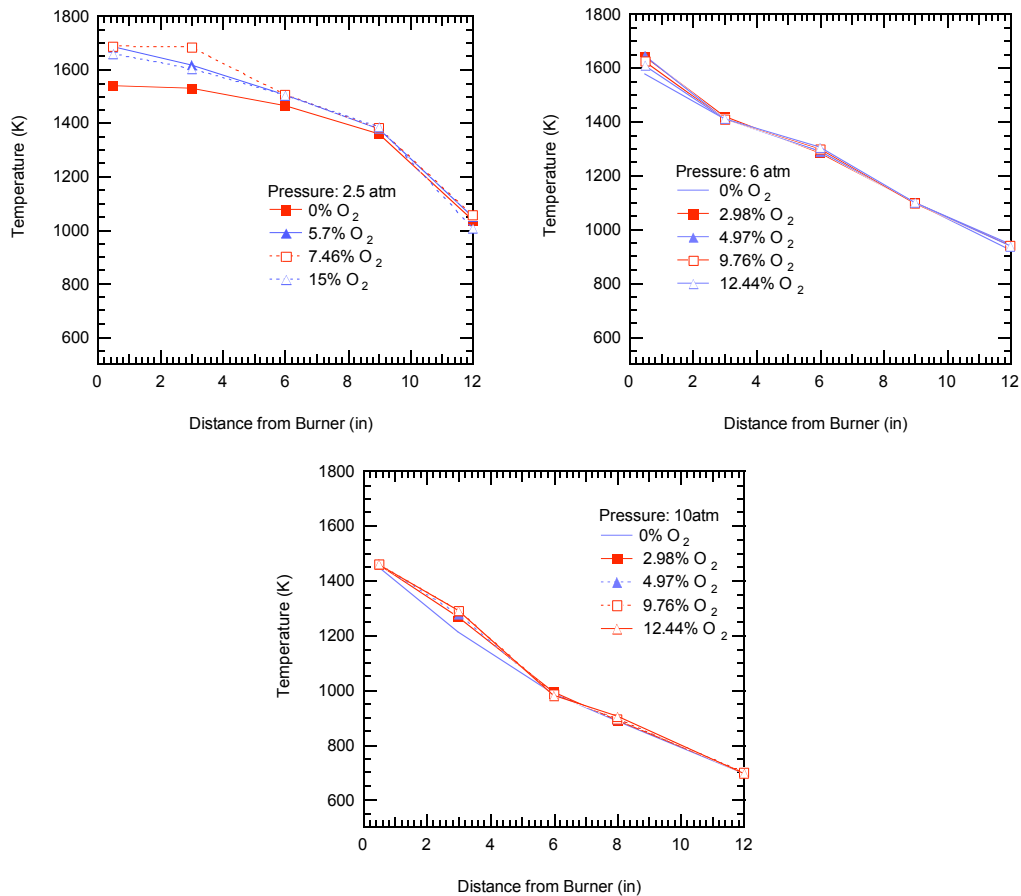


Figure 3.1. Measured gas temperature profiles in the HPFFB at different pressures and oxygen concentrations.

3.4 Results and Discussion

3.4.1 Variations in Char Properties during Combustion

Figures 3.2-3.5 show the mass release for four sets of coal combustion experiments vs. O₂ molar fractions at different pressures. Mass release is reported here based on (a) the parent daf coal (solid lines), and (b) the initial char collected at 0.5% O₂ (dashed lines).

The change in char properties vs. post-flame O₂ concentration for a given is thought to be small.

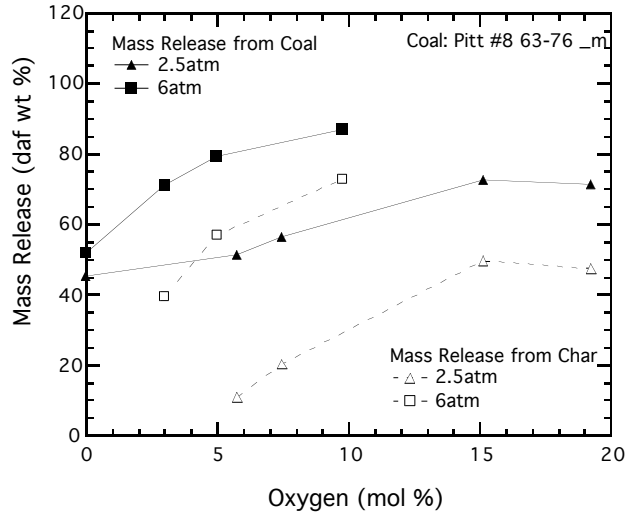


Figure 3.2. Measured mass release of Pitt #8 coal (90-125 μm) during combustion experiments at different pressures and O_2 concentrations. Open symbols represent the data on a %char burnout basis, whereas closed symbols are normalized to the initial amount of dry ash-free coal.

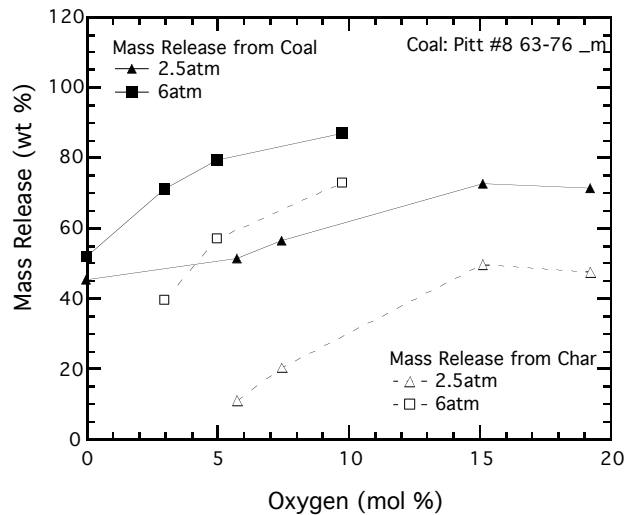


Figure 3.3. Measured mass release of Pitt #8 coal (63-76 μm) during combustion experiments at different pressures and O_2 concentrations. Open symbols represent the data on a %char burnout basis, whereas closed symbols are normalized to the initial amount of dry ash-free coal.

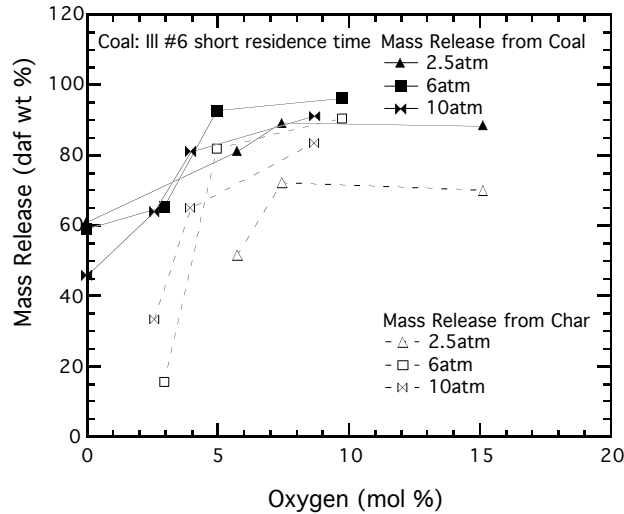


Figure 3.4. Measured mass release of Ill #6 coal (short reaction distance) during combustion experiments at different pressures and O₂ concentrations. Open symbols represent the data on a %char burnout basis, whereas closed symbols are normalized to the initial amount of dry ash-free coal.

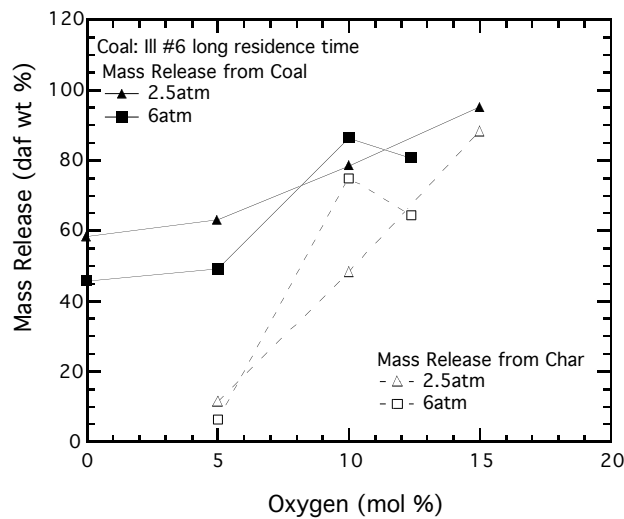


Figure 3.5. Measured mass release of Ill #6 coal (long reaction distance) during combustion experiments at different pressures and O₂ concentrations. Open symbols represent the data on a %char burnout basis, whereas closed symbols are normalized to the initial amount of dry ash-free coal.

Unfortunately, due to the constraint of achieving similar temperature profile, the residence times varied for each pressure conditions. This also changes the particle

temperature profile. All of these factors made it difficult to interpret the mass release data directly, and hence the mass release data were modeled using the CBK model.

Figure 3.6 shows of N_2 BET surface areas of chars collected at different post-flame O_2 conditions and pressures. In this study, higher O_2 concentrations corresponded to higher extent of burnout (Figures 3.2-3.5) and lower N_2 surface areas. As shown for the Pitt #8 chars, the N_2 surface areas initially increase vs. O_2 concentration for some pressure conditions and then decrease at elevated pressures.

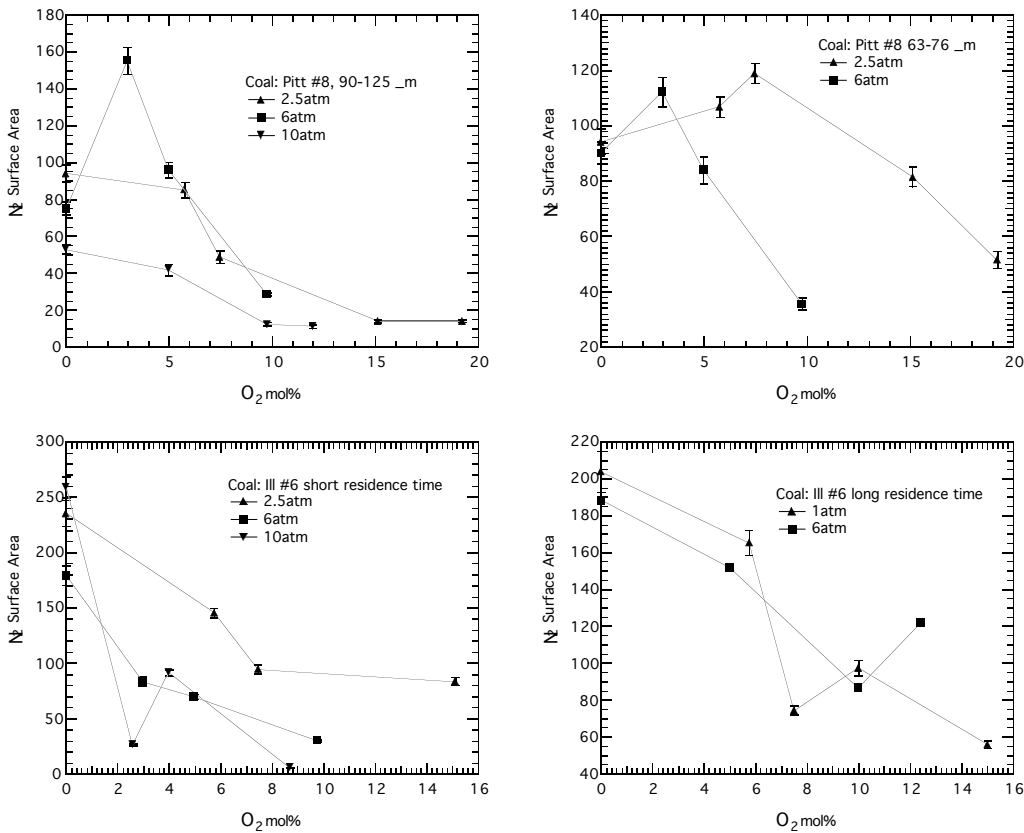


Figure 3.6. Nitrogen surface areas of char particles during combustion experiments at different pressures and O_2 concentrations.

No such initial increase in N_2 surface area was observed for the Ill #6 coal chars, or for some of the pressures for the Pitt #8 coal chars. For Ill #6 coal at both long and short residence time experiments, N_2 surface areas decrease with the increase of burnout. The change of char surface area with burnout is related to the evolution of pore structure. For the Pitt #8 coal chars, the opening of closed-off pores contributes to the initial increase of

surface area, followed by decreases in surface area due to the merging and coalescing of pores (Mitchell, 2003). The evolution of pore structure with burnout of Ill #6 coal did not display the initial increase, possibly caused by the different character of pore structure. Values of d/d_0 for the char samples, determined based on the initial coal diameter, are plotted versus the O_2 concentrations in Figure 3.7. The values of d/d_0 are calculated using the same method described in Chapter 2, which assumes a constant packing ratio. Values of d/d_0 , calculated based on the char produced at 0.5 mol% O_2 , are plotted against char burnout in Figure 3.8. The particle diameter ratio swelling ratio based on coal decreased with increasing O_2 concentration for all four conditions. For the Pitt #8 coal, the larger size coal reached a larger diameter ratio than the smaller size coal. The swelling ratio based on the char generally decreased with increasing char burnout. However, values of

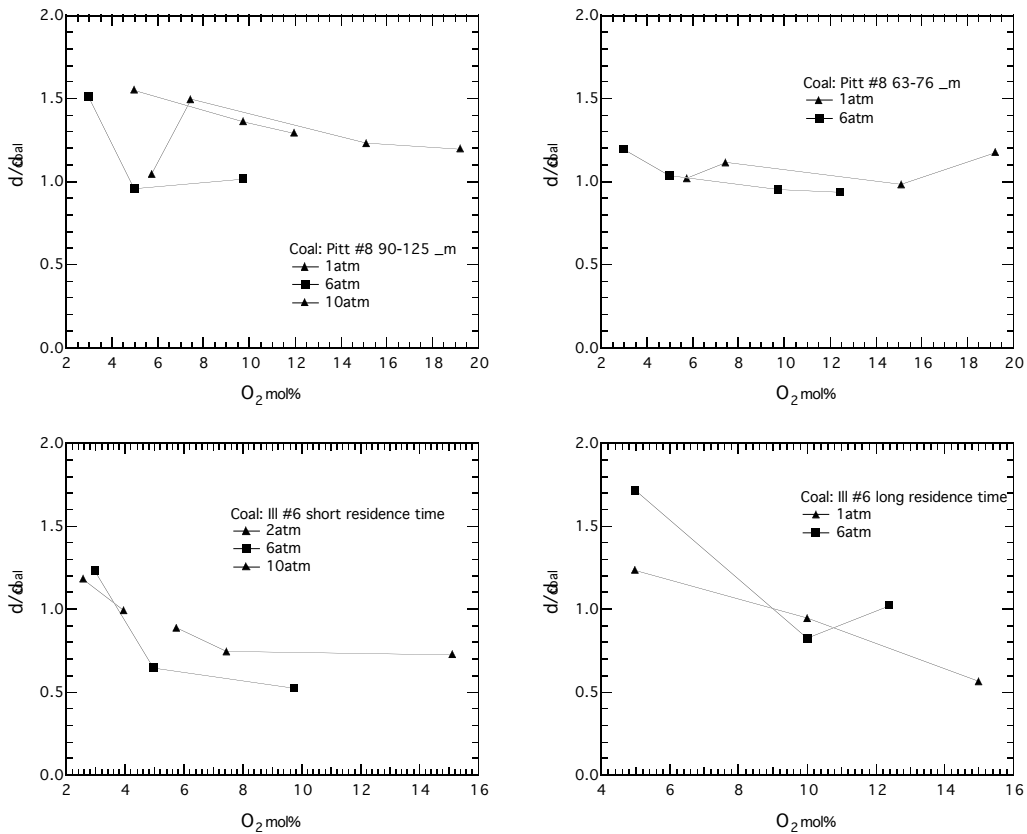


Figure 3.7 Diameter ratios of char particles during combustion experiments at different pressures and O_2 concentrations. The initial coal diameters were taken from measurements of unreacted coal.

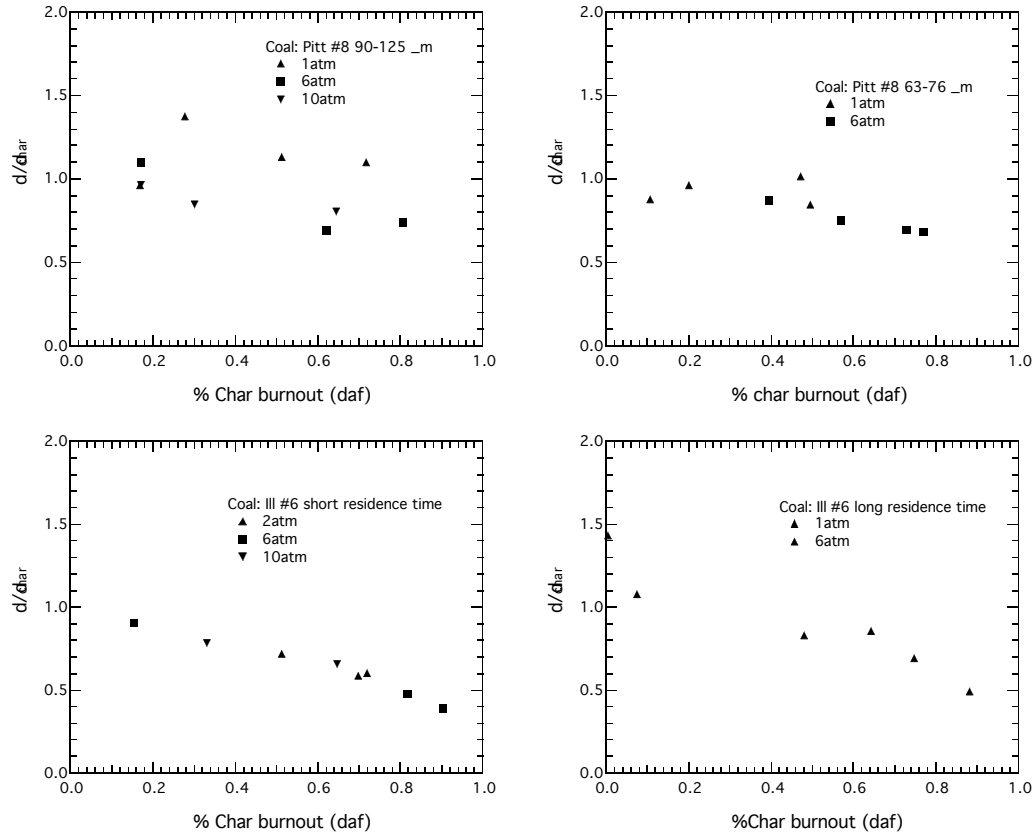


Figure 3.8 Diameter ratios of char particles during combustion experiments at different pressures and O₂ concentrations. Initial char diameters for normalization are taken from char formed at 0.4 mol% O₂ concentration.

d/d_{char} greater than one were obtained, such as for the Pitt #8 90-125 i m char. This is possibly caused by the uncertainty of experiment condition, or the effect of varying O₂ content. In contrast, the diameter ratio (based on coal) of Ill #6 char in Figure 3.7 decreased quickly with increased O₂ concentration, and the diameter ratio based on char decreased to 0.5 at about 85% burnout, regardless of the experimental condition or the O₂ concentration.

3.4.2 Modeling of Gas and Particle Temperature Profiles

The gas and particle temperature profiles are critical in order to precisely model the char oxidation process. Gas temperature and particle velocity profiles for each condition were modeled using FLUENT. The centerline gas temperature profile for each condition was measured and used to validate the reliability of modeling results. The model assumed that

the inlet natural gas is reacted instantaneously to equilibrium. The composition of post-flame products was modeled using an equilibrium code, and was then used as input parameters in the FLUENT calculation. The geometry of the FLUENT modeling is shown in Figure 3.9. The reaction tube length is 321 mm, and the radius is 25 mm. The radius of the feeding tube is 2.38 mm.

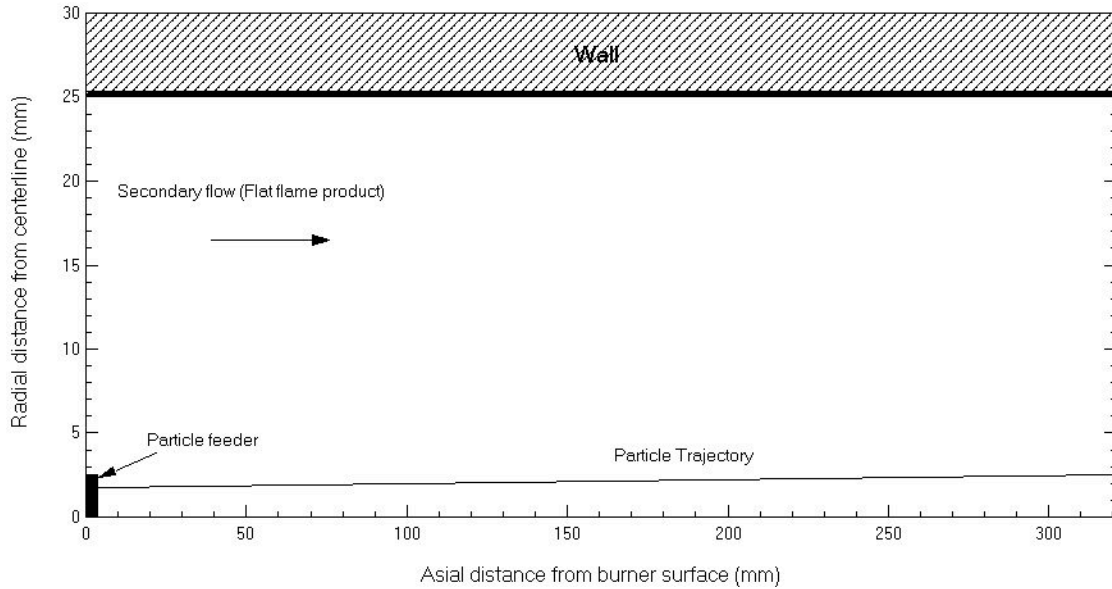


Figure 3.9. Geometry and particle trajectory used in the FLUENT calculations.

Coal particles entrained by N_2 entered the reaction zone through a centerline feed tube. The average inlet radial entrance location of particles is assumed to be the area-averaged radius of the feeding tube, which is 1.68 mm from the centerline. Since the particle temperature is affected by the injection position, the area-averaged is reasonable based on the assumption that the particle is evenly distributed in the entraining N_2 flow. The primary gas velocity was set close to the secondary velocity in these experiments to minimize the radial dispersion of the particle. Observations of the particle trajectory at the outlet of the reaction tube indicated that particles flowed along the centerline. In this study, several coal particle size ranges were used, which includes 63-76 μm , 90-125 μm , and 74-90 μm . Average particle sizes of 69.5 μm , 107.5 μm , and 82 μm were used in the modeling. Since coal (not char) was used in combustion experiments, it is important to model both the pyrolysis and combustion reactions. In this study, the CPD model was used to calculate the time needed for coal pyrolysis. The combustion process was

assumed to begin after the end of pyrolysis. The particle velocity profile was partitioned accordingly.

Figure 3.10 compares the modeled gas centerline temperature profile with the measured temperature profile at 6 atm. To simulate the dramatic heat loss occurred at elevated pressure, wall temperature was decreased with increasing reaction length. By adjusting the wall temperature profile, good agreement was achieved between the modeled and measured gas centerline temperature profile. Once the gas temperature was modeled correctly, the velocity profile from the model was used. The modeled gas temperature profile is comparable with measured temperature profile, except for the temperature point closest to the burner. This is possibly caused by a departure of the thermocouple bead from the centerline.

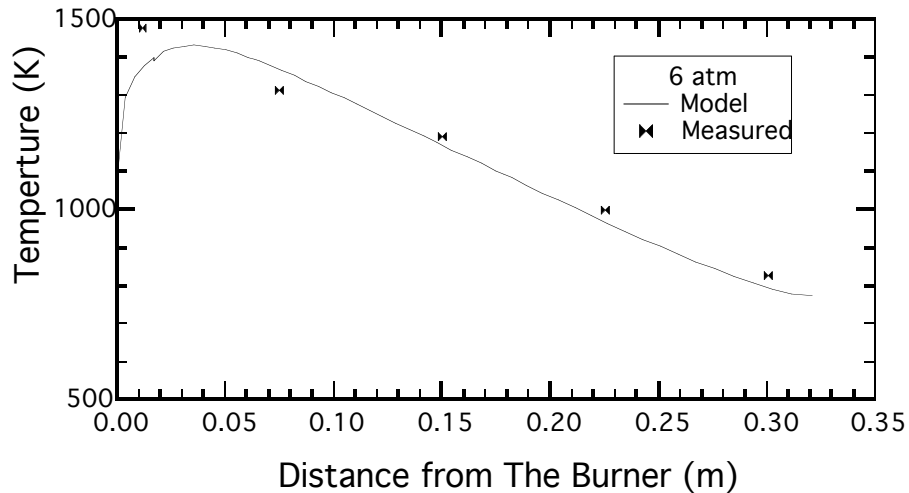


Figure 3.10. Measured and predicted centerline gas temperature profiles for Pitt #8 coal at 6 atm.

Figure 3.11 shows the calculated particle velocity profiles of Pitt #8 (90-125 μ m) at pressures of 2.5, 6, and 10 atm. The velocity decreased dramatically with increased pressure because the gas has a higher density at elevated pressure. In the experiment, the flow rate of inlet gas was increased somewhat to compensate for the decrease in gas velocity. However the compensation was limited because of the necessity (a) to maintain the laminar flow pattern of the reaction gas flow, (b) to stabilize the flat flame, and (c) to

achieve a similar gas temperature profiles. These limitations made it impossible to perform experiments at isothermal conditions and similar residence times. The calculated temperature and velocity profiles were therefore used in char combustion modeling, and transient calculations were performed.

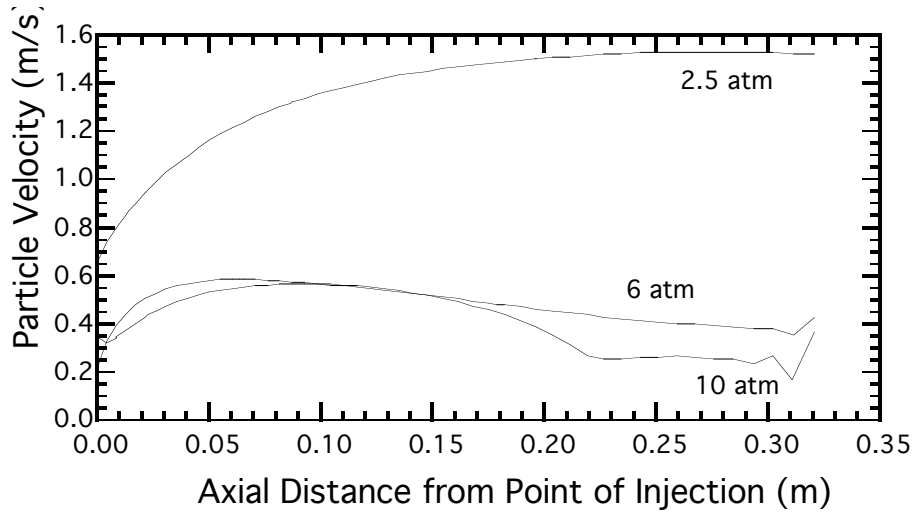


Figure 3.11. Predicted centerline particle velocity profiles for Pitt #8 coal.

3.4.3 High Temperature Char Combustion Modeling

3.4.3.1 Modeling of char combustion process using n-th order kinetic

The n^{th} order kinetic expression, also known as the power-law kinetic expression, usually has a form:

$$r_{gas} = kP_{O_2}^n = A \exp(-E/RT) P_{O_2}^n \quad (3.1)$$

This is the most widely used kinetic form in engineering calculations to account for the oxidation of carbon:



This simple reaction actually exhibits complex kinetic behavior. Among the many kinetic forms published, the n-th order kinetic expression is the simplest form. This form has often been criticized due to its lack of theoretical foundation. Consistent power law behavior was observed in several TGA studies (Hecker et al., 2003; Suuberg et al., 1988), but power law behavior failed to predict the char combustion behavior at high

temperature and high pressure (Monson et al., 1995). Recently, Hurt and Haynes (2004) postulated that surface chemical heterogeneity may result in n-th order kinetic behavior.

In this section, n-th order kinetics were used to model the high-temperature, high-pressure coal combustion kinetic data obtained in this project. Char Burnout Kinetics model 8 (CBK8) was used to model the char combustion process. CBK8 is a kinetics package that describes char oxidations relevant to pulverized fuel combustion processes (Hurt et al., 1998) that uses n-th order intrinsic kinetics. In addition, a separate version of Hurt's model that includes a e-step surface mechanism (CBK/E) was also used (Niksa et al., 2003).

Both CBK8 and CBK/E incorporate a new correlation for the coal swelling ratio (Benfell, 2001):

$$Sw_1 = \begin{cases} 8.67 - 0.0833C_{daf}, & 89 \leq C_{daf} \leq 92 \\ 0.0458 + 0.01459C_{daf}, & 72 \leq C_{daf} < 89 \\ 1.0, & C_{daf} < 72 \end{cases} \quad (3.3)$$

Where C_{daf} denotes the daf carbon content of parent coal, and Sw_1 represents the swelling ratio at atmospheric pressure. A correlation which involves the effect of operating pressure is:

$$Sw = \begin{cases} Sw_1^{0.7143+2.857P_T}, & 0.1 \leq P_T \leq 0.8 \\ Sw_1^{3.5-0.625P_T}, & 0.8 \leq P_T \leq 4.0 \end{cases} \quad (3.4)$$

where P_T is the total pressure in MPa.

Figure 3.12 shows the comparison of the swelling ratios during devolatilization for Pitt #8 and Ill #6 coals that were measured vs. the values calculated using Benfell's correlation. The results from Benfell's model overestimate the swelling ratios of Pitt #8 and underestimate the swelling ratios of Ill #6. This discrepancy is possibly caused by the fact that this correlation does not account for heating rate. Due to the lack of agreement, the measured swelling ratios were used in the char combustion modeling, instead of using the correlation of Benfell.

In the CBK8 model, the initial starting char mass subsequent to pyrolysis is input via a variable named “high-temperature volatile yield (HTVL)”. However, starting char mass changes with pressure. The most rigorous modeling effort is to integrate a complex coal devolatilization model. In this study, coal particle temperature and velocity profiles obtained from FLUENT calculations were used as input for the CPD model. The coal pyrolysis time and volatile yield were calculated from the CPD model calculation and used as input parameters in the char combustion modeling.

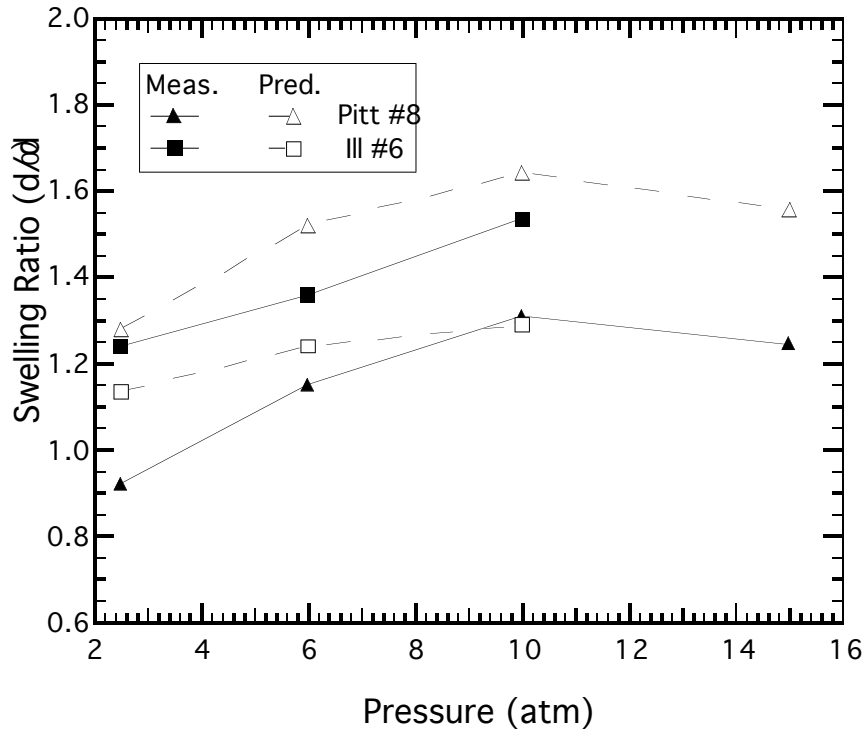


Figure 3.12. Comparison of swelling ratios of Benfell’s model and measured swelling ratios during devolatilization.

CBK8 uses an n-th order relation to calculate the CO/CO₂ ratio, and this relation was used here. The distributed activation energy model of thermal annealing and the ash inhibition model in the CBK models were also used. The CBK models were developed from coals similar to those used in this study and are therefore thought to be applicable.

The n-th order combustion model of char has three parameters: (1) the pre-exponential factor A, (2) the activation energy E, and (3) the Oxygen order n. The Oxygen order n

was assumed to be 0.5 based on Hurt's recommendation (1998). The pre-exponential factor A was correlated with coal carbon mass fraction, and was calculated as follows:

$$A = 10^{14.969 - 0.746 C_{daf}} \quad (3.5)$$

The values of the pre-exponential factor (A) were calculated for the two coals used in this study, are shown in the Table 3.4:

Table 3.4 Pre-exponential Factor (A) Used in CBK8

Coal	A (g/(g*sec*(mol/m ³) ^{0.5}))
Pitt # 8	3.214 × 10 ⁸
Ill # 6	1.019 × 10 ⁹

Using a single pre-exponential factor for each coal provides a basis for comparing char reactivity, which is reflected by the activation energy only. The activation energy E was optimized to find the best fit to the measured burnout data. Figure 3.13 shows a parity plot of the predicted vs. measured burnouts using CBK8. Figure 3.14 is the activation energies (E) used to obtain the best fit of the experimental measurements.

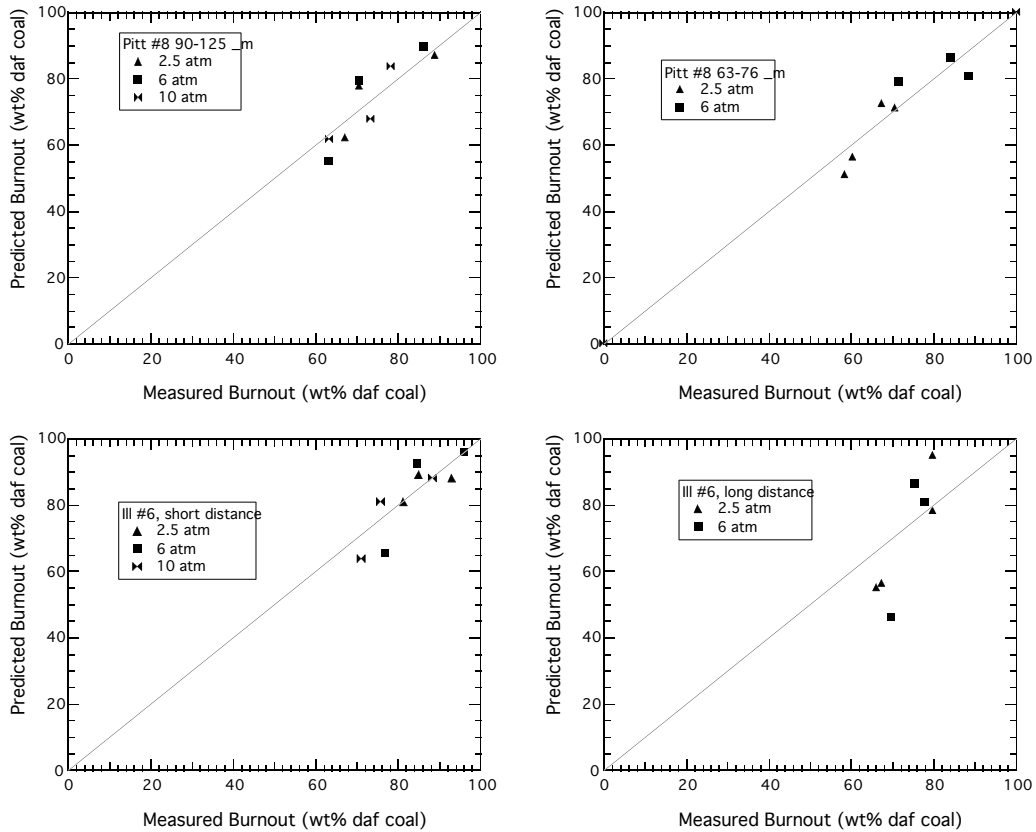


Figure 3.13. Predicted burnouts using of CBK8 versus measured burnouts for the four combustion conditions.

The resulting error between the modeling results of CBK 8 and the measured values of mass release or each coal char are listed in Table 3.5. The relative error is calculated using following equation:

$$\text{Relative error} = \sqrt{\frac{\sum_{i=1}^n (p_i^p - p_i^0)^2}{n}} \quad (3.6)$$

where n is the number of the records modeled; p_i^p is the prediction for the i^{th} record; p_i^0 is the measured value.

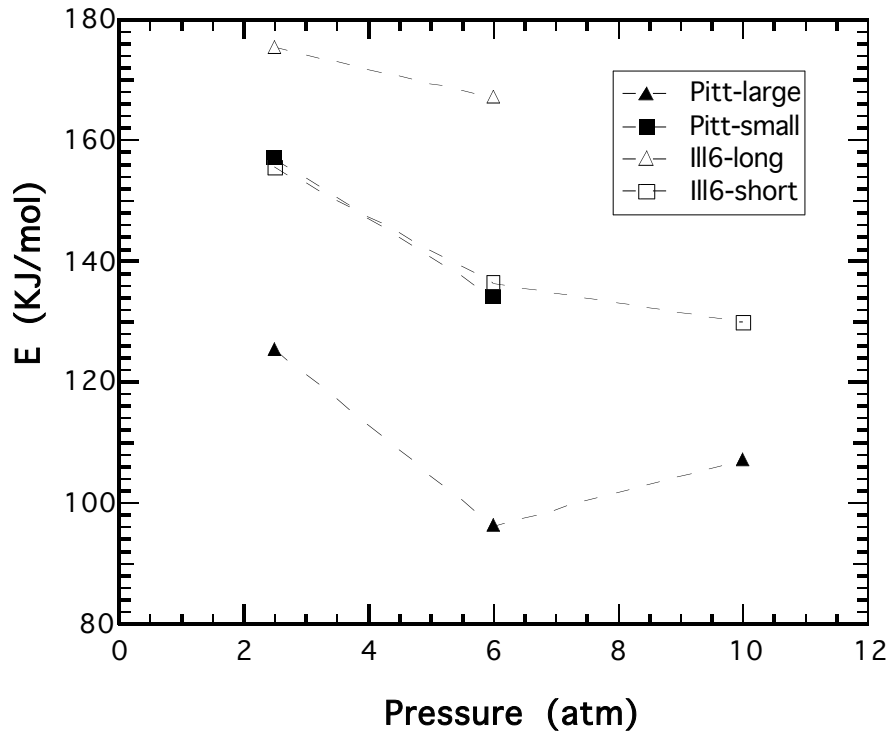


Figure 3.14. Modeled Activation Energy (E) of the best fit for the different pressures.

Table 3.5 Error between Calculations and Measured Values of Mass Release

Coal chars	Error (%)
Pitt #8 large	7.98
Pitt #8 small	8.08
Ill #6 long reaction distance	7.09
Ill #6 short reaction distance	18.20

3.4.3.2 Modeling of Char Combustion Process using 3-Step Kinetics

The Char Burnout Kinetics Extension model (CBK/E) was developed by Hurt et al. (1998), and then was later modified to include a three-step kinetic (Hurt and Calo, 2001):



This model was recently evaluated by comparison with several sets of high-pressure char combustion data (Niksa et al., 2003). Using one adjustable kinetic parameter A_{30} (pre-exponential factor of reaction 3.9) and default values for all other parameters, the model was shown to agree with the reported combustion behavior in many experiments. However, for low-rank coals, the values of A_{30} at high pressure are lower by just over half an order-of-magnitude than those at atmospheric pressure.

In the evaluation of CBK/E (Niksa et al., 2003), all of the data were obtained from combustion experiments on chars produced at atmospheric pressure. In contrast, the major objective of this study is to perform experiments on chars at the same pressure at which they were formed. The char burnout data (Figures 3.2-3.5) are modeled in this section using the CBK/E model.

In the CBK/E model, the char oxidation mechanism includes three reactions Eq. 3.7-3.9. Each reaction is a quasi-global reaction and has a pre-exponential factor A and an activation energy E . The overall rate and CO/CO_2 ratio are controlled by these parameters as follows (Hurt and Calo, 2001):

$$r = \frac{k_1 k_2 P_{O_2}^2 + k_1 k_3 P_{O_2}}{k_1 P_{O_2} + k_3 / 2} \quad (3.10)$$

$$CO/CO_2 = \frac{k_3}{k_2 P_{O_2}} \quad (3.11)$$

Among the six parameters A_1 , A_2 , A_3 , E_1 , E_2 , and E_3 , all activation energies were assigned based on the published char kinetic data (Niksa et al., 2003). The initial pre-exponential factor for k_3 (Step 3) is used to normalize the pre-exponential factors k_1 and k_2 . Thus the controlling parameter for three-step mechanism is the value of pre-exponential factor of reaction 3.9 (A_{30}). The values of E_1 , E_2 , E_3 , and A_{20}/A_{30} , A_{30}/A_{10} are listed in the Table 3.6.

Table 3.6 Kinetic Parameters Used in CBK/E

E_1 (kJ/mol)	25
E_2 (kJ/mol)	117
E_3 (kJ/mol)	133.8
A_1/A_{30}	1.0×10^6
A_2/A_{30}	5.0×10^4

The CBK/E model also uses a generalized internal effectiveness factor and a power-law exponent that relates density changes to the extent of burnout. Proper values were assigned to the kinetic and other submodels. The CBK/E model was included as a subroutine in an optimization software package OptdesX (Parkinson et al., 1992) in order to adjust the kinetic parameters (A_{30}) within pre-set values between 1.0×10^7 and 1.0×10^9 (Niksa et al., 2003) to best fit the experimental data.

Figure 3.15 shows the resulting comparisons of calculated and measured burnouts for the four conditions: Pitt #8 large particle size; Pitt #8 small particle size; Ill #6 short reaction distance; and Ill #6 long reaction distance. Because A_{30} is coal rank dependent and is also affected by the char formation pressure, a unique A_{30} was calculated for different pressures at each condition by minimizing the square error between model predictions and the data.

Effectively, A_{30} represents the “reactivity” of the char, and CBK/E does not have a mechanism to deal with the effect of pressure on char characteristics. Therefore, the variation of A_{30} is a measure of the effect of formation pressure on char reactivity.

The resulting errors associated with the best fit coal burnout results from CBK/E at different conditions, as shown in Figure 3.15, are listed in Table 3.7. The optimal values of A_{30} with pressure are shown in Figure 3.16.

Table 3.7 Error of the CBK/E model results

Coal chars	Error (wt%)
Pitt #8 large	10.44
Pitt #8 small	8.99
Ill #6 long reaction distance	7.88
Ill #6 short reaction distance	20.23

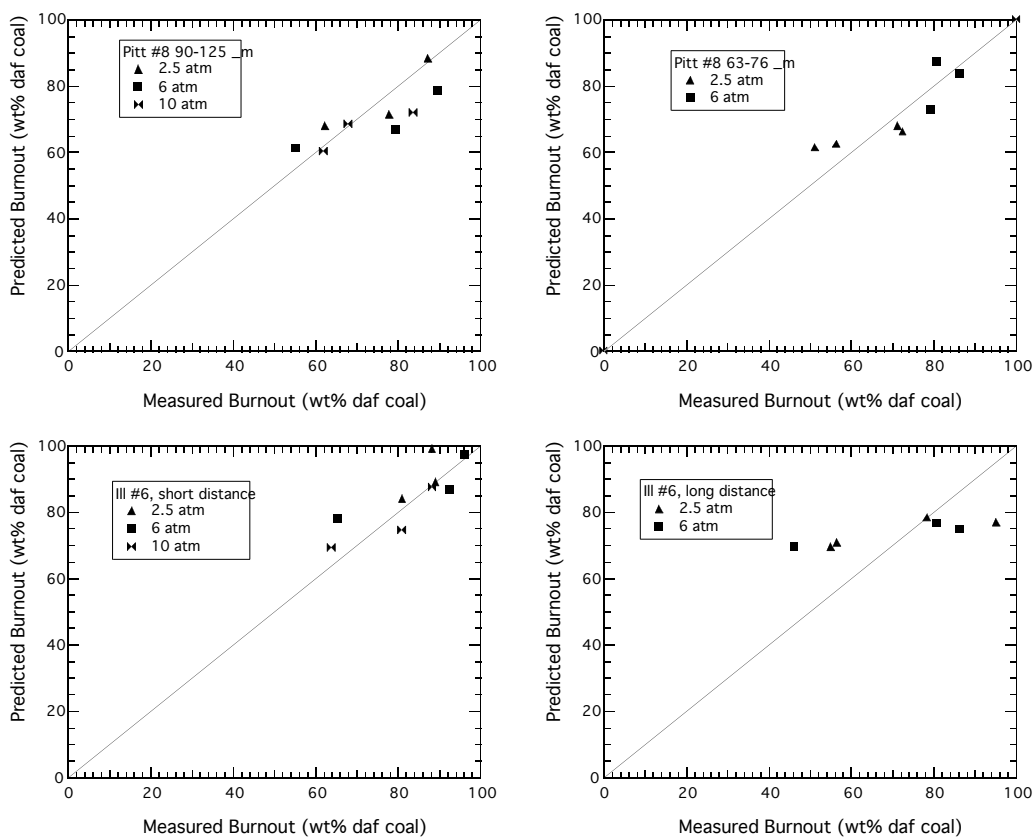


Figure 3.15. Predicted burnouts using CBK/E versus measured burnouts for the four combustion conditions.

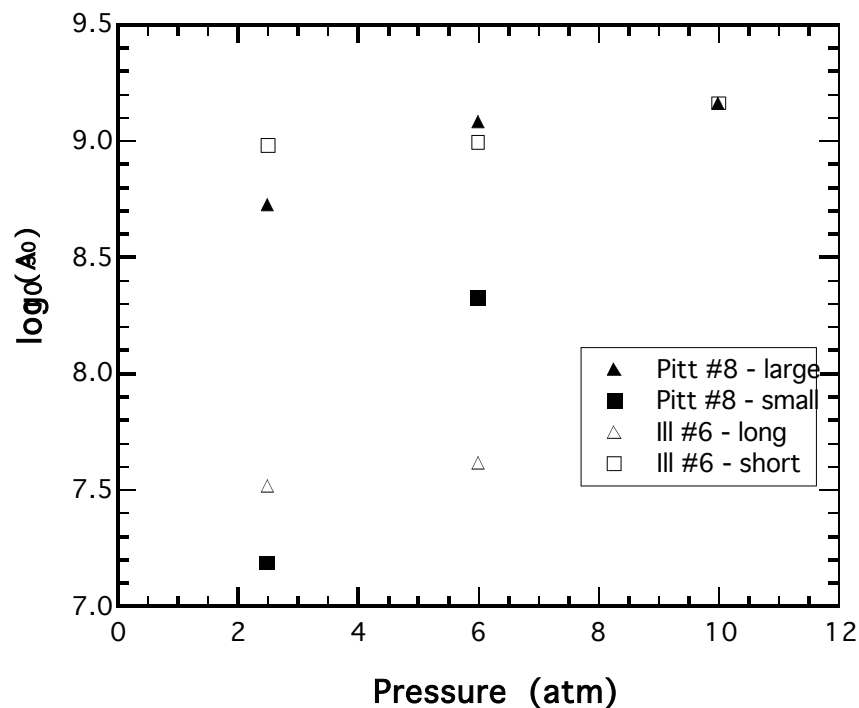


Figure 3.16. Best-fit values of A_{30} for the four combustion conditions.

3.4.3.3 Discussion

Both an n^{th} -order (CBK8) and a 3-step surface mechanism (CBK/E) were used to model char combustion for two coals as a function of pressure. The n^{th} -order modeling results indicated that activation energies decreased by about 20% as pressure increased from 20 to 10 atm. The values of E calculated were within the range of 100 to 180 kJ/mol (24~43 kcal/mol), which is the range of reported activation energy in the most char oxidation experiments. The decreased activation energy with elevated pressure represents the increasing reactivity with increasing pressure.

Drastic changes in activation energy with pressure were reported by Monson et al. (1995), although their results were influenced by using chars formed only at atmospheric pressure and by the limitations of their 2-color pyrometer. It is not clear that the n^{th} -order kinetic model is correct, and hence a more mechanistic model was also used.

The CBK/E model was compared with the high pressure char oxidation data obtained in this project. Only one adjustable parameter (A_{30}) was used in the CBK/E calculations, with reasonable results. However, a different value of A_{30} was needed for each experimental condition for each coal, indicating that the effect of pressure on char properties affected reactivity as well.

The effect of the total pressure on char oxidation kinetics has been studied for decades, and the reported results do not seem consistent. Several reviews (Hong, 1999; Niksa et al., 2003; Wall et al., 2002) and the literature review of this chapter summarize the previous elevated pressures char oxidation studies. The char oxidation data available for comparison to this study have to meet the requirements such as high-temperature (Zone II temperature), pulverized coal size ($<100 \mu\text{m}$), and single particle behavior. Among the data that meet these criteria are:

1. Monson (1992), who reported that char oxidation rate increased with increasing pressure from 1-5 atm, then decreased at pressure from 5-15 atm;
2. Joutsenoja et al. (1999) and Saastamoinen et al. (1996), who reported that char burnout rate decreased at elevated total pressure
3. Cope et al. (1989) and Wall et al. (1999), who found that increasing total pressure increased the char oxidation rate.

Though it is not the mission of this study to analyze these data, comprehensive analysis can be found in three reviews (Hong, 1999; Niksa et al., 2003; Wall et al., 2002). The diversity of different results may be caused by the experimental technique and/or the respective data analysis.

It is well-known that char burnout is a function of char properties (e.g., ρ , pore structure and evolution, internal surface area, and elemental composition), reaction kinetics, and reaction conditions (e.g., P_{O_2} , T_p , and P_{tot}).

Several theoretical factors play roles in the change of char reaction rate with increasing pressure:

1. Bituminous coal chars undergo a plasticity stage during pyrolysis, thus char

formed at high pressure has a more oriented surface (Niksa et al., 2003) and lower surface area, which is associated with lower reactivity.

2. Char formed at high pressure has higher hydrogen content, which may be related to more reactive char.
3. Elevated total pressure can restrain the gas diffusion coefficient, thus decreasing the reactivity at high temperature (Zone II or Zone III combustion).
4. At constant total pressure, increased oxygen partial pressure (P_{O_2}) can increase the char oxidation reactivity until the char surface is saturated. At high temperature, a higher P_{O_2} is needed to achieve surface saturation because of the increased reaction rate (or faster desorption of surface complexes) (Roberts and Harris, 2000).
5. The effect of mineral matter is primarily responsible for the high-reactivity of low-rank coal, especially at low temperatures, although this effect becomes less important at high temperatures. The role of catalytic mineral matter at high pressure is still unclear (Niksa et al., 2003).

The complexity of char combustion reactions makes it difficult to develop a comprehensive model including all mechanisms. The CBK/E model was a good attempt at using a surface mechanism, but still required one adjustable parameter A_{30} that was a function of pressure. Hurt developed correlations for A_{30} based on pressure and coal type, but notes that a complete mechanistic description is still unavailable (Niksa et al., 2003). However, this mechanism (in CBK/E) may be useful for engineering calculations.

3.5 Chapter 3 Conclusions

High-pressure, high-temperature char combustion experiments were performed in a HPFFB for two coals: Pitt #8 and Ill #6. Char samples were collected and analyzed. The following phenomena were observed:

- (1) Within the total pressure range from 2.5 to 10 atm, char burnout increased with increasing O_2 concentration at constant total pressure.
- (2) N_2 surface areas for Pitt #8 chars increased at early stages of burnout and then decreased with increasing burnout. N_2 surface areas for Ill #6 chars always decreased with increasing burnout. The evolution of pore structure with burnout contributed to the change of N_2 surface area. The difference in the surface area behavior between the two coals may be caused by the different character of pore structure.
- (3) The particle diameter ratio based on coal ($d/d_{\text{coal},0}$) decreased with increasing O_2 concentration for all four conditions. For the Pitt #8 coal, the larger size coal achieved a larger swelling ratio than the smaller size coal. The diameter ratio based on the char ($d/d_{\text{char},0}$) generally decreased with increasing char burnout. The diameter ratio (based on coal) of Ill #6 char decreases quickly with increased O_2 concentration, and the diameter ratio based on char decreased to 0.5 at about 85% burnout rate, regardless of the experimental condition or the O_2 concentration.

The gas temperature and velocity profiles were modeled using Fluent. The coal pyrolysis process was modeled using the CPD model. The results from these two models were used as input parameters for the char burnout model. Both n^{th} -order kinetics and 3-step surface kinetics were used to model the experimental results. Only one kinetic parameter was used to fit the experimental char burnout data:

1. Activation energy (E) was used as a fitting parameter for the n^{th} -order kinetic model (CBK8), and

2. A_{30} was used as a fitting parameter for the 3-step model (CBK/E).

Both CBK8 and CBK/E achieved reasonable agreement with the char combustion data. The modeling results showed that the char oxidation rate increased with increasing total pressure. A different value of E or A_{30} was necessary for each pressure condition for each coal. This means that a one-point calibration is necessary for every condition before CBK/E or CBK8 is capable of predicting char burnout.

The result obtained here that char reactivity increases with increasing total pressure is different than reported by some investigators. Some of that difference may be due to the fact that many previous investigators produced their starting char at atmospheric pressure only, rather than at the pressure where reactivity was measured (as was done in this study).

Chapter 3 References

- Alvarez, D., A. G. Borrego and R. Menendez, "Unbiased Methods for the Morphological Description of Char Structures," *Fuel*, **76**: 1241 (1997).
- Anthony, D. B. and J. B. Howard, "Coal Devolatilization and Hydrogasification," *AIChE J.*, **22**: 625-656 (1976).
- Arendt, P. and K. H. Heek, "Comparative Investigation of Coal Pyrolysis under Inert gas and H₂ at Low and High Heating Rates and Pressures up to 10 MPa," *Fuel*, **60**: 779-787 (1981).
- Bailey, J. G., A. G. Tate, C. Diessel and T. F. Wall, "A Char Morphology System with Applications to Coal Combustion," *Fuel*, **69**, (225) (1990).
- Banin, V. R. M. and B. Veeffkind, "Kinetic Study of High-Pressure Pulverized Coal Char Combustion: Experiments and Modeling," *Fuel*, **76**: 945-949 (1997).
- Bautista, J. R., W. B. Russel and D. A. Saville, "Time-Resolved Pyrolysis Product Distribution of Softening Coals," *Ind. Eng. Chem. Fundm.*, **25**: 536-544 (1986).
- Benfell, K. E., Assessment of Char Morphology in High Pressure Pyrolysis and Combustion. Department of Geology, The University of Newcastle. (2001)
- Benfell, K. E., G.-S. Liu, D. Roberts, D. J. Harris, J. A. Lucas, J. G. Bailey and T. F. Wall, "Modelling Char Combustion: the Influence of Parent Coal Petrography and pyrolysis pressure on the Structure and Intrinsic Reactivity of its Char," *Proceedings of the Combustion Institute*, **28**: 2233-2241 (2000).
- Cai, H. Y., A. J. Guell, I. N. Chatzakis, J. Y. Lim, D. R. Dugwell and R. Kandiyoti, "Combustion Reactivity and Morphological Change in Coal Chars: Effect of Pyrolysis Temperature, Heating Rate and Pressure," *Fuel*, **75**: 15-24 (1996).
- Chitsora, C. T., H.-J. Muhlen, K. H. v. Heek and H. Juntgen, "The Influence of Pyrolysis Conditions on the Reactivity of Char in H₂O," *Fuel Process. Technol.*, **15**: 17-29 (1987).
- Cloke, M., E. Lester and W. Gibb, "Characterization of Coal with Respect to Carbon Burnout in p.f.-fired Boilers," *Fuel*, **76**: 1257-1267 (1997).
- Cope, R., L. D. Smoot and P. Hedman, "Effects of Pressure and Coal Rank on Carbon Conversion in an Entrained-coal Gasifier," *Fuel*, **68**: 807 (1989).
- Croiset, E., M. C., R. J.-P. and R. J.-R., "The Influence of Pressure on Char Combustion Kinetics," *Proceedings of the Combustion Institute*, **26**: 3095-3102 (1996).
- Essenhigh, R. H., Chemistry of Coal Utilization (Chapter 19). M. A. Elliott, New York, (1981).
- Essenhigh, R. H. and G. C. Yorke, "Reaction Rates of Single Coal Particles: Influence of Swelling, Shape, and Other Factors," *Fuel*, **44**: 177-186 (1965).
- Fatemi, M. Effect of Pressure on Pyrolysis of a Sub-Bituminous Coal in an Entrained-Flow Reactor. *Am. Chem. Soc. Div. Fuel Chem.*, **32** (3) 117-124 (1987).
- Fletcher, H. T., A. R. Kerstein, R. J. Pugmire and D. M. Grant, "Chemical Percolation Model for Devolatilization. 2. Temperature and Heating Rate Effects on Product Yields," *Energy & Fuels*, **4**: 54 (1990).

- Fletcher, T. H., "Time-Resolved Particle Temperature and Mass Loss Measurements of a Bituminous Coal During Devolatilization," *Combustion and Flame*, **78**: 223-236 (1989).
- Fletcher, T. H., "Swelling Properties of Coal Chars During Rapid Coal Pyrolysis and Combustion," *Fuel*, **72**, (11): 1485-1495 (1993).
- Gale, T. K., C. H. Bartholomew and T. H. Fletcher, "Decreases in the Swelling and Porosity of Bituminous Coals During Devolatilization at High Heating Rates," *Combustion and Flame*, **100**: 94-100 (1995).
- Gao, H., S. Murata, M. Nomura, M. Ishigaki, M. Qu and M. Tokuda, "Experimental Observation and Image Analysis for Evaluation of Swelling and Fluidity of Single Coal Particles Heated with CO₂ Laser," *Energy & Fuels*, **11**: 230-238 (1997).
- Genetti, D., T. H. Fletcher and R. J. Pugmire, "Predicting ¹³C NMR Measurements of Chemical Structure of Coal Based on Elemental Composition and Volatile Matter Content," *Energy and Fuels*, **13**: 60-68 (1999).
- Grant, D. M., T. H. Fletcher, R. J. Pugmire and A. R. Kerstein, "Chemical Model of Coal Devolatilization using Percolation Lattice Statistics," *Energy & Fuels*, **3**: 175 (1989).
- Griffin, T. P., J. B. Howard and W. A. Peters, "Pressure and Temperature Effects in Bituminous Coal Pyrolysis: Experimental Observations and a Transient Lumped-parameter Model," *Fuel*, **73**: 591-601 (1994).
- Hambly, E. M., The Chemical Structure of Coal Tar and Char During Devolatilization. Chemical Engineering Department, Brigham Young University. (1998)
- Hecker, W. C., M. P. Madsen, R. S. Michael, J. W. Allen, R. J. Sawaya and T. H. Fletcher, "High Pressure Intrinsic Oxidation Kinetics of Two Coal Chars," *Energy and Fuels*, **17**: 427-432 (2003).
- Hong, J., Modeling Char Oxidation as a Function of Pressure Using an Intrinsic Langmuir Rate Equation. Chemical Engineering Department, Brigham Young University. (1999)
- Hong, J., W. C. Hecker and T. H. Fletcher, "Modeling High Pressure Char Oxidation Using Langmuir Kinetics with an Effectiveness Factor," *Proceedings of the Combustion Institute*, **28**: 2215-2223 (2000).
- Hurt, R. H. and J. M. Calo, "Semi-Global Intrinsic Kinetics for Char Combustion Modeling," *Combustion and Flame*, **125**: 1138-1149 (2001).
- Hurt, R. H. and B. S. Haynes, "On the Origin of Power-Law Kinetics in Carbon Oxidation," *Proceedings of the Combustion Institute*: in Press (2004).
- Hurt, R. H., J. Sun and M. Lunden, "A Kinetic Model of Carbon Burnout in Pulverized Coal Combustion," *Combustion and Flame*, **113**: 181-197 (1998).
- Joutsenoja, T., J. Saastamoinen, M. Aho and R. Hernberg, "Effects of Pressure and Oxygen Concentration on the Combustion of Different Coals," *Energy & Fuels*, **13**: 130-145 (1999).
- Kajitani, S. and N. Suzuki. Study on Coal Pyrolysis Property in Pressurized Entrained Flow Coal Gasifier. 12th International Conference on Coal Science, Cairns, Australia (No. 10C4) (2003).
- Khan, M. R. and R. G. Jenkins, "Thermoplastic Properties of Coal at Elevated Pressures : 1. Evaluation of a High-pressure Microdilatometer," *Fuel*, **63**: 109 (1984).

- Lee, C. W., R. G. Jenkins and H. H. Schobert, "Structure and Reactivity of Char from Elevated Pressure Pyrolysis of Illinois No.6 Bituminous Coal," *Energy & Fuels*, **6**: 40-47 (1992).
- Lee, C. W., A. W. Scaroni and R. G. Jenkins, "Effect of Pressure on the Devolatilization and Swelling Behaviour of a Softening Coal during Rapid Heating," *Fuel*, **70**: 957-965 (1991).
- Lester, E. and M. Cloke, "The Characterisation of Coals and Their Respective Chars Formed at 1300°C in a Drop Tube Furnace," *Fuel*, **78**: 1645 (1999).
- Lester, E., M. Cloke and M. Allen, "Char Characterisation Using Image Analysis Techniques," *Energy & Fuels*, **10**: 696 (1996).
- Lester, T. W., W. R. Seeker and J. F. Merklin, "The Influence of Oxygen and Total Pressure on the Surface Oxidation rate of Bituminous Coal," *Proceedings of the Combustion Institute*, **18**: 1257 (1981).
- Ma, J., Soot Formation from Coal Pyrolysis. Chemical Engineering Department, Brigham Young University. (1996)
- Mathias, J. A., High Pressure Oxidation Rates for Large Particles. Mechanical Engineering Department, Brigham Young University. (1996)
- Matsuoka, K., Z.-x. Ma, H. Akiho, Z.-g. Zhang, A. Tomita, T. H. Fletcher, M. A. Wojtowicz and S. Niksa, "High-pressure Coal Pyrolysis in a Drop Tube Furnace," *Energy & Fuels*, **17**: 984-990 (2003).
- Mitchell, R. E., "Characterization of Variations in Char Reactivity and Mode of Particle Buring During Combustion of Pulverized Solids," *Final report for NSF Grant # CTS-9903403*, Stanford, California, (2003).
- Monson, C. R., Char Oxidation at Elevated Pressures. Mechanical Engineering Department, Brigham Young University. (1992)
- Monson, C. R., G. J. Germane, A. U. Blackham and L. D. Smoot, "Char Oxidation at Elevated Pressure," *Combustion and Flame*, **100**: 669-683 (1995).
- Moors, J. H. J., Pulverised Char Combustion and Gasification at High Temperature and Pressure. Technique University of Eindhoven. (1998)
- Niksa, S., G. Liu and R. H. Hurt, "Coal Conversion Submodels for Design Applications at Elevated Pressures. Part I. Devolatilization and Char Oxidation," *Progress in Energy and Combustion Science*, **29**, (5): 425-477 (2003).
- Oh, M. S., W. A. Peters and J. B. Howard, "An Experimental and Modeling Study of Softening Coal Pyrolysis," *AIChE J.*, **35**: 775 (1989).
- Parkinson, A., R. Balling, J. Free, J. Talbert, D. Davidson, G. Gritton, L. Borup and B. Busaker, "OptdesX A Software System For Optimal Engineering Design," (1992).
- Perry, S., A Global Free-Radical Mechanism for Nitrogen Release During Devolatilization Based on Coal Chemical Structure. Chemical Engineering Department, Brigham Young University. (1999)
- Ranish, J. M. and P. L. J. Walker, "High Pressure Studies of the Carbon-Oxygen Reaction," *Carbon*, **31**: 135-141 (1993).
- Reichelt, T., T. Joutsenoja, H. Spliethoff, K. R. G. Hein and R. Hernberg, "Characterization of Burning Char Particles Under Pressurized Conditions by Simultaneous *in situ* Measurement of Surface Temperature and Size," *Proceedings of the Combustion Institute*, **27**: 2925-2932 (1998).

- Roberts, D. G. and D. J. Harris, "Char Gasification with O₂, CO₂, and H₂O: Effects of Pressure on Intrinsic Reaction Kinetics," *Energy & Fuels*, **14**: 483-489 (2000).
- Roberts, D. G., D. J. Harris and T. F. Wall, "On the Effects of High Pressure and Heating Rate during Coal Pyrolysis on Char Gasification Reactivity," *Energy & Fuels*, **17**: 887-895 (2003).
- Saastamoinen, J. J., M. J. Aho, J. P. Hamalainen, R. Hernberg and T. Joutsenoja, "Pressurized Pulverized Fuel Combustion in Different Concentrations of Oxygen and Carbon Dioxide," *Energy & Fuel*, **10**: 121-133 (1996).
- Seebauer, V. P. J. and G. Staudinger, "Effects of Particle Size, Heating Rate and Pressure on Measurement of Pyrolysis Kinetics by Thermogravimetric Analysis," *Fuel*, **76**: 1277-1282 (1997).
- Sha, X. Z., Y. G. Chen, J. Cao, Y. M. Yang and D. Q. Ren, "Effects of Operating Pressure on Coal Gasification," *Fuel*, **69**: 293 (1990).
- Sheng, C. and J. L. T. Azevedo, "Modeling the Evolution of Particle Morphology During Coal Devolatilization," *Proceedings of the Combustion Institute*, **28**: 2225 (2000).
- Solomon, P. G. and D. G. Hamblen. Chemistry of Coal Conversion. New York, Plenum Press. (1985)
- Solomon, P. R. and T. H. Fletcher, "Impact of Coal Pyrolysis on Combustion," *Proceedings of the Combustion Institute*, **25**: 463-474 (1994).
- Strezov, V., J. A. Lucas and T. F. Wall. Effect of Pressure on the Swelling of Density Separated Coal Particles. Int. Symp. on Utilisation of Coal and Biomass, Newcastle, Australia ISUCB-03 (2003).
- Sun, C. L., Y. Q. Xiong, Q. X. Liu and M. Y. Zhang, "Thermogravimetric Study of the Pyrolysis of Two Chinese Coals Under Pressure," *Fuel*, **76**: 639-644 (1997).
- Suuberg, E. M., Peters, W.A., and Howard, J.B. *Proceedings of the Combustion Institute*, **17** 117 (1978).
- Suuberg, E. M., M. Wojtowicz and J. M. Calo, "Reaction Order for Low Temperature Oxidation of Carbon," *Proceedings of the Combustion Institute*, **22**: 79-87 (1988).
- Van Heek, K. H. and H.-J. Muhlen. Fundamental Issues in Control of Carbon Gasification Reactivity, Kluwer Academic Publishers. (1991)
- Wall, T., H. Wu, K. Benfell, G. Liu and G. Bryant. The Influence of Pressure in pf Combustion and Gasification: Char Structure, Reactivity, and Ash Character. Fifth International Conference on Technologies and Combustion Technologies for a Clean Environment 733-739 (1999).
- Wall, T. F., L. Gui-su, W. Hong-wei, D. G. Roberts, K. E. Benfella, S. Gupta, J. A. Lucas and D. J. Harris, "The Effects of Pressure on Coal Reactions during Pulverised Coal Combustion and Gasification," *Progress in Energy and Combustion Science*, **28**: 405-433 (2002).
- Wu, H., G. Bryant, K. Benfell and T. Wall, "An Experimental Study on the Effect of System Pressure on Char Structure of an Australian Bituminous Coal," *Energy & Fuels*, **14**: 282-290 (2000).
- Yeasmin, H., J. F. Mathews and S. Ouyang, "Rapid Devolatilisation of Yallourn Brown Coal at High Pressures and Temperatures," *Fuel*, **78**: 11-24 (1999).
- Yu, J., J. Lucas, V. Strezov and T. Wall, "Swelling and Char Structures from Density Fractions of Pulverized Coal," *Energy & Fuels*, **17**: 1160-1174 (2003).

- Yu, J.-L., V. Strezov, J. Lycas, G.-S. Liu and T. Wall, "A Mechanistic Study on Char Structure Evolution During Coal Devolatilization - Experiments and Model Predictions," *Proceedings of the Combustion Institute*, **29**: 467-473 (2002).
- Zhang, H. and T. H. Fletcher, "Nitrogen Transformations during Secondary Coal Pyrolysis," *Energy and Fuels*, **15**: 1512-1522 (2001).
- Zygourakis, K., "Effect of Pyrolysis Conditions on the Macropore Structure of Coal-Derived Chars," *Energy & Fuels*, **7**: 33-41 (1993).